Inaugural dissertation

for

obtaining the doctoral degree

of the

Combined Faculty of Mathematics, Engineering and Natural Sciences

of the

Ruprecht - Karls - University

Heidelberg

Presented by

M.Sc. Jasmin Onistschenko

Born in: Ludwigshafen am Rhein, Germany

Oral examination: 18.10.2024

Stem cell homeostasis in medaka neuromasts – Keratin 15 as a regulator of proliferation

Referees: Prof. Dr. Lázaro Centanin

Prof. Dr. Steffen Lemke

Abstract

Stem cells have the remarkable ability to constantly self-renew and create cellular diversity. Adult stem cells in particular are of great interest as they form the pool of cells that provides continuous replacement of vanished cells both in physiological conditions and upon injury. The neuromast of the posterior lateral line in medaka (*Oryzias latipes*) is an exceptional model to study adult stem cells. As fish grow throughout their entire lives and the neuromasts of the lateral line are continuously exposed to the environment, the neuromasts have constantly active stem cells that react to the need of new cells. So far, the dynamics of neuromast stem cells (NSCs) has not been studied in detail and their regulation has remained elusive. In this thesis, I investigated the proliferation of NSCs by timelapse imaging using *keratin 15 (k15)* expression as a stem cell marker. This showed that NSCs are highly proliferatively active stem cells in homeostasis. Furthermore, nuclei of the NSCs migrate within the cell in a temporally correlated manner at certain cell cycle steps, resembling interkinetic nuclear migration in which mitosis occurs exclusively on the apical side of the cell. Following the expression of *k15* during the cell cycle also revealed that *k15* expression is heterogeneous among NSCs, being upregulated in dividing stem cells. Keratins are generally known as markers for stem cells, but their function in stem cell regulation remains unclear. In this work, I therefore investigated the link between the stem cell marker K15 and the behaviour of NSCs by combining fluorescent transgenic lines, 4D imaging and clonal genetic approaches for gain- and loss-of-function of K15. Overexpression of *k15* in NSCs resulted in reduced stem cell proliferation visualised by the incorporation of the base analogue bromodeoxyuridine (BrdU). This showed that fewer NSCs underwent S-phase. This result was further confirmed by timelapse imaging, in which fewer stem cells underwent mitosis compared to the wildtype. In contrast, the NSCs of the K15 mutants exhibited increased proliferation detected by BrdU incorporation and timelapse imaging. In addition, neuromast with a mutant K15 showed morphological changes ranging from very small to very large and elongated neuromasts. Clonal analyses in chimeric neuromasts revealed a differential short and long-term behaviour for overexpressing *K15* in NSCs. My results suggest that K15 not only serves as a stem cell marker but is also involved in stem cell regulation and stem cell fate. Furthermore, a single-cell RNA sequencing atlas of medaka epithelial cells was generated which forms the basis to further elucidate the regulation of all cell types in the neuromast. Taken together, this work provides new insights into how

stem cells are regulated under homeostatic conditions and emphasises the importance of keratins as stem cell markers as regulators of stem cells.

Zusammenfassung

Stammzellen haben die bemerkenswerte Fähigkeit, sich einerseits selbst zu erneuern und andererseits dabei eine zelluläre Vielfalt zu schaffen. Vor allem adulte Stammzellen sind von großem Interesse, da sie den Zellpool bilden, der sowohl das physiologische Gleichgewicht aufrechterhält als auch bei Verletzungen für den kontinuierlichen Ersatz verlorener Zellen sorgt. Neuromasten des hinteren Seitenlinienorgans von Medaka *(Oryzias latipes)* sind ein besonders gut geeignetes Modellsystem zur Untersuchung von adulten Stammzellen.

Da Fische ihr ganzes Leben lang wachsen und die Neuromasten des Seitenlinienorgans ständig der Umwelt ausgesetzt sind, haben sie ständig aktive Stammzellen. Bisher wurde das Verhalten von Neuromast-Stammzellen noch nicht im Detail untersucht und deren Regulierung noch nicht aufgedeckt. In dieser Arbeit untersuchte ich die Zellproliferation von Neuromast-Stammzellen mit Hilfe von Zeitrafferaufnahmen unter Verwendung der Expression von *keratin 15 (k15)* als Stammzellmarker. Dabei zeigte sich, dass Neuromast-Stammzellen in der Homöostase hoch proliferativ aktive Zellen sind. Darüber hinaus wandern die Zellkerne der Neuromast-Stammzellen entsprechend dem Zellzyklus, ähnlich wie bei der interkinetischen Kernwanderung, bei der die Mitose ausschließlich an der apikalen Seite einer Zelle stattfindet. Die Zeitrafferaufnahmen haben auch gezeigt, dass die Expression von *k15* unter den Neuromast-Stammzellen heterogen ist und in sich teilenden Stammzellen *k15* hochreguliert wird. Keratine sind generell als Marker für Stammzellen bekannt, aber ihre Funktion bei der Stammzellregulation ist bisher unklar. In dieser Arbeit habe ich deshalb den Zusammenhang zwischen dem Stammzellmarker K15 und dem Verhalten von Neuromast-Stammzellen untersucht, indem ich fluoreszierende transgene Linien, Zeitrafferaufnahmen und klonale genetische Ansätze für eine Über- und Unterexpression der Funktion von K15 kombiniert habe. Die Überexpression von *k15* in Neuromast-Stammzellen führte zu einer verringerten Stammzellproliferation, die durch den Einbau des Basenanalogons Bromdesoxyuridin (BrdU) sichtbar gemacht wurde. Dies zeigte, dass weniger Neuromast-Stammzellen die S-Phase durchlaufen. Dieses Ergebnis konnte durch Zeitrafferaufnahmen weiter bestätigt werden, bei denen im Vergleich zum Wildtyp weniger Stammzellen eine Mitose durchliefen. Dahingegen wiesen die Neuromast-Stammzellen der K15-Mutanten eine erhöhte Proliferation auf, die durch BrdU-Inkorporation und Zeitrafferaufnahmen nachgewiesen werden konnte. Darüber hinaus zeigten Neuromasten mit mutiertem K15 morphologische Veränderungen, die von sehr kleinen bis hin zu sehr großen und verlängerten Neuromasten reichten. Klonale Analysen in chimären

Neuromasten zeigten ein unterschiedliches Kurz- und Langzeitverhalten bei der Überexpression von K15 in Neuromasten-Stammzellen. Meine Ergebnisse legen nahe, dass K15 nicht nur als Stammzellmarker dient, sondern auch an der Stammzellregulation beteiligt ist. Zusätzlich wurde ein Einzelzell-RNA-Sequenzierungsatlas von Medaka-Epithelzellen erstellt, der die Grundlage für die weitere Aufklärung der Regulation aller Zelltypen im Neuromast bildet. Insgesamt liefert diese Arbeit neue Erkenntnisse darüber, wie Stammzellen unter homöostatischen Bedingungen reguliert sind und unterstreicht die Bedeutung von Keratinen als Stammzellmarker als Regulatoren von Stammzellen.

Graphical abstract

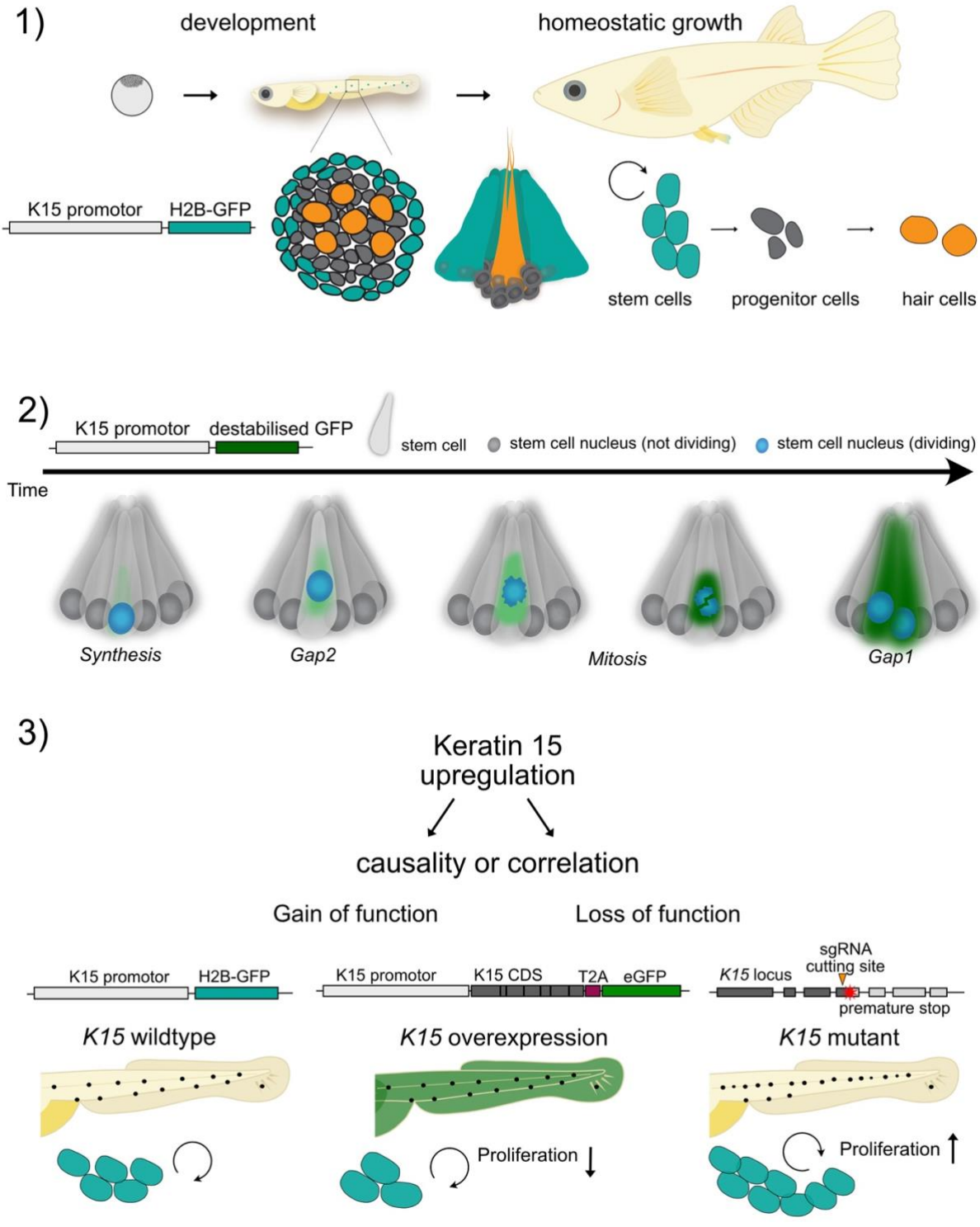

* Schemes partially adapted from (Seleit, Krämer, et al. 2017; Groß et al. 2022)

Contents

Abstract I

Zusammenfassung III

Graphical abstract V

Abbreviations XI

1 Introduction 1

1.1 The origin of stem cells 1

1.2 Adult stem cells 1

1.3 Regulation of adult stem cells 2

1.4 Stem Cell Division 3

1.5 The cell cycle and its influence on cell fate 4

1.6 Adult stem cell marker 5

1.7 Keratins as epithelial stem cell marker 6

1.8 Interkinetic nuclear migration (INM) as a cell fate decision 8

1.9 Medaka as a model organism to study stem cells 9

1.10 Posterior lateral line medaka to study stem cells 10

1.11 Keratin 15 as neuromast stem cell marker 11

2 Aims of this study 13

2.1 Understanding stem cell behaviour of neuromast stem cells 13

2.2 The influence of Keratin 15 on neuromast stem cells 13

3 Results 15

3.1 Neuromast stem cells actively proliferate during homeostasis 15

3.2 Neuromast stem cells oscillate according to the cell cycle 18

3.3 Apical positioning of centrosome 20

3.4 The stem cell marker K15 is heterogeneously expressed in neuromast stem cells 22

3.5 Endogenous tagging of K15 24

3.6 K15 expression is upregulated during G2-M phase in NSCs 25

3.7 K15 overexpression decreases neuromast stem cell proliferation 26

3.8 K15 mutants display increase in neuromast stem cell proliferation 29

3.9 Transplantations affected the proliferation of neuromast stem cells 33

3.10 Transplanted K15 oe stem cells outcompeted wt stem cells 36

3.11 Transplanted K15 mut stem cells do not impact the proliferation of stem cells 37

3.12 Single cell RNA sequencing of medaka epithelial cells revealed niche cell marker 38
3.13 Identification of epithelial fin cells by scRNA seq: 41
4 Discussion 43
4.1 Neuromast stem cells (NSCs) actively proliferate during homeostasis 43
4.2 Increased anterior proliferation of NSCs in post-embryonic growth 45
4.3 Proliferation control in NSCs 46
4.4 NSCs oscillate according to the cell cycle, reminiscent of interkinetic nuclear migration 47
4.5 Upregulation of Keratin 15 in NSCs during apical migration in G2/M phase 49
4.6 K15-GFP fusion impacts embryonic development in medaka 50
4.7 K15 acts as proliferation pacer 51
4.8 K15 influences cell fate: 52
4.9 ScRNA seq data to identify marker genes in neuromasts 54
5 Conclusion 57
6 Materials and Methods 59
6.1 Materials 59
6.1.1 Medaka fish lines 59
6.1.2 cDNA templates from 20k library 59
6.1.3 Oligo pools 59
6.1.4 Plasmids 61
6.1.5 Primers 62
6.1.6 sgRNAs 63
6.1.7 Chemicals and reagents 64
6.1.8 Media and solutions 66
6.1.9 Enzymes and buffers 69
6.1.10 Antibodies and conjugates 69
6.1.11 Kits 70
6.1.12 Consumables 70
6.1.13 Equipment 71
6.1.14 Software and Applications 72
6.2 Methods 73
6.2.1 Fish Husbandry 73
6.2.2 Hatching of embryos 73
6.2.3 Mounting 73
6.2.4 Fixation of fish 73
6.2.5 Whole-mount immunostaining 73

6.2.6 BrdU incorporation and staining 74
6.2.7 Imaging 75
6.2.8 Image processing 75
6.2.9 Data processing 75
6.2.10 4-Di-2-ASP staining 75
6.2.11 Microinjection of one-cell stage Medaka 75
6.2.12 Transplantation of blastulae 76
6.2.13 Whole mount *in*-situ hybridisation 76
6.2.14 Probe design for HCR RNA-FISH 77
6.2.15 HCR™ RNA-FISH 77
6.2.16 Genotyping 78
6.2.17 Polymerase Chain Reaction (PCR) 78
6.2.18 Agarose gel electrophoresis 78
6.2.19 Gel extraction 79
6.2.20 PCR clean-up 79
6.2.21 Restriction Digest 79
6.2.22 DNA ligation 79
6.2.23 Transformation of Shot® Mach1TM-T1R Chemically Competent *E. coli* 79
6.2.24 Extraction of plasmid DNA 80
6.2.25 Sequencing 80
6.2.26 Single cell dissociation 80
6.2.27 Library preparation and sequencing 81
References ***83***
Declaration ***93***
Acknowledgments ***95***
Publications ***99***
List of Figures ***101***
List of Tables ***103***

Abbreviations

3D	three dimensions
4D	four dimensions
4-Di-2-ASP	4-(4-diethylaminostyryl)-1-methylpyridinium iodide
and1	actinodin
BCIP	5-Brom-4-chlor-3-indoxylphosphat
BrdU	Bromodeoxyuridine
Cas	CRISPR-associated system
CDS	coding sequence
CRISPR	clustered regularly interspaced short palindromic repeats
crRNA	crispr RNA
d2-GFP	destabilised GFP
DAPI	4', 6-diamidino-2-phenylindole
DNA	deoxyribonucleic acid
dpf	days post fertilisation
E. coli	*Escherichia coli*
eGFP	enhanced GFP
ERM	Embryonic rearing medium
EtOH	Ethanol
fwd	forward
G1	Gap1-phase
G2	Gap2-phase
GFP	green fluorescent protein
h	Hour
H2B	histone H2B
H_2O	Water
HCR	hybridisation chain reaction
INM	Interkinetic nuclear migration
I-SceI	meganuclease I-SceI
K	keratin
Krt1c19e	Keratin 1c19e
K15	Keratin 15

l	litre
M	mitosis
MeOH	methanol
min	minute
mRNA	messenger RNA
mut	mutant
mYFP	membrane yellow fluorescent protein
NBT	nitro blue tetrazolium
NGS	Natural goat serum
NSCs	Neuromast stem cells
Oe	overexpression
PCNA	Proliferating cell nuclear antigen
PFA	Paraformaldehyde
PTW	phosphate buffered saline plus Tween 20
rev	Reverse
RFP	red fluorescent protein
RNA	ribonucleic acid
S	synthesis
sec	Seconds
sgRNA	single guide RNA
T2A	thosea asigna virus 2A
TAE	tris-acetate-EDTA
Tg	Transgene
UTR	untranslated region
Wnt	Wingless/Integrated
wt	Wildtype
x	-fold

1 Introduction

1.1 The origin of stem cells

Understanding the origin of life has been of interest since centuries and remains one of the most fundamental questions in science to this day. Many researchers followed their curiosity to identify what life means and what its key requirements are. Unicellular organisms such as prokaryotes (like bacteria and archaea), which were found 3.5 billion years ago, can already be defined as living organisms (Schopf and Packer 1987). They were able to metabolize, grow, respond to external stimuli, reproduce, and adapt to their environment over the course of evolution. Over time, multicellular organisms have formed and developed different forms of cells depending on the organization of the organism. This required cellular specification and diversification, leading to the high complexity and individuality of life (Novikoff 1945). One important cell type which has evolved are stem cells. Choanoflagellates, unicellular protists, show a close resemblance to choanocytes in sponges and are known to be the closest unicellular relatives to animals (Brunet and King 2017). In recent studies which compared the different sponge cells with choanoflagellates, it was found that choanoflagellates already show similar properties of stem cells in higher complex animals, such as the expression of myc, which is characteristic of pluripotent stem cells (Sogabe et al. 2019). Stem cells are essential and the prerequisite for multicellular organisms since these are the cells which maintain homeostasis and generate differentiated tissue (Kumar et al. 2010). During evolution, the specification into stem cells not only appeared in the animal kingdom but also in plants. In both systems, stem cells are the source of cells to produce new cells and generate differentiated progeny. Moreover, animal and plant stem cells share similar properties as in maintaining a stem cell niche, regulating the activity of stem cells, and similar molecular signalling as retinoblastoma, controlling the fate of the cells (Burkhart and Sage 2008; Scheres 2007). This co-evolution of stem cells highlights their fundamental need in multicellular organisms.

1.2 Adult stem cells

Stem cells have the unique ability to generate new stem cells while also being able to produce differentiated cells. Stem cells can be subdivided into two groups, embryonic and adult (somatic) stem cells. They can be characterised by their potency. While early embryonic stem cells have a high potency and can differentiate into any cell type, the potency decreases over

the course of development as the tissue becomes more specified, from pluripotent to multipotent and sometimes even to unipotent (Ding and Schultz 2004). In the mammary gland, both multipotent and unipotent population of adult mammary gland stem cells are found, in which the multipotent stem cells can differentiate to myoepithelial and luminal mammary cells, while the unipotent stem cells only differentiate into either myoepithelial or luminal cells. These different adult stem cell populations of the mammary gland are characterised by their distinct expression of keratins which are used as stem cell markers (Zhou et al. 2019; Van Keymeulen et al. 2011). Once development has concluded, most of the cells in an organism have lost their high capacity and differentiated into a tissue-specific cell type. However, small groups of cells stay in an undifferentiated state and form the pool of tissue-specific adult stem cells. The process from pluripotent embryonic stem cells, which are capable of producing every cell type in the organism, to adult stem cells, that only generate a few cell types, is known as fate restriction (Henion and Weston 1997).

1.3 Regulation of adult stem cells

The amount, potency, and behaviour of adult stem cells varies greatly between different organisms and tissues. Some adult stem cells are continuously active to maintain homeostasis and respond to injuries such as in the skin, whereas other remain quiescent (Blanpain and Fuchs 2006; de Morree and Rando 2023). It is known that stem cells can rest in dormant states called quiescence and be reactivated when needed (Pietras, Warr, and Passegué 2011). The haematopoietic system is one very well studied example for a stem cell pool where it could be shown that the quiescent stem cells can be reactivated and give rise to all cell types from the blood system (McCulloch and Till 1962). Other stem cell pools are more restricted to their cell fate, e.g., the liver which is able to generate new hepatocytes and bile duct epithelial cells (Douarin 1975). The Müller Glia cells in the retina of medaka are only able to regenerate once (Lust and Wittbrodt 2018). As a fundamental basis for homeostasis and regeneration, stem cell regulation needs to be studied to understand how the tightly controlled stem cells can adapt to difficult and changing conditions. Dysregulation can result in loss of tissue integrity and diseases, such as cancer (Morrison and Kimble 2006). Cancerogenic cells display a high similarity to normal stem cells as they can self-renew and share similar molecular pathways for self-renewal, such as Notch, Wnt, and Hedgehog (Reya et al. 2001). In many cases, cancer involves accumulated mutations in stem cells that start dividing uncontrollably and form tumours (Passegué et al. 2003). In acute myeloid leukaemia (AML), acquired mutations in hematopoietic stem cells have been found to be the main cause of the disease (Hope, Jin, and

Dick 2004). In the intestine, mutations in the Wnt pathway of crypt stem cells lead to the formation of neoplasia (Barker et al. 2009). Therefore, it is of great importance to understand how stem cells are regulated in homeostasis to better understand how such diseases can be prevented and treated.

1.4 Stem Cell Division

Stem cells can act in two division modes, symmetric and asymmetric. In the symmetric division mode, stem cells either give rise to two stem cells or two differentiated cells. Whereas in the asymmetric division mode, one stem cell and one differentiated cell is generated (Fig 1). Which division mode is chosen depends on the tissue and the need of new differentiated progeny. In the brain of adult mice, neural stem cells usually divide symmetrically and alternate between self-renewal and the generation of olfactory neurons (Obernier et al. 2018). Drosophila neuroblasts normally divide asymmetrically. Once the machinery of asymmetric division is interfered, neuroblasts divide symmetrically, resulting in tumour formation (Morrison and Kimble 2006). So far it is not fully known how stem cell division is regulated but the microenvironment, called niche, seems to be of high importance. The niche can interfere with the behaviour of stem cells and influence the division mode. Stem cells closer to the niche tend to stay stem cells, whereas cells further away from their niche become progenitor and mature cells (Schofield 1978). The microenvironment of stem cells can be very different depending on the stem cell system. In the haematopoietic system, the bone marrow is the niche, and bone marrow stromal cells and the extracellular matrix play important roles in regulating the haematopoietic stem cells (Woods and Guezguez 2021). In the adult mammalian brain, the subventricular zone form the niche of neural stem cells and is modulated by neighbouring cells such as progenitor and differentiated cells, but also by the vasculature which secrete growth factors to influence neural stem cell behaviour (Lee et al. 2012). These diverse components of each stem cell niches make it difficult to study the stem cell niche interaction. Interestingly, in the posterior lateral line of medaka, the niche is defined by a single cell type called border cells, which constructs the microenvironment of neuromast stem cells (Seleit, Krämer, et al. 2017; Onistschenko et al. 2023).

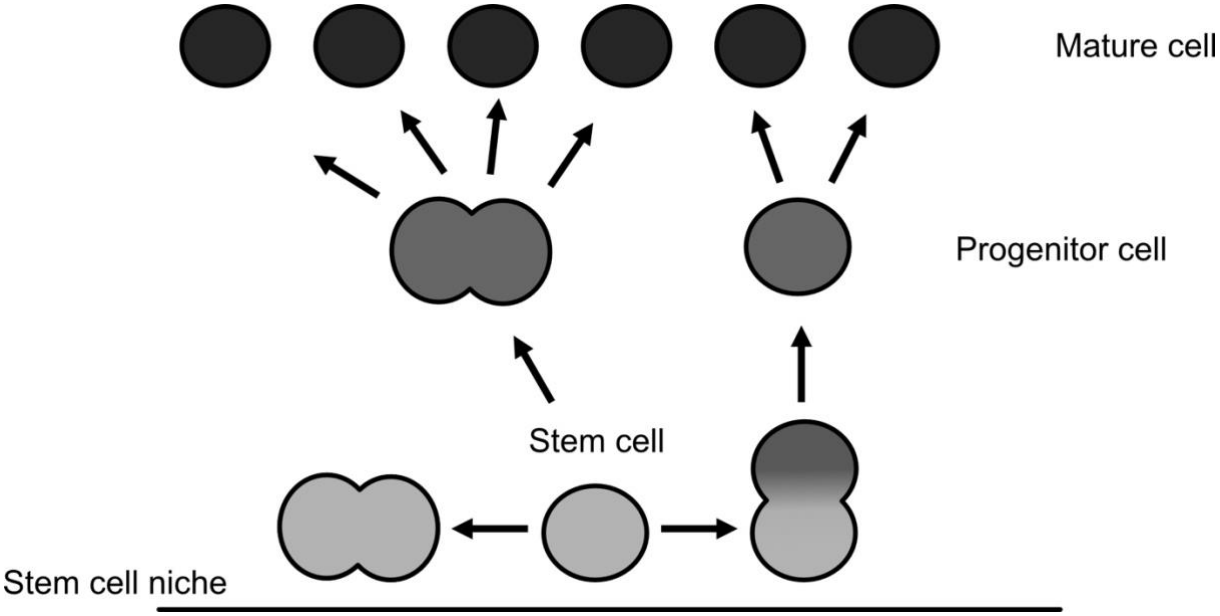

Figure 1: Representation of symmetric and asymmetric division of stem cells.
Stem cells can divide symmetrically and thereby generating two stem cells or two progenitor cells. Whereas in the asymmetric division mode, the stem cell divides by generating one progenitor cells and one stem cell. Daughter cells closer to the niche rather stay stem cells, whereas daughter cells further away differentiate into progenitor and mature cells.

1.5 The cell cycle and its influence on cell fate

Cell division is essential for the formation of multicellular organisms and embryonic development is characterized by a massive increase in the number of cells from which different cell types will develop (Brunet and King 2017). In adult organisms, cell division is restricted to stem and progenitor cells (Gonzalez and Bernad 2012). The cell cycle can be divided into several phases whose function is to ensure the proper replication of a cell. It can essentially be separated into mitosis and interphase. During mitosis (M-phase), the actual cell division takes place. The DNA condenses into chromosomes, which are then separated during mitosis by the mitotic spindle. The interphase consists of a series of events. One important event is the synthesis phase (S-phase), in which the DNA content is duplicated. In between M- and S-phase, two phases called gap phases (G1 and G2) take place. The G1 phase is the stage after

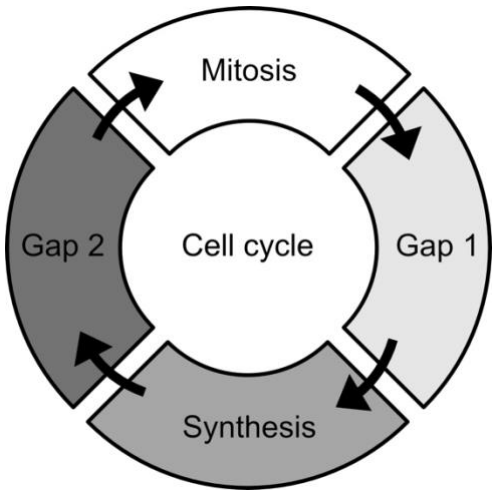

Figure 2: Schematic drawing of the cell cycle. The cell cycle can be subdivided into four phases: Mitosis, gap 1, synthesis and gap 2 phase.

mitosis and G2 occurs after S-phase (Park and Koff 2001) (Fig. 2). These are important pauses for the growth of the cell and the replication of proteins and cell organelles. These phases are also crucial for monitoring whether the conditions are right for the continuation of S- or M-phase (Bertoli, Skotheim, and de Bruin 2013). Cyclin-dependent kinases therefore control the progression of the cell cycle. Cyclin proteins initiate certain check-points, that the cell can continue in its cell cycle program or rest longer in a specific phases (Malumbres 2014). P53 is a protein that is well known as a tumour suppressor because it can interrupt the cell cycle. In doing so, P53 pauses the cell cycle to give the cell more time to ensure that the correct DNA content is produced and DNA damage is repaired (Donehower et al. 1992). After mitosis, the cell can also enter a longer resting phase, where the cell is not actively cycling anymore. This phase is called G0 and is characterised as a quiescent state (Cheung and Rando 2013). How long cells stay in quiescent and whether they are reactivated depends on the stem cell system. The cell cycle can also be used to decide the cell fate of the cell. Depending on which signals are transmitted, the cell cycle either progresses or rests. Various signals during the G1 phase can determine whether a stem cell undergoes self-renewal or starts to differentiate. In human embryonic stem cells (hESC), it was demonstrated that cyclin D expression in G1 promote neuroectoderm differentiation whereas expression of activin and nodal drive differentiation to endoderm (Pauklin and Vallier 2013). Taken together, this shows that the cell cycle is a dynamic process which must be adapted and controlled at the individual cell level.

1.6 Adult stem cell marker

Adult stem cells are present in all multicellular organisms, and many of them have already been characterized and studied (Ma et al. 2009; Blanpain and Fuchs 2006). However, adult stem cells are poorly represented compared to other cells in the body and constitute only a small group of cells. In addition, adult stem cells are embedded in their respective tissues and are not always easy to distinguish from other cells (Ferraro, Celso, and Scadden 2010). This difficulty in differentiation and rarity represents a major challenge in researching adult stem cells. It is therefore of great importance to have reliable markers to identify stem cells. It has long been of interest to identify individual adult stem cell markers. Intensive studies have been carried out on the hierarchical organization of the hematopoietic system to identify its individual markers for their various differentiation states. The transmembrane protein CD34 was identified to be an important marker for the hematopoietic lineage, since these CD34 + cells are able to reconstitute the full hematopoietic lineage (Link et al. 1996). In later studies of the intestine, researchers could identify the marker leucine-rich-repeat containing G-protein-coupled

receptor 5 (Lgr5) as a marker for the intestinal crypt cells which are known to be the stem cells (Barker et al. 2007). The neural adult stem cells could be classified using GFAP and Nestin among others as markers. In the subventricular zone, astrocytes are acting as the stem cells of the adult mammalian brain and generate new neurons. These astrocytes are characterised as GFAP + (Doetsch et al. 1999). Nestin is used as neural stem cell marker in the central nervous system (CNS) during development as well as in the adult brain, but is also found in endothelial progenitor cells in CNS (Suzuki et al. 2010). Both GFAP and Nestin belong to the family of intermediate filaments (Zerlin, Levison, and Goldman 1995). Interestingly, intermediate filaments often serve as molecular markers for stem cells and the differentiation status of cells. Typical examples are vimentin in mesenchymal cells after epithelial to mesenchymal transition (EMT) or keratins in epithelial cells (Mendez, Kojima, and Goldman 2010; Sjöqvist et al. 2021; Dmello et al. 2019). In the hair bulge of human and mice, Keratin 15 is used as stem cell marker (Lyle et al. 1998; Liu et al. 2003). Especially Keratins are regularly used to determine the identity of epithelial cells and are used in cancer progression research.

1.7 Keratins as epithelial stem cell marker

Intermediate filaments are essential proteins of the cytoskeleton in a variety of cells such as neurons, muscle, and epithelial cells. Other than actin and microtubules which are polymers of individual proteins, intermediate filaments form clusters of various proteins. They share a common structure, the central rod domain, which is important for forming heterodimers with other intermediate filament proteins (Fig. 3).

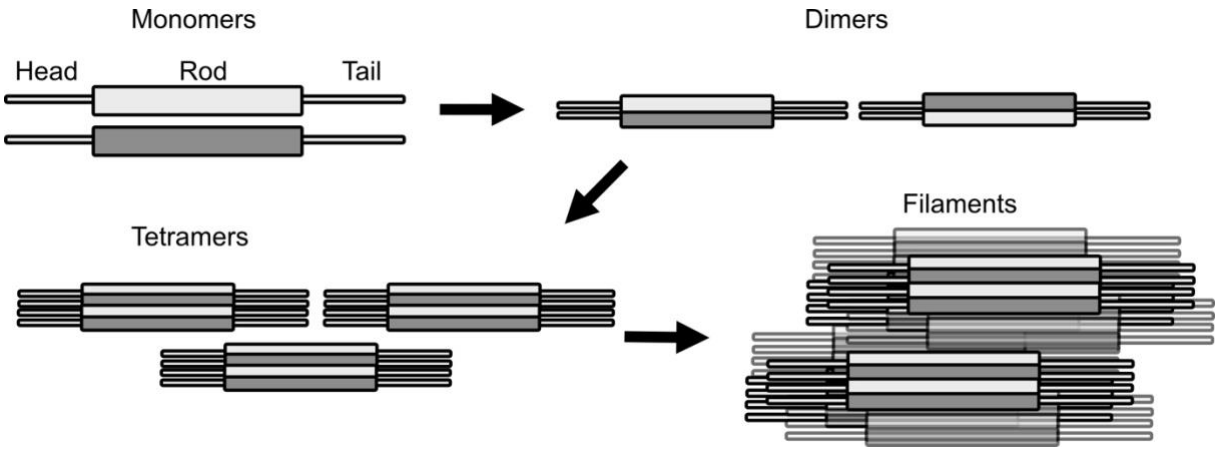

Figure 3: Schematic representation of intermediate filament assembly. Monomers are structured in a central rod domain flanked by a head and a tail domain. These monomers form dimers which then assemble to tetramers which form the individual filaments.

These heterodimers then cluster together and form tetramers which then form the filaments, spanning through the cytoplasm of the cell (Cooper. 2000). They are very compacted and display a high stability which is why they are known to serve as structural support of cells and help to resist mechanical forces (Aebi et al. 1983). Intermediate filaments can be subdivided into six groups according to their similarity of amino acids: Type 1 keratins, type 2 keratins, vimetins and desmins, neurofilaments, lamins and nestin. All of them are expressed in particular tissues and have specific functions according to the cell type (Cooper. 2000).

Keratins belong to the first and second group of intermediate filaments and can therefore be subdivided into type 1 and type 2 keratins according to their feature of being acidic (type 1) or neutral (type 2). Interestingly, a type 1 keratin always forms a heterodimer with a type 2 keratin. Therefore, the expression of both classes is important for proper functionality. The formation of individual keratin heterodimers gives information about the distinct cell types. It is known that the expression of keratin pairs is not only tissue specific, but also dependent on the differentiation state (Coulombe and Omary 2002; Schwarz et al. 2015). Keratin 8 always forms heterodimers with Keratin 18 and is expressed in simple epithelial cells. Keratin 5 clusters together with Keratin 14 being expressed in epidermal stem cells of the epidermis. Therefore, the profile of keratins can be used to analyse the identity of specific tissues and cells. Keratins are not only often used as stem cell markers, but also serve as markers for cancer progression. Often, in carcinogenic tissues the expression pattern of keratins is altered. Reduced expression of K8 and K20 in colorectal cancer correlates with decreased survival rate of the patients (Knosel et al. 2006). The presence of K5/K6 and K17 was found to be correlated with a negative impact on survival in breast cancer (Cheang et al. 2008). The knowledge of altered keratin expression in malignant tissue is fundamental to better understand cancer. The alteration in keratin expression in cancer shows that keratin expression can change when cells are dysregulated. Whether the change in keratin expression is the cause of the cell fate/behaviour change has not yet been clarified. Therefore, it is of high importance to better understand how keratin expression affect the fate of a cell.

1.8 Interkinetic nuclear migration (INM) as a cell fate decision

During the cell cycle, major changes need to occur to get from one cell to two. On the one hand the DNA needs to be duplicated and separated, but also the cytoskeleton components need to be doubled and rearranged to split into two cells after mitosis. Interestingly, in some cells the position of the nucleus changes depending on the cell cycle phase (Fig. 4). Nearly one century ago, Sauer detected that nuclei in the neural tube of chick embryos oscillate according to the cell cycle and that mitosis occurs exclusively at the apical site (Sauer 1935). He named this process interkinetic nuclear migration (INM). He identified this by measuring the nucleus size according to its position within the cell. This migration could be confirmed by pulse labelling cells in S-phase with different lengths with Bromodeoxyuridine (BrdU) and H^3-thymidin (Sauer and Walker 1959). Later, this process was observed via time lapse imaging where radial glia cells undergo INM (Noctor et al. 2001). INM was mainly found in vertebrate pseudostratified epithelial tissue such as the brain and retina but is not restricted to neuronal tissue in vertebrates. It can also be observed in the *Drosophila* wing disc or *Nematostella* ectoderm (Meyer, Ikmi, and Gibson 2011). This shows that INM is a common feature of stratified tissue across the taxonomy.

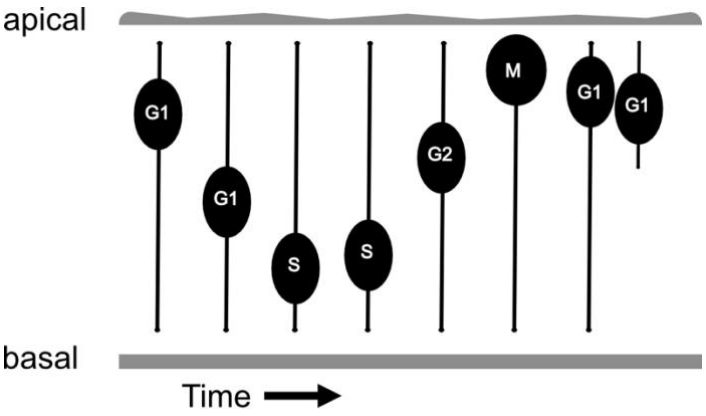

Figure 4: Illustration of interkinetic nuclear migration, displaying how nuclei migrate according to the cell cycle phases. Mitosis takes place at the apical site, whereas the other cell cycle phases are not associated to one side of the cell.

The cause behind it is still under current debate. Possibly, INM is used as a way to create space for nuclei to undergo mitosis. Very compacted cells where nuclei are all located on one side of the cell might not be able to divide at this position. Therefore, nuclei need to migrate more apically to have more room for the division (Lee and Norden 2013). Another plausible explanation could be that different markers or cell organelles are expressed at specific locations in the cells. Prominent examples are apical-basal polarity markers within a cell. In order to pass on certain markers to both daughter cells, the nuclei must migrate apically to pass on the markers to both daughter cells (Del Bene et al. 2008). This concept might explain the influence of INM on asymmetric vs. symmetric division and therefore cell fate. In the case of asymmetric division, for example, only one cell receives the apical markers and thus retains stemness, whereas the other cell is destined to differentiate due to the absence of the markers. In addition,

the centrosomes also might play an essential role. It has been shown that the centrosomes are oriented more apically in the cell in cells undergoing INM, which means that the nucleus, in order to undergo mitosis, must migrate apically to reach the centrosome (Miyata 2008).
Although the question of why INM takes place is not yet clear, many researchers are trying to understand how INM works and how the nucleus can migrate within the cell. The cytoskeleton plays an important role in the migration of the nucleus. In the cerebral cortex of mice, they identified that the migration during G2 is an active process where the nucleus migrates along microtubules via dynein (Tsai et al. 2005). In zebrafish retina, they observed by blocking myosin with blebbistatin that the apical migration was also stopped, suggesting an active role of actomyosin in INM (Norden et al. 2009). The basal migration in G1 however, is thought to be a more passive process (Kosodo et al. 2011). All in all, the cytoskeleton seems to have a high impact on the migratory process and the inhibition of certain components affect INM. It highlights that INM is very diverse and the mechanistic behind INM can change depending on the different tissue and the organism. Nevertheless, the proper regulation of INM during the cell cycle is crucial and might be a key regulator of cell fate.

1.9 Medaka as a model organism to study stem cells

The Japanese rice fish medaka (*Oryzias latipes)* is a fresh water living species which is an ideal model system to study developmental and stem cell related questions. Medaka embryogenesis is extrauterine, and both embryos and hatchlings are transparent, enabling the study of processes both during embryonic and post-embryonic development *in vivo*. Moreover, fish have the capacity for lifelong growth and therefore constantly require active adult stem cells. Embryogenesis is rapid and embryos hatch after 7 days when raised at 28°C (Iwamatsu 2004). Due to its high inbreeding capability and daily production of embryos, medaka provides a defined genetic background to study stem cells in a reproducible manner. The small genome size of 800 Mb and many already established techniques in medaka constitute the ideal experimental conditions for studying stem cells (Kirchmaier et al. 2015). Meganuclease induced transgenesis enabled to generate fluorescent transgenic lines for stem cells in medaka (Grabher and Wittbrodt 2007; Seleit, Krämer, et al. 2017). In addition, CRISPR/Cas9 has been established in medaka, which allows precise interference in the desired gene involved in the regulation of stem cells, for example (Stemmer et al. 2015). All this makes medaka the optimal model system for the study of adult stem cells.

1.10 Posterior lateral line medaka to study stem cells

Adult stem cells are the key requirement for homeostasis and post-embryonic growth. However, stem cells are not always easy to study *in vivo,* as they are usually few in number and embedded in their niches and therefore not easily accessible. The posterior lateral line in medaka is an excellent model to study stem cells as they are exposed to the surface of the skin. Hence, stem cells are easily accessible for imaging and experimental manipulation. The posterior lateral line is a sensory system in fish and amphibians which is important to help them navigate within the water, hunt prey, and swim in a swarm (Dijkgraaf 1963). It is composed of individual organs called neuromasts. Neuromasts feature clear structural composition and consists of only four different cell types: Niche, stem, progenitor, and differentiated cells (Fig 5 B). The differentiated cells are hair cells which are the sensory part of this organ. The hair cells are connected to nerves which transmit the signals allowing the fish to detect the water flow. In addition, the hair cells of the neuromasts are continuously exposed to the environment and thus, require constant replenishment. Hence, the stem cells are steadily active and can be examined under various conditions. In medaka, the hair cells can be visualised by the expression of *eyes absent 1 (eya1)* (Seleit et al. 2017).

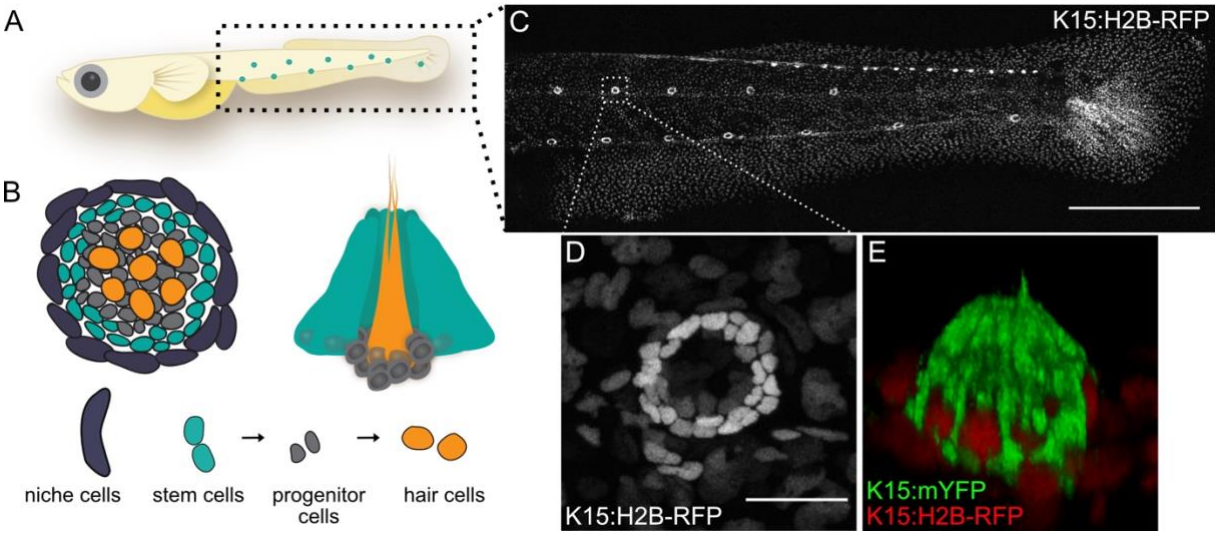

Figure 5: Posterior lateral line of medaka: (A) Scheme of a medaka hatchling showing in turquois dots the pattern of neuromasts from the posterior lateral line. (B) Schematic drawing of a neuromast, displaying the organisation of the individual cell types adapted from (Seleit, Krämer, et al. 2017, Groß et al. 2022). The niche cells (dark blue) surround the stem cells (turquois). The stem cells embed the progenitor cells (grey) and in the middle of the organ the hair cells (orange) are located. (C) Confocal image of a medaka hatchling displaying the expression of *keratin 15* in the epithelium and in the neuromast stem cells via Tg(K15:H2B-RFP). Scale bar indicates 100 µm. (D) Zoom-in of one neuromast visualised via Tg(K15:H2B-RFP). Scale bar shows 25 µm. (E) 3D reconstruction of a neuromast labelling the nuclei and the membranes of neuromast stem cells via Tg(K15:H2B-RFP) and Tg(K15:mYFP). This shows the elongated shape of neuromast stem cells, where nuclei are located basally in the cell.

The progenitor cells called support cells which are located between hair and stem cells are the pool of cells which are known to generate new hair cells upon loss (Thomas and Raible 2019). The stem cells, named mantle cells, show a distinctly elongated morphology. From a lateral view, the stem cells form a volcano-like shape where nuclei are located basally in the cell (Fig. 5 E). Due to their shape, the stem cells surround the support and hair cells. As an outer ring, the stem cells are embraced by the niche cells which are called border cells. In previous studies from our lab on the neuromast niche, it was shown that the niche originates from a different lineage than the stem cells. Newly formed neuromasts do not have niche cells but during the migration to their final position, epithelial cells are transformed and change fate to form the niche cells (Onistschenko et al. 2023; Seleit, Krämer, et al. 2017).

During development, the posterior lateral line is established by a migrating primordium which deposits clusters of cells at regular places from anterior to posterior. These first clusters of cells then migrate ventrally and form the ventral neuromasts. Cells from the ventral organ together with interneuromast cells then migrate out to the midline in order to form the secondary organs called midline neuromasts. At the end, a zigzag-like pattern of neuromasts distributed in the midline and ventral side of the fish is present (Fig. 5 A, C) (Seleit, et al. 2017). This migration is dependent on a proper expression of specific receptor and ligands which are expressed in the epithelium. Disrupting the epithelium by inducing a keratin 15 mutation in its coding sequence, our lab could show that the disorganization of the epithelium leads to malformation of the posterior lateral line pattern (Seleit et al. 2022).

Neuromasts were not able to migrate in the normal way and primary neuromasts were often stuck in the midline. Therefore, the epithelium of the tail needs to be intact to properly form the posterior lateral line.

1.11 Keratin 15 as neuromast stem cell marker

The epithelium and the neuromast stem cells are described as keratin 15 + (K15) cells (Fig. 5 C, D). Previous lineage tracing experiments in our lab have shown that the stem cells of the neuromast are the pool of cells which give rise to the entire neural lineage and that the neuromast is clonally organised. Furthermore, ablation experiments showed that these K15 + cells are the stem cells of this organ, as they were able to reconstitute the neuromast organ (Seleit, Krämer, et al. 2017). The transgenic K15 lines, generated in our lab, display homogenous expression of *k15* in the stem cells (Fig. 5 D, E).

However, proving the expression of the transgenic lines by *in situ* hybridisation revealed heterogenous expression of *k15* (Groß 2022). In preliminary results, using a destabilized

transcriptional K15 reporter, I detected heterogenous expression of *k15* in both epithelial and stem cells *in vivo*. To date, it is not known where this heterogeneity comes from and whether K15 influences stem cell regulation. In this thesis, the heterogeneity of stem cells is explored during homeostasis and the question of how K15 is involved in stem cell regulation due to different levels of *k15* expression is investigated.

2 Aims of this study

The aim of this study was to understand two things about medaka neuromast stem cells:

2.1 Understanding stem cell behaviour of neuromast stem cells

Neuromasts consist of many stem cells compared to progenitor or differentiate cells. Although, hair cells continuously need to be replaced, it is surprising that most of the cells of a neuromast are stem cells, even if they are not the direct source of hair cell replacement. So far, little is known about how these stem cells are organised within the stem cell pool. Using pulse chase labelling, I studied the proliferation of the individual stem cells to understand whether there are different pools of stem cells. Moreover, I used time lapse imaging to follow how neuromast stem cells divide *in vivo.*

2.2 The influence of Keratin 15 on neuromast stem cells

In medaka neuromast stem cells, Keratin 15 (K15) is used as a stem cell marker. In previous results, I could see that the expression of *k15* is not homogenous. Therefore, I was interested in understanding the role of K15 in neuromast stem cells to see if it affects stem cell behaviour. I generated transgenic lines to induce *k15* overexpression and *k15* mutation to understand the role of K15 in the context of gain and loss of function.

3 Results

3.1 Neuromast stem cells actively proliferate during homeostasis

Understanding how adult stem cells are regulated is essential for multicellular organisms, as these are the cells that maintain tissues during homeostasis and after injury. Thus, the regulation of adult stem cells is very dynamic and must always adapt to external conditions (Graf and Stadtfeld 2008). The neuromast stem cells (NSCs) of the posterior lateral line are constantly challenged to maintain the stem cell pool while adapting to the need for new hair cells that are constantly exposed to environmental conditions. To characterize the organisation of NSCs as well as the proliferative state of different stem cell populations I performed BrdU (Bromodeoxyuridine) label retention experiments as an indicator for proliferation activity. I used different pulse (incubation with BrdU) and chase (incubation after the pulse without BrdU) durations. During the pulse, BrdU is incorporated into the cells, which are in the S phase during this time; whereas during the chase, the fate of the stem cell can be followed. Cells that no longer divide so frequently retain the signal, whereas those that divide frequently lose the signal. 7 days post fertilised (dpf) Medaka hatchlings were treated with a 48 h BrdU pulse and a seven day-long chase. In these neuromasts, most stem cells were labelled (77%), indicating high stem cell activity within 48 h (Fig 6A and D). This reveals that most NSCs are proliferatively active and remain stem cells over the course of the 7 days. The spatial distribution of BrdU + stem cells did not show significant bias. In order to visualise possible proliferation heterogeneity among NSCs, I reduced the exposure time for BrdU to 16 h and 6 h. In that case, the average ratio of BrdU positive cells was 35% after 16 h and 22 % after 6 h (Fig. 6B, C and D). The positional analysis of BrdU+ stem cells showed no directional dependency. This indicated that actively proliferating stem cells are located throughout the organ (Fig. 6E).

The shorter BrdU pulse of 6 h resulted in 22 % of NSCs labelled and these were distributed along the outer rim of a neuromast. I wanted to use the dispersed labelling of NSCs as a proxy to study their lineage progression to infer their cell division mode; whether NSCs divide symmetrically or asymmetrically. Unfortunately, the percentage of labelled cells was still too high to unambiguously annotate clones. I then decided to change the experimental approach and incorporate a 4D analysis in stem cell behaviour *in vivo*.

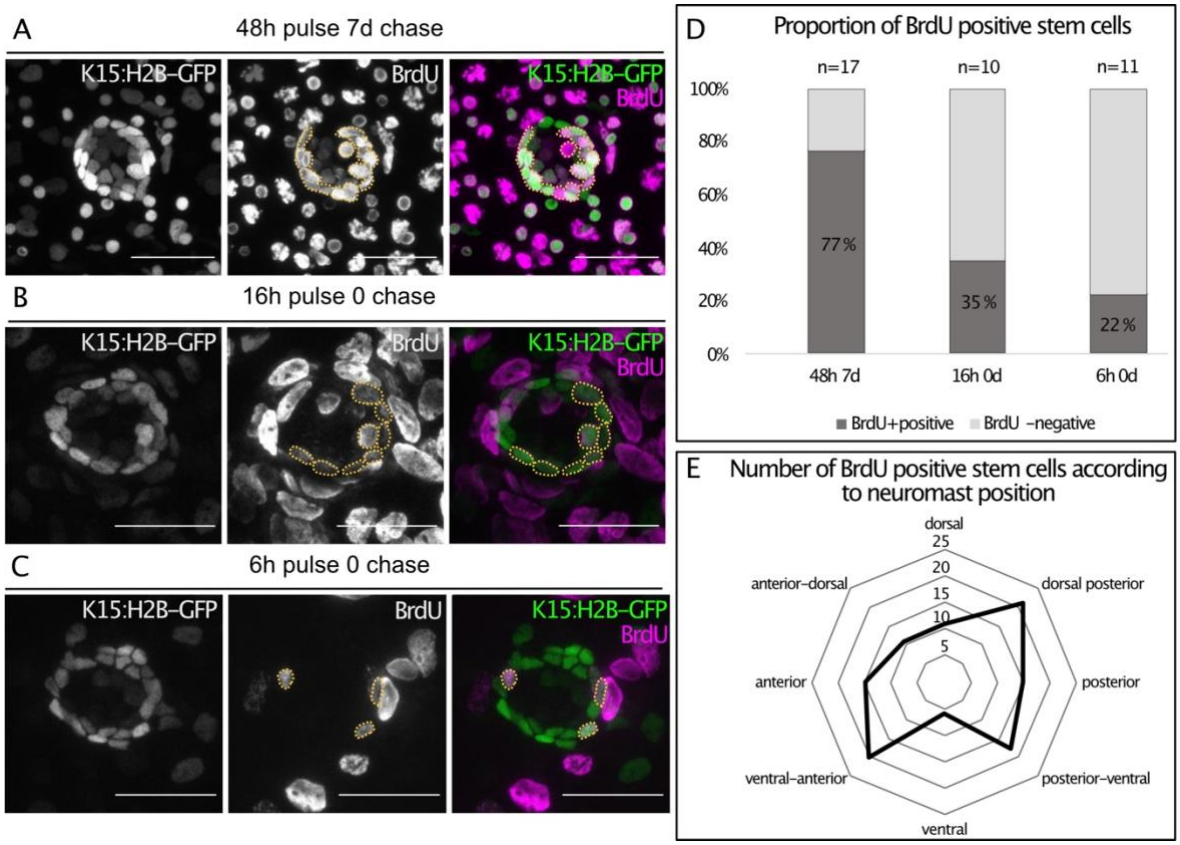

Figure 6: Proliferation activity of neuromast stem cells in homeostasis

(A-C) For all BrdU incorporation experiments 7dpf hatchlings from Tg(K15:H2B-GFP) were used and incubated for the respective times. Left, H2B-GFP + neuromast stem cells are displayed, in the middle, BrdU staining is shown and, in the right, the merge of both channels (K15:H2B-GFP in green and BrdU in magenta). Scale bar indicates 25 µm. (A) Neuromast shown after 48 h BrdU pulse and 7 d chase. (B) Neuromast after 16 h BrdU pulse and (C) after 6 h are shown. (D) Bar plot displays the proportions of BrdU + stem cells in comparison to all stem cells per neuromast in percentage after the different BrdU pulses. For 48h BrdU pulse and 7 d chase, 17 neuromasts from 3 hatchlings were analysed (317/ 412 BrdU+ neuromast stem cells). For 16 h BrdU pulse, 10 neuromasts from 2 hatchlings were analysed (74/210 BrdU+ stem cells) and for 6 h BrdU pulse, 11 neuromasts from 2 hatchlings were measured (40/177 BrdU+ stem cells) (E) Analysis of proliferation according to position within the neuromast from 16 h and 6 h BrdU pulse. The grid lines show how often BrdU+ stem cells were found at the specific positions.

Tracking stem cell proliferation by using BrdU staining only showed a snapshot of the cells that were in S phase during this period of the pulse, but it is not possible to interfere with their proliferation behaviour *in vivo*.

Medaka neuromasts are very exposed to the surface of the skin and are therefore easily accessible for live imaging. In addition, medaka embryos are quite resistant for time-lapse imaging over several hours. This allowed me to perform time-lapse imaging of 7 dpf Tg(K15:H2B-FP) medaka hatchlings visualising the nuclei of neuromast stem cells to understand the behaviour of stem cell *in vivo.* Imaging was performed every 15 min over a period of approximately 18 h. Nuclei in mitosis were clearly identifiable by the condensation

of chromosomes, followed by a division into two separate nuclei (Fig. 7A, A´). In wildtype neuromasts, I observed that roughly three individual stem cells divided per neuromast (mean= 2,66) (Fig. 7B) over the 18 h period. The divisions of the NSCs took place sequentially and in non-neighbouring cells. Additionally, I quantified the position of stem cells undergoing mitosis which revealed a tendency for stem cells to divide more frequently at the anterior side of the neuromast.

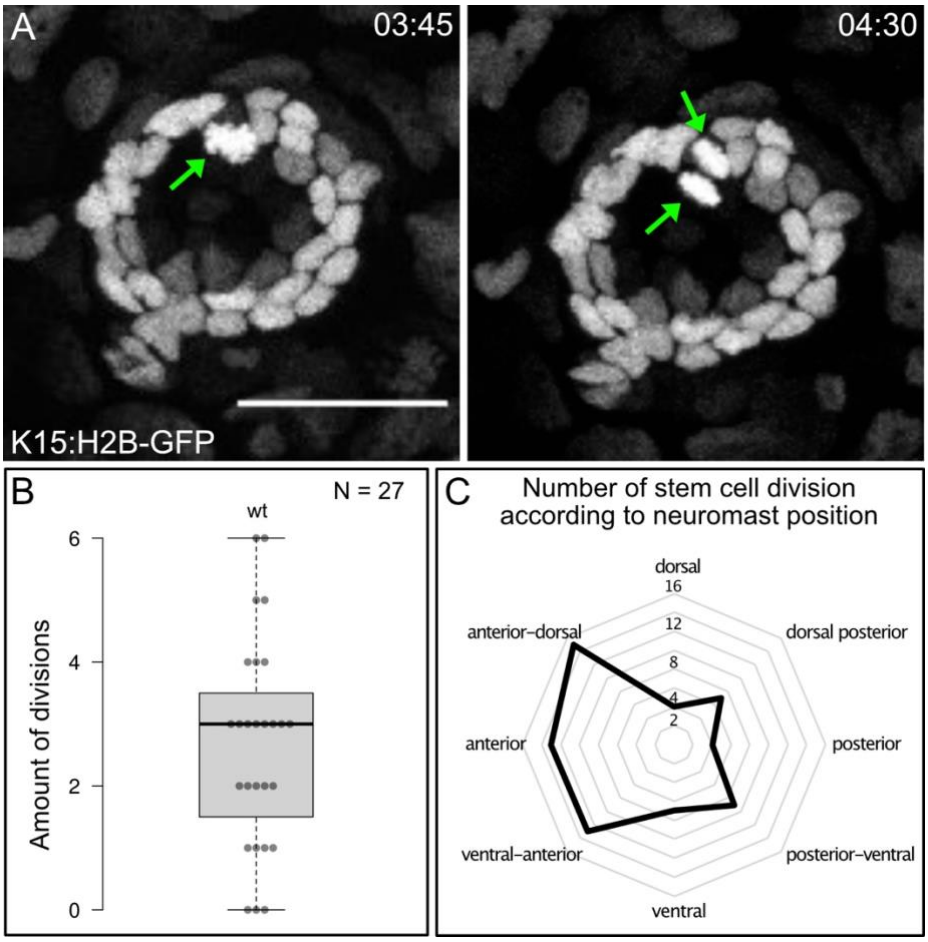

Figure 7: Active proliferation of neuromast stem cells *in vivo*

(A) Neuromast showing H2B-GFP+ neuromast stem cell nuclei in Tg(K15:H2B-GFP) from a timelapse movie. Neuromasts were imaged every 15 min over 18 h. At 03:45 h one nucleus is highly condensed suggesting mitosis, indicated by a green arrow. At 4:30 this nucleus has divided into two, indicated by two green arrows. Scale bar shows 25 µm. (B) Boxplot is showing the number of stem cell divisions within 18 h of imaging. In total 27 neuromasts from 6 embryos were imaged. 72 stem cell divisions could be observed. (C) Analysis of stem cell proliferation according to position within in the neuromast via time lapse imaging. The grid lines show how many stem cells have divided at the specific positions.

When comparing the *in vivo* 4D data to the BrdU pulses, it immediately became clear that the number of NSCs that actually underdo mitosis within 18 h is lower than the number of NSCs actively undergoing S-phase within a similar time frame (Mitosis: 12.6 %; BrdU: 35 %). In contrast to the homogenously distributed BrdU + stem cells previously described in the pulse chase experiments, the actual location of stem cells undergoing mitosis seems to be biased towards the anterior side of the neuromasts.

These results indicated that stem cells that have already copied their DNA content do not necessarily proceed directly into mitosis and that the actual division takes place preferentially anteriorly within the neuromast.

3.2 Neuromast stem cells oscillate according to the cell cycle

When looking at the general disposition of stem cells within the neuromast in a lateral cross section, I found that the majority of stem cell nuclei are located basally in the cell (Fig. 8A-A´´´). Occasionally I found nuclei that were displaced more apically (Fig. 8 B-B´´´). Until now it was not clear why the nuclei are arranged differently within the NSCs.

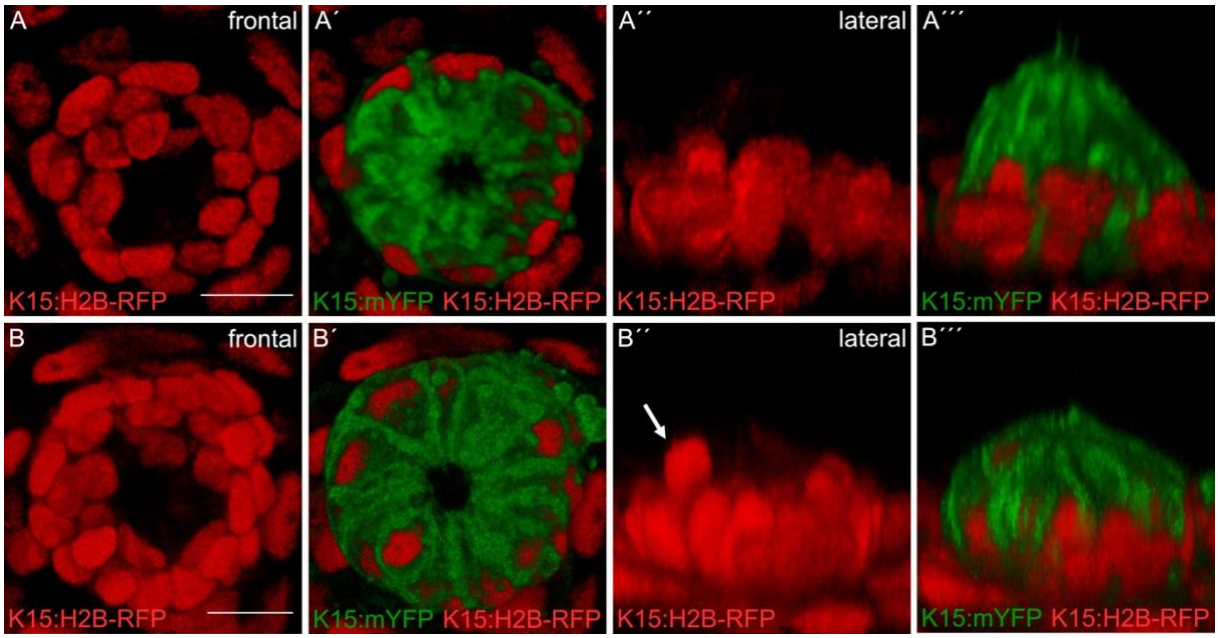

Figure 8: Variable positioning of NSC nuclei

3D reconstruction of H2B-RFP+ nuclei from Tg(K15:H2B-RFP) together with membrane-YFP from Tg(K15:mYFP) showing the localisation of nuclei within NSCs. (A) Frontal view of H2B-RFP expression shown in red. Scale bar indicates 10 µm. (A´) shows the merge of H2B-RFP+ and membrane-YFP in green from the frontal view. (A´´) shows the lateral view of H2B-RFP+ nuclei and (A´´´) displays the merge of H2B-RFP+ and membrane-YFP in the lateral view. Nuclei are uniformly localised at the basal site of NSCs. (B-B´´´) shows another neuromast with similar description as in (A-A´´´), but displaying variable positioning of NSC nuclei, highlighted with a white arrow in (B´´).

Following the individual nuclei in 4D imaging, I was able to follow the migration of nuclei in NSCs. I observed how individual stem cell nuclei migrated more apically, underwent mitosis, and then migrated back basally (Fig. 9) by live imaging H2B-GFP+ NSCs from Tg(K15:H2B-GFP). As soon as the nucleus had moved upwards, it took about 1 hour until the condensation of the chromosomes could be seen. The actual division into two nuclei then only took about 30 minutes (Fig 9B). In contrast, the downward migration of the nuclei was less organised in terms of time, and often one nucleus was down faster than the other. This indicates that NSCs oscillate according to the cell cycle, where mitosis usually occurs at a more apical plane compared to all other cell cycle phases. By analysing 54 divisions I found that in 81 % (apical: 44, basal: 10) nuclear division occurred apically. This process is known as interkinetic nuclear migration (INM).

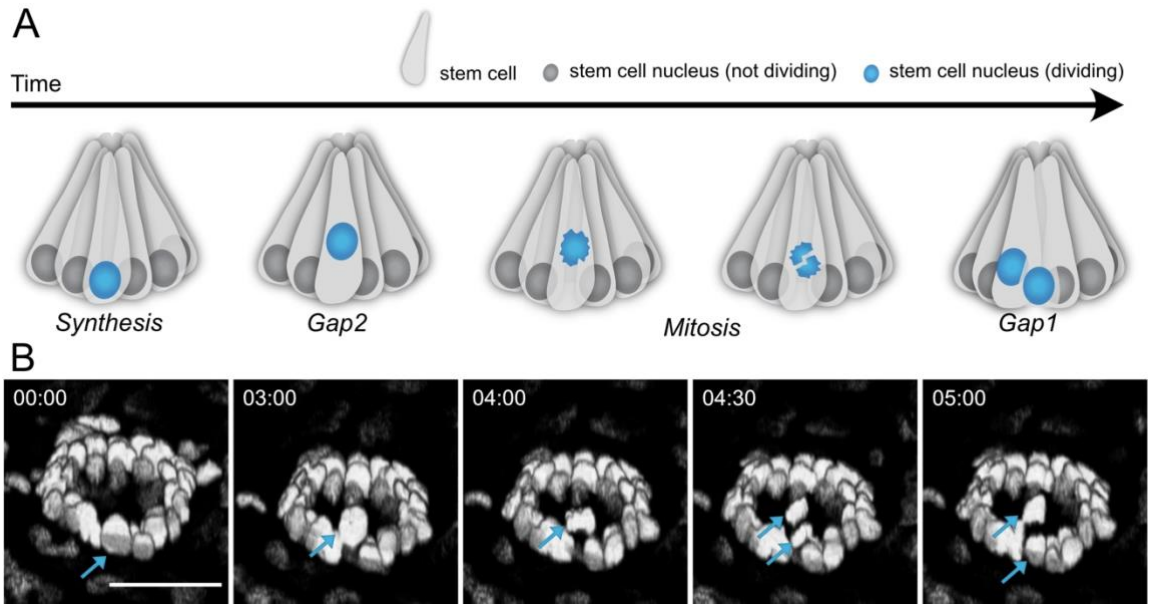

Figure 9: Neuromast stem cells undergo interkinetic nuclear migration

(A) Schematic illustration of a 3D drawn neuromast displaying interkinetic nuclear migration progressing through the cell cycle. In Gap 2 nucleus migrates up, condensation and division happen in mitosis and downwards migration in Gap1. (B) 3D reconstruction of H2B-GFP+ neuromast stem cell nuclei from Tg(K15:H2B-GFP). Depicted timepoints show the distinct cell cycle phases as previously described. Blue arrows highlight the dividing stem cell nuclei. Scale bar indicates 25 µm.

3.3 Apical positioning of centrosome

From previous studies on the cause of INM, it was proposed that centrosomes are one reason for nuclei to migrate apically (Miyata 2008). Centrosomes are the microtubule organisation centres which are essential for chromosomal segregation during mitosis. γ-tubulin localises at centrosomes since they are required for the microtubule nucleation of the centrosomes (Hoffmann 2021). If centrosomes are located apically within a cell, nuclei need to migrate to the centrosomes to properly divide during mitosis. To test this hypothesis, I utilised γ-tubulin to visualise the localisation of centrosomes within neuromasts. Antibody staining against γ-tubulin revealed that the centrosomes are indeed located more apically within the cell (Fig. 10A, A′, A′′). At the position of nuclei, no γ-tubulin-expression was detected (Fig. 10B, B′, B′′). The lateral view of the neuromast showed the local separation of nuclei and centrosomes (Fig. 10C, C′, C′′). Since neuromasts are highly compacted with cells, it was difficult to judge which centrosome belongs to which cell. Therefore, I designed a construct to drive a γ-tubulin-mCherry fusion under the *K15* promotor to ensure expression in the neuromast stem cells. I injected this into the Tg(K15:H2B-GFP) to visualise the stem cell nuclei. In the injected generation, I was able to see partial expression of γ-tubulin *in vivo* also more apical compared to the stem cell nuclei (Fig. 10D, D′, D′′). Unfortunately, the imaging of the centrosomes could only be carried out for a short period of time, as the signal would otherwise be bleached out. Therefore, no time-lapse imaging could be performed to follow the process of cell division and migration of the nuclei to the centrosomes *in vivo*.

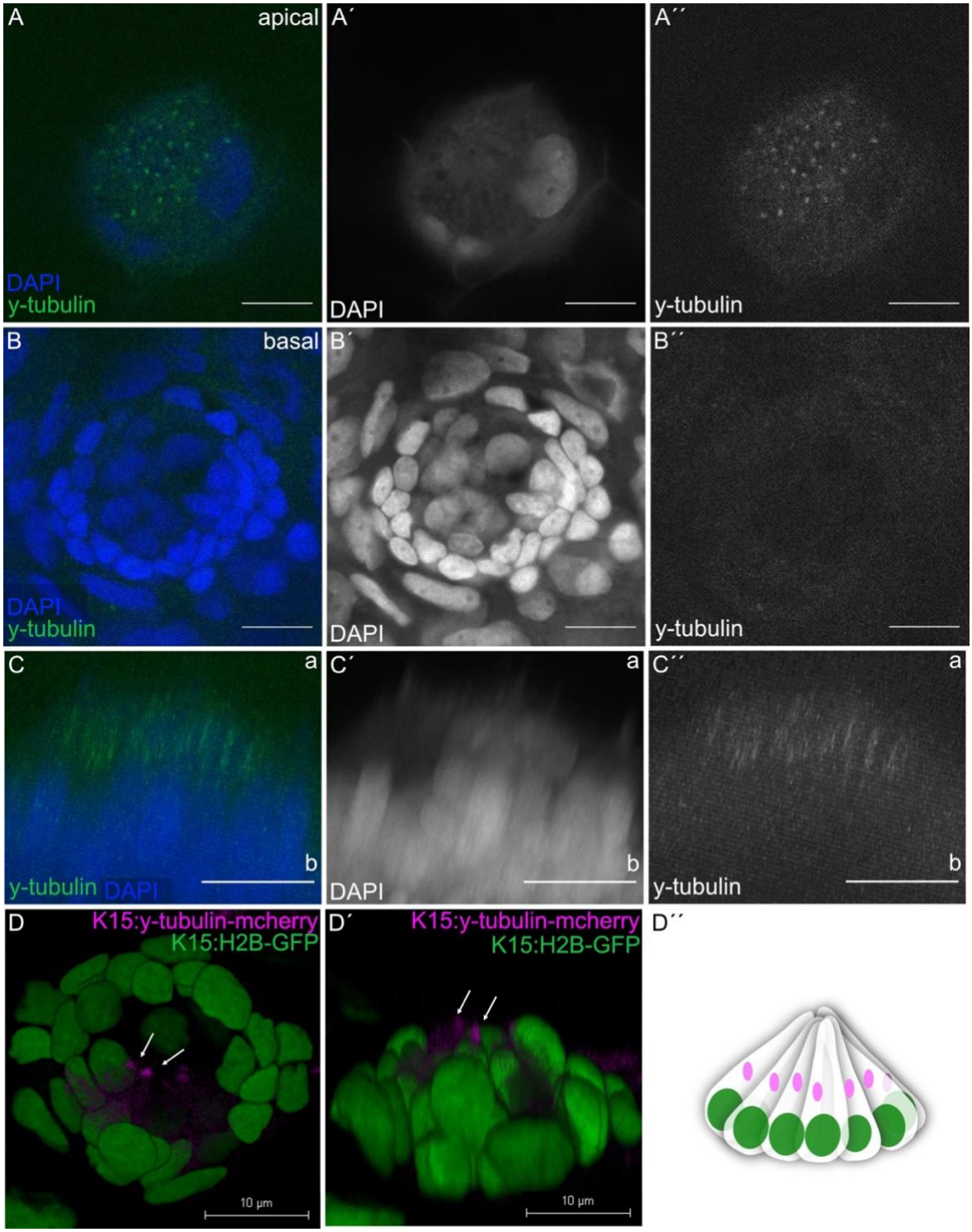

Figure 10: Apical localisation of centrosome in neuromast stem cells

(A-C) Neuromast from a 7 dpf hatchling stained against γ-tubulin was imaged at different positions to localise centrosomes (γ-tubulin in green, DAPI in blue). (A-A´´) Neuromast imaged at apical position, (B-B´´) represented at a lower plane. (C-C´´) Lateral view of the neuromast, highlighting the position of centrosomes at the apical site of the cell. Apical (a) and basal (b) gives the orientation of the neuromast. (D-D´) 3D reconstruction of H2B-GFP+ neuromast stem cell nuclei from Tg(K15:H2B-GFP) injected with a γ-tubulin-mcherry fusion under the *K15* promotor. Partial γ-tubulin-mCherry expression (magenta), showing apical localisation of centrosomes indicated by white arrows. Scale bar indicates 10 µm. (D´´) Schematic representation of a neuromast, highlighting the position of stem cell nuclei and centrosomes.

3.4 The stem cell marker K15 is heterogeneously expressed in neuromast stem cells

Using K15 as a marker for the NSCs, we have generated stable transgenic lines to follow neuromast stem cell behaviour. The Tg(K15:H2B-RFP) displays a very strong and homogenous expression in epithelial cells and in neuromast stem cells (Fig. 11C, C′). To validate the expression pattern of our Tg(K15:H2B-FP), *in situ* hybridisation against *k15* mRNA was performed. As indicated by the transgenic line, *in situ* hybridisation showed that *k15* is expressed in epithelial cells and in neuromast stem cells. However, the expression seemed to be more heterogenous compared to the stable transgenic line. To further examine this, a classical RNA *in situ* hybridisation and a hybridisation chain reaction (HCR) RNA *in situ* hybridisation against *k15* was performed. In order to be able to distinguish *k15* levels between cells, I used HCR. In both *in situ* hybridisation techniques, I could see strong expression of *k15* in the epithelium and a rather weak and heterogenous expression in the neuromast (Fig. 11A, B, B′). In the HCR it was even clearer that neuromast stem cells express *k15* at a low level, while the expression in some areas of the neuromast appeared to be more intense than in others (Fig. 11 A). In summary, *in situ* hybridisation against *k15* showed that on the one hand the transgenic line for K15 is representing the same expression pattern, and on the other hand, that *k15* expression varies in the intensity among individual epithelial and neuromasts cells. Since fluorescent proteins with nuclear localization are known to be very stable, these reporters are not well suited to study dynamic changes that occur faster than the half-life of the reporter protein (Li et al. 1998).

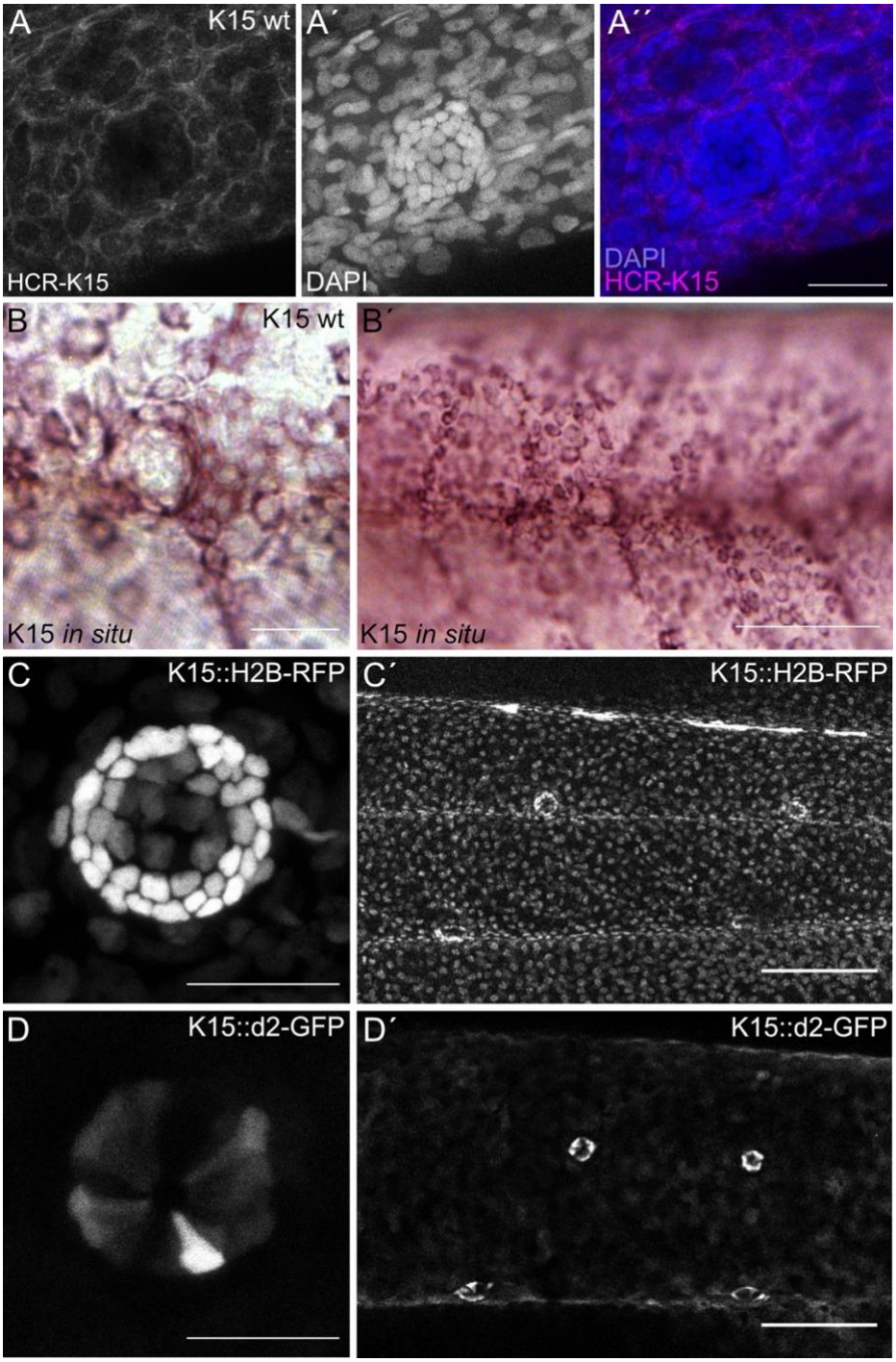

Figure 11: Heterogenous expression of Keratin 15 in epithelial and neuromast stem cells:
7 dpf hatchlings were used for all *in situ* hybridisations. (A-A´´) Detection of *K15* mRNA by hybridisation chain reaction (HCR) RNA *in situ* hybridisation with the fluorophore 647 showing in (A) *K15* mRNA expression in a neuromast, in (A´) the DAPI channel and in (A´´) the merge of both channels (DAPI in blue and K15 mRNA in magenta). (B-B´) Displaying the *K15* mRNA expression detected by *in situ* hybridisation with NBT/BCIP. (B) shows a zoom in of a neuromast, scale bar of 25 µm. (B´) shows the K15 mRNA expression in the tail region of the embryos, scale bar is 100 µm. (C-C´) Depiction of H2B-RFP+ neuromast stem cells of the Tg(K15:H2B-RFP) showing in (C) a zoom in of a neuromast, scale bar is 25 µm. (C´) shows a depiction of the tail of the embryo, scale bar 100 µm. (D- D´) Image of the same embryo from (C) depicting the GFP+ neuromast stem cells of the Tg(K15:d2GFP), showing the destabilised expression of *K15.* In (D) zoom in of the neuromast, scale bar 25 µm and in (D`) image of the tail, scale bar 100 µm.

To overcome this issue of stability due to nuclei localisation in the transgenic line, I made use of a previously generated transgenic line from the lab, driving a destabilised GFP under the *K15* promotor to have a less stable fluorescent protein, mimicking actual *k15* expression. Imaging this destabilised transgenic line showed that the expression of *k15* is heterogenous and more similar to what I saw in the *in-situ* hybridisation (Fig. 11D, D´). Both in the epithelium and in the neuromast, I detected patchy expression of *k15*. Some neuromast stem cells showed only weak GFP expression, whereas other where strongly GFP-positive (Fig. 11D). This indicates that the *K15* promotor is not always active and *k15* is dynamically expressed.

3.5 Endogenous tagging of K15

To further understand the basis of heterogenous *k15* expression in neuromasts *in vivo,* I endogenously tagged K15 using CRISPR/Cas9 by inducing homologous directed repair (Seleit, Aulehla, and Paix 2021). To do so, I generated different GFP donor constructs with homologous overhangs compatible with the K15 locus, together with different sgRNA to induce homologous directed repair and integrate the GFP into the region of interest (N- terminal and C- terminal). 898 embryos were injected at one-cell stage and screened for GFP expression. Only few embryos showed GFP positive cells in the enveloping layer and some in the skin (GFP+ = 72/898)

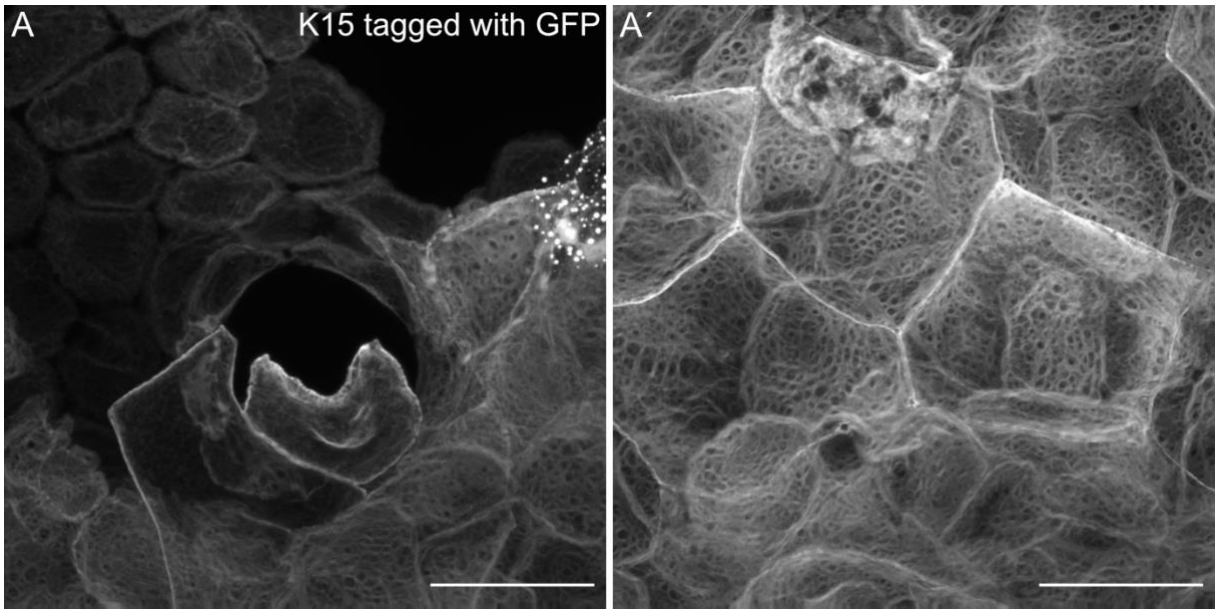

Figure 12: K15 localisation in epithelial cells displaying the fin network of K15
K15 expression in skin epithelial cells detected by endogenous N-terminal tagging of the K15 open reading frame with GFP. (A) Depicting *K15* expression in epithelial cells surrounding a neuromast. (A´) Epithelial cells, displaying the fine network of K15 throughout a cell. Scale bar indicates 25 µm.

Table 1: Quantification of injected embryos for the endogenous tag of K15

	Injected embryos	GFP+ positive
C-terminal tagging	589	17
N-terminal tagging	309	55
Total	898	72

In these injected embryos, a fine network of GFP expression was observed that is compatible with the structure of the intermediate filaments. This indicated successful endogenous labelling of K15. I was also able to hit epithelial cells surrounding the neuromast, but I never succeeded in obtaining GFP expression within NSCs (Fig. 12). GFP-positive embryos often showed severe developmental abnormalities and did not make it to the hatchling stage. Only those with very weak expression, mostly in the enveloping layer hatched but never carried the integration in the germ line (14/898). Hence, no transgenic line could be established. The overall low number of GFP-positive cells and the absence of GFP -positive cells in the neuromast indicated the difficulty to label K15 *in vivo*. The death of most GFP positive embryos further emphasised that functional *K15* expression appears to be critical for the progression of embryonic development. In an alternative approach, I designed a construct in which the K15 coding sequence is tagged via a flexilinker to GFP under the *K15* promotor. Also here, all GFP positive embryos had issues in development and did not hatch. Therefore, direct fusions and endogenous tagging of K15 in medaka was not feasible, pointing towards functional relevance of K15 in medaka development.

3.6 K15 expression is upregulated during G2-M phase in NSCs

The assessment of the different K15 transgenic lines and the *in-situ* hybridisations have shown that the promotor of *K15* was heterogeneously active. To understand if this heterogeneity is functionally relevant for neuromast stem cells, I analysed the Tg(K15:d2-GFP) line over time and tracked changes in GFP expression. I performed time lapse imaging using a double transgenic, Tg(K15:H2B-RFP) and Tg(K15:d2GFP) to follow the promotor activity estimated by detection of destabilised GFP and at the same time tracking the migration and condensation of NSCs which undergo mitosis. I observed that the GFP expression in neuromast stem cells changed over time during the cell cycle. I detected that some stem cells started to express GFP strongly during mitosis (Fig. 13B, 2:00). I tracked the process of INM in the stem cells via the Tg(K15:H2B-RFP) and during the upwards migration of a mitotic active cell, GFP expression was highly upregulated (Fig. 13).

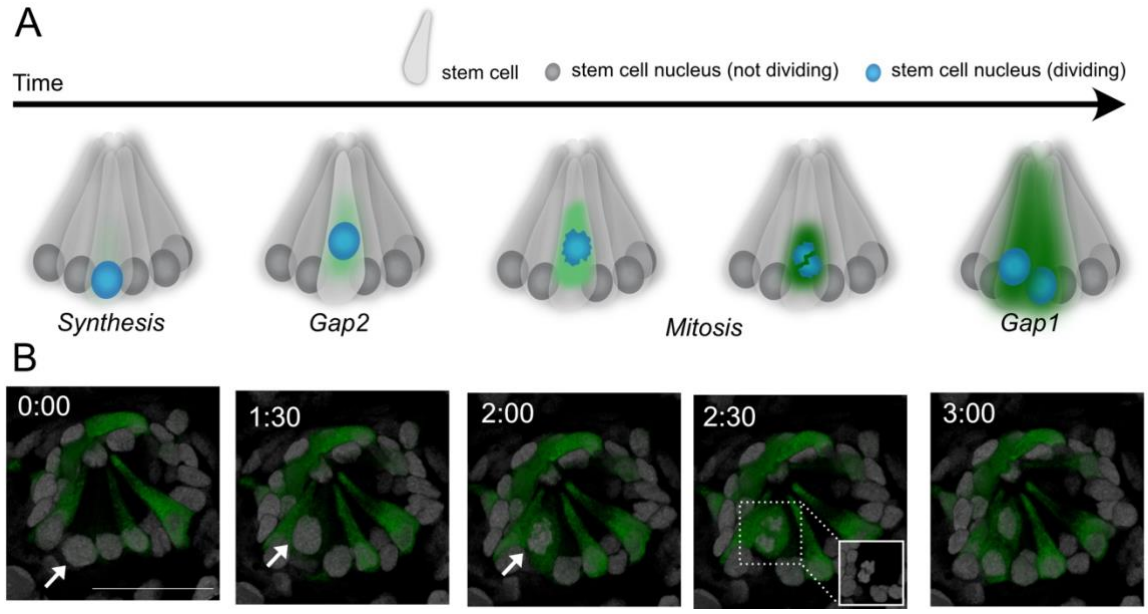

Figure 13: Dynamic expression of K15 during the cell cycle in neuromast stem cells:
(A) Schematic illustration of a 3D drawn neuromast displaying interkinetic nuclear migration progressing through the cell cycle together with *K15* expression in green. (B) 3D reconstruction of H2B-RFP+ neuromast stem cell nuclei from Tg(K15:H2B-RFP) and GFP+ cells from Tg(K15:d2-GFP). Depicted timepoints show key moments of cell cycle phases. In Gap 2, the nucleus migrates up, condensation, division and upregulation of *K15* expression happen in mitosis and downwards migration in Gap1. Scale bar indicates 25 µm.

Once division finished, both daughter cells migrated basally but retained strong GFP signal. Over the 18 h of imaging, I never saw the GFP expression reducing to levels before mitosis in 4 hatchlings. With the tools available to me, I cannot distinguish between correlation or causality of K15 levels and cell cycle stage. Therefore, I have started to develop genetic tools to investigate this aspect.

3.7 K15 overexpression decreases neuromast stem cell proliferation

To figure out whether the expression of *k15* plays a role during cell cycle in neuromast stem cells, I focussed on gain- and loss-of-function experiments. Seeing that *k15* was upregulated during the cell cycle, I tested how neuromast stem cells behave in a K15 gain-of-function paradigm. Therefore, I designed a construct containing the coding sequence of K15, driven by the *K15* promotor. To prevent the fusion of the K15 and GFP proteins, I chose a T2A linker sequence to separate GFP from K15 to be able to follow its expression *in vivo* (Fig 14A) (Liu, Chen et al. 2017). Together with Africa Temporal, a student from the Molecular Biosciences Master Program who worked under my supervision for 8 weeks, we injected this construct into

medaka wildtype embryos. In the injected embryos, I saw strong GFP expression across the body of the embryo, including NSCs. These embryos were then used to generate a transgenic line. Both, the injected and incrossed founder embryos did not show any phenotypes regarding the positioning and amount of neuromasts (Fig. 14C).

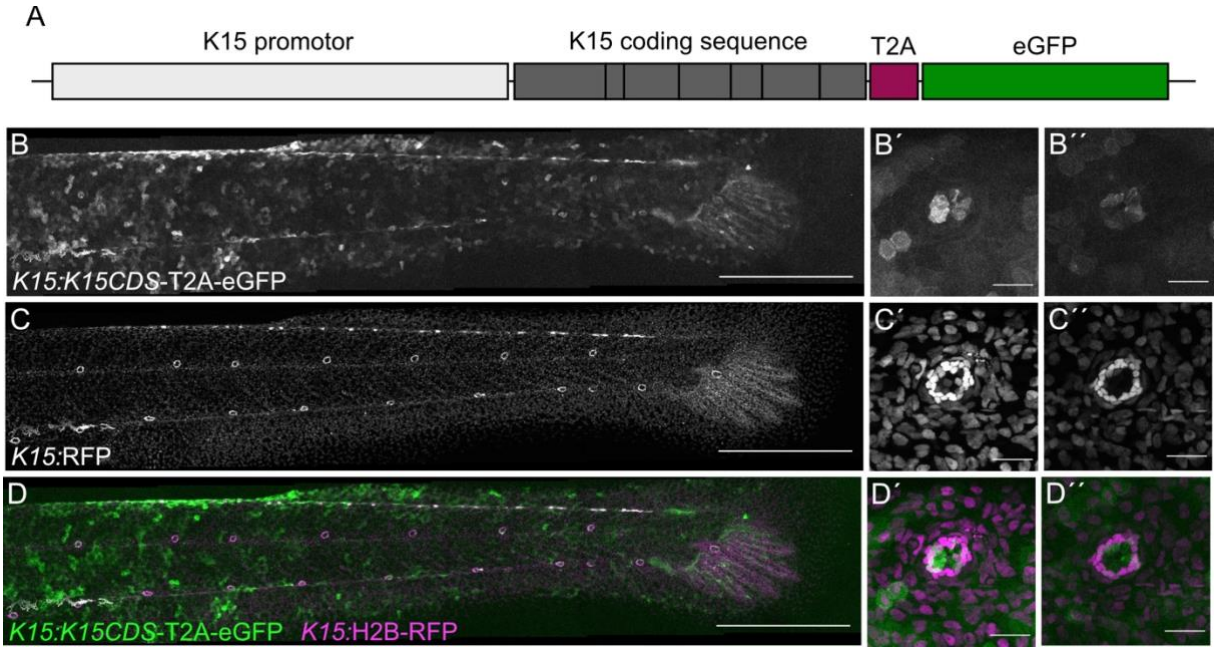

Figure 14: Generation of K15 overexpression

(A) Illustration of the K15 overexpression construct, consisting of the *K15* promotor driving the K15 coding sequence which is linked via a T2A sequence to a GFP. (B-D) 7 dpf Hatchling showing the double expression of GFP from Tg(K15:K15CDS-T2A-eGFP) and H2B-RFP expression from Tg(K15:H2B-RFP) in epithelial cells and neuromast stem cells. (B) Shows the tail of the hatchling expressing GFP by Tg(K15:K15CDS-T2A-eGFP), scale bar displays 500 µm. (B´, B´´) show zoom ins into two neuromasts depicting the differential *K15* overexpression of the individual neuromast stem cells. Scale bar 25 µm. (C, C´, C´´) Shows H2B-RFP+ of the same neuromasts with Tg(K15:H2B-RFP) to visualise the neuromast stem cells. (D, D´, D´´) Displaying the merge of both channels, having the Tg(K15:K15CDS-T2A-eGFP) in green and the Tg(K15:H2B-RFP) in magenta.

However, the embryos showed heterogenous GFP expression. In I-SceI-mediated transgenesis, the DNA donor constructs are integrated into the genome at random positions, whereby several copies can also be integrated (Grabher and Wittbrodt 2007). By breeding all GFP+ embryos, I therefore obtained different alleles with different expression. In order to have a more stable expression across the individual embryos, I performed *in-situ* hybridisations against the different crosses of fish. I selected one founder fish, giving the strongest and most stable expression of GFP and outcrossed these (Fig. 14B, B´, B´´). To confirm an increase of *k15* expression in the transgenic line, I used HCR *in-situ* hybridisation to check the expression levels of *k15* and compared those to wildtype samples. I measured the integrated intensity of the HCR channel by using the sum of the pixel values in the neuromast (RawInDen) and normalised it

by the integrated intensity of DAPI. This showed that I have higher *k15* expression levels in neuromasts from the Tg(K15:K15-T2A-EGFP) compared to wildtype (Fig. 15A, A´, A´´) (K15 wt RawInDen mean = 0,206645888; K15 oe RawInDen mean = 0,3467457).

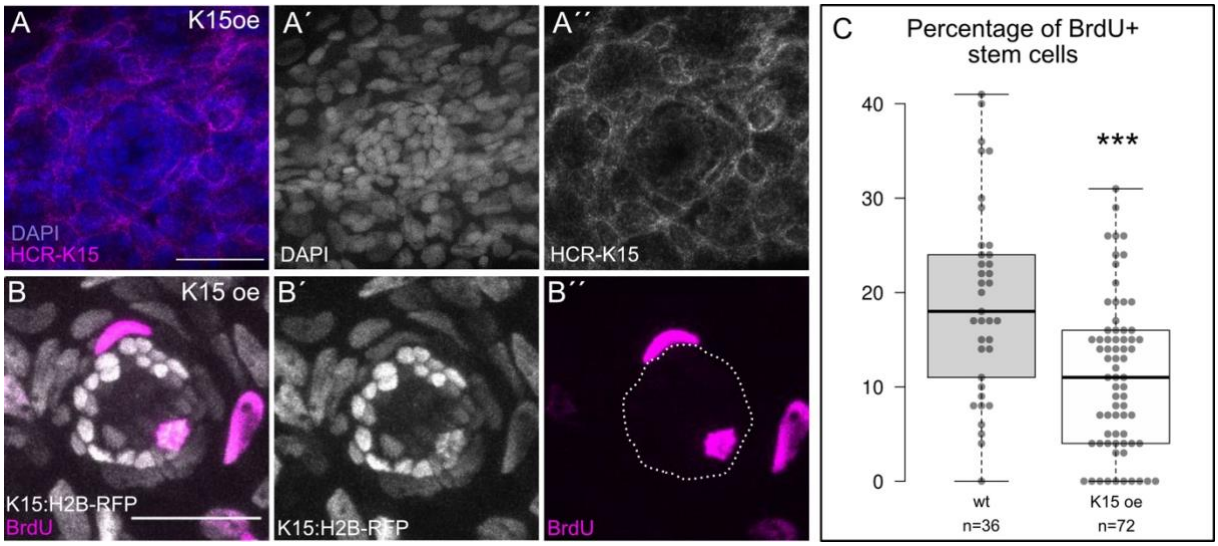

Figure 15: Reduced proliferation in K15 oe shown by BrdU incorporation
(A) Detection of *K15* mRNA by hybridisation chain reaction (HCR) RNA *in situ* hybridisation with the fluorophore 647 in a 7dpf K15 oe hatchling, showing the *K15* mRNA expression in magenta and DAPI in blue in a neuromast. Scale bar indicates 25 µm. (A´) Split of the same neuromast in the DAPI channel. (A´´) Split of the same neuromast showing *K15* mRNA expression. (B) Neuromast showing BrdU + cells after BrdU incorporation assay of a 6 h BrdU pulse in a 7 dpf K15 oe hatchling, displaying BrdU in magenta and the H2B-RFP+ neuromast stem cells in grey by Tg(*K15*:H2B-RFP). Scale bar shows 25 µm. (B´) Shows H2B-RFP+ neuromast stem cells in Tg(*K15*:H2B-RFP) and (B´´) the BrdU incorporated cells. Dotted line indicates the boundaries of the neuromast to show which BrdU + cells belong to the neuromast. (C) Boxplot is showing the percentage of how many stem cells were BrdU + after a 6 h BrdU pulse comparing wildtype to K15 oe (t-test = 0,0001).

To understand which effect a higher level of *k15* expression has on the stem cells, I first performed BrdU staining's to assess the proliferation activity. I used the same 6 h BrdU pulse as previously described in the wildtypes (wt) to compare the proliferation rate of K15 overexpression (K15 oe) and wt. This revealed that stem cells from the K15 oe proliferated less than the wt. In the wt, 19 % of the NSCs were in S-phase during this 6 h pulse (analysed neuromasts n=36; amount of embryos N=6). In the K15 oe, only 11 % were proliferatively active (n= 72; N=10). This showed a significant decrease in proliferation in the K15 oe compared to the wt, indicating that K15 oe alters the proliferation of NSCs (Fig. 15B, C). Time-lapse imaging of K15 oe neuromasts using the same conditions as in previous experiments with wt neuromasts (every 15 min for up to 18 h) confirmed that stem cell proliferation in K15 oe is reduced in contrast to the wt (Fig. 16A) (analysed neuromasts n=30; amount of embryos N=7, amount of division D= 45). K15 oe neuromast stem cells also showed defects in cell division. In 9 % of the divisions (4/45), I observed that the nuclei migrated up to start mitosis, condensed,

but then failed to divide. In cases where nuclei failed to divide, already separated nuclei came together again and collapsed, leading to cell death (Fig. 16B). Such failure in division was never observed in the wt (0/72). In addition, I quantified the apical migration of stem cell nuclei in the K15 oe. In 55 % of the analysed neuromasts, I found nuclear division occurring apically (apical: 26, basal: 21). In the wt, apical migration occurred in 81 % (apical: 44, basal: 10) of divisions. This showed that the migration during the cell cycle is significantly affected in K15 oe (p=0.006). These phenotypes of reduced proliferation, problems during division, and altered INM in the K15 oe indicated that the proper regulation of K15 is of great importance.

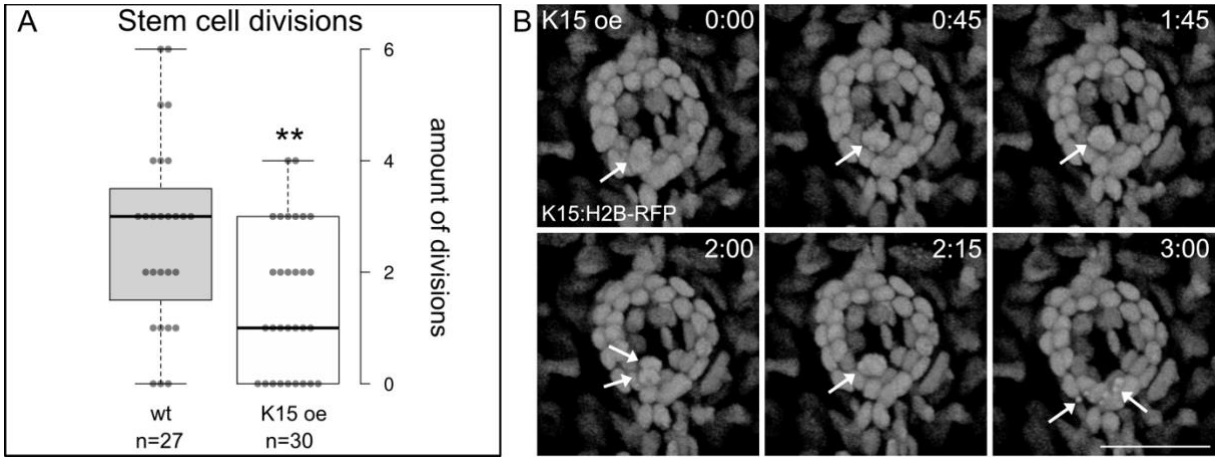

Figure 16: K15 overexpression negatively affects stem cell proliferation
(A) Boxplot showing the neuromast stem cell divisions detected by live imaging comparing the amount of division of wildtype to K15 oe (t-test = 0.0048). (B) 3D reconstruction of H2B-RFP+ neuromast stem cells from Tg(K15:H2B-RFP) of K15 oe displaying failure in division. At 0:00, nucleus is migrating up and from 0:45 onwards it is trying to divide. At 2:00, already two separated nuclei can be seen which then come back together at 2:15. At 3:00 this nucleus collapses fully, seen by small speckles, indicated by white arrows. Scale bar shows 25 μm.

3.8 K15 mutants display increase in neuromast stem cell proliferation

The gain-of-function analysis of K15 indicated that K15 affects the proliferation of stem cells. To better understand the role of K15 in NSCs, K15 mutants were generated by using CRISPR/Cas9 injecting two guide RNAs targeting exon 3. Previously, the lab had generated homozygous K15 mutant lines which were phenotypically characterised by defective neuromast positioning. They exhibited a disruption of the typical zig-zag pattern of the neuromasts, as many neuromasts remained stuck in the midline. Therefore, this phenotype was named stuck in the midline (SIML) (Seleit et al. 2022). However, this transgenic line was lost after a couple of generations. Therefore, I generated a new transgenic mutant K15 line (K15

mut), having two base pair insertions and one base pair change at one of the guide RNA sites, resulting in a premature stop codon (Fig. 17A). In these homozygous K15 mutants, I observed in 50 % of the cases the SIML phenotype (Fig. 17B, C). Ventral neuromasts have failed to migrate ventrally during development due to a disruption in the epithelium and consequently more neuromast are placed in the midline (Seleit et al. 2022).

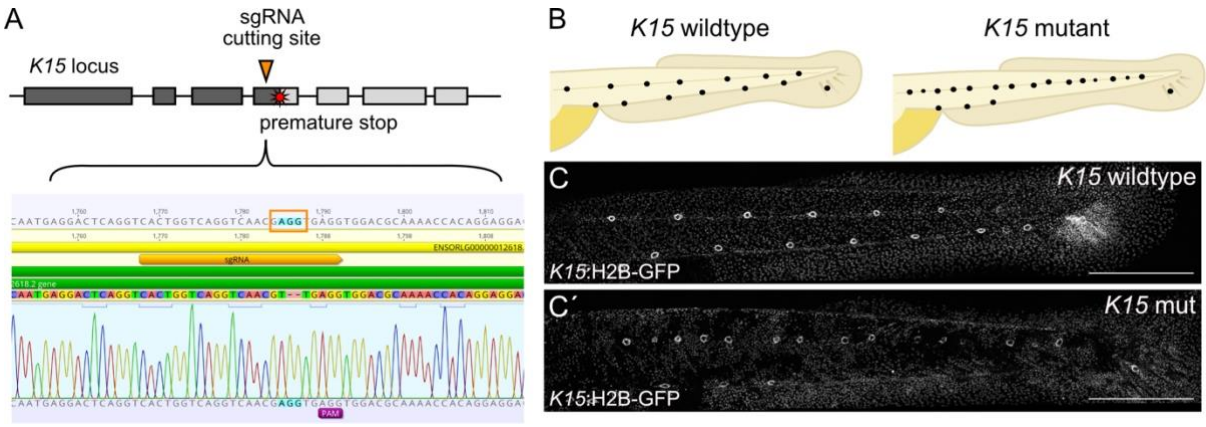

Figure 17: Generation of K15 mutants via CRISPR/cas9
(A) Representation of how the K15 mutant was generated. In the upper panel a scheme of the K15 locus with the corresponding sgRNA cutting site and the indication of the premature stop. In the lower panel, sequencing results of K15 mutants showing a two base pair insertion and a one base pair change from a T to A induced by the sgRNA. (B) Schematic drawings from the tail of hatchlings representing the neuromast positioning of K15 mutants and wildtypes. (C) Neuromast pattern of K15 wildtype showing H2B-GFP+ epithelial and neuromast stem cells by Tg(K15:H2B-GFP) displaying the normal distribution of neuromasts. (C´) Neuromast pattern of K15 mutants visualised H2B-GFP+ epithelial and neuromast stem cells from Tg(K15:H2B-GFP), showing an abnormal pattering of neuromast.

This phenotype of disorganization in the epithelium, however, could also be seen in the other 50% K15 mut without SIML phenotype. Via genotyping, I proved that all embryos with or without SIML phenotype were homozygous mutants. Moreover, many neuromasts in the K15 mut exhibited abnormal shapes. In the wt, neuromast stem cells were tightly organised in a ring-like shape (Fig. 11C). In the K15 mut, neuromasts were elongated and the stem cells were less organised as in the wt. Other neuromasts were underdeveloped only consisting out of clusters of K15 positive cells (Fig. 19A-A´´´). To prove that my generated K15 mut line was indeed a mutant for K15, I checked the *k15* expression in K15 mut by performing HCR *in situ* hybridisation. Compared to the wt, K15 mut showed reduced to no *k15* expression, proving that this K15 mutation is affecting the production of *k15* mRNA (Fig. 18A, A´, A´´). In the wildtype, I observed a strong expression of K15 in the epithelium (Fig 11A), whereas in the K15 mutants only few speckles were visible (Fig 18A-A´´). This confirmed that in the K15 mutants, *k15* expression is strongly reduced. To investigate how this altered *k15* expression impacted the

stem cell proliferation, I performed a BrdU staining as described before using a 6 h BrdU pulse of 7 dpf hatchlings. This revealed that stem cells are significantly over proliferating in comparison to wt (p= 0,00000025). In the wildtypes 19 % of stem cells are BrdU positive after a 6 h pulse (analysed neuromasts n=36; amount of embryos N=6) whereas in the K15 mut 32% of stem cells were BrdU positive (n=86; N=6) (Fig. 18 B-B´´, C).

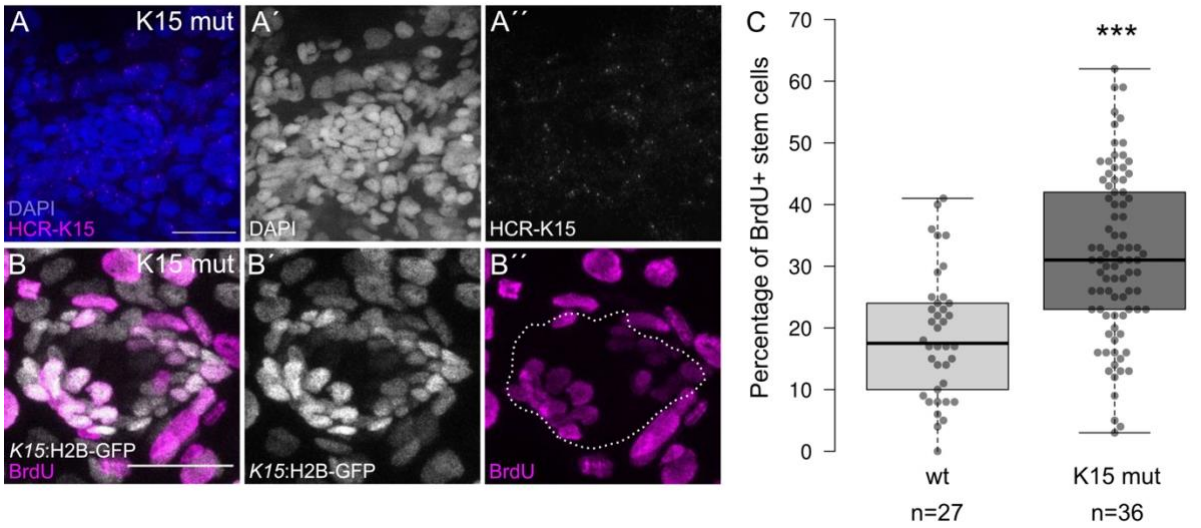

Figure 18: Increased proliferation in K15 mut shown by BrdU incorporation
(A) Detection of *K15* mRNA by hybridisation chain reaction (HCR) RNA *in situ* hybridisation with the fluorophore 647 in a 7dpf K15 mut hatchling, showing the *K15* mRNA expression in magenta and DAPI in blue in a neuromast. Scale bar indicates 25 µm. (A´) Split of the same neuromast in the DAPI channel. (A´´) Split of the same neuromast showing *K15* mRNA expression. (B) Neuromast showing BrdU + cells after BrdU incorporation assay of a 6 h BrdU pulse in 7 dpf K15 mut hatchlings, displaying BrdU in magenta and the H2B-GFP+ neuromast stem cells in grey by Tg(*K15*:H2B-GFP). Scale bar shows 25 µm. (B´) Shows H2B-GFP+ neuromast stem cells in Tg(*K15*:H2B-GFP) and (B´´) the BrdU incorporated cells. Dotted line indicates the boundaries of the neuromast to show which BrdU + cells belong to the neuromast. (C) Boxplot shows the percentage of BrdU + stem cells after a 6 h BrdU pulse comparing wildtype to K15mut (t-test = 0,00000025).

I performed time-lapse imaging of K15 mut as previously described (every 15 min up to 18 h imaging) which confirmed the over-proliferation effect of K15 mut neuromast stem cells as observed in the BrdU incorporation experiments. In the wt, stem cells divided on average 2- 3 times within 18 h (analysed wt neuromasts n=27; amount of embryos N=6, amount of division D= 72). In the K15 mut, on average 3- 4 stem cells divided and sometimes even up to 7 division could be tracked within 18 h of imaging which never occurred in wt (analysed K15 mut neuromasts n=36; amount of embryos N=4, amount of division D= 139) (Fig. 19B, C). Sometimes, the divisions occurred simultaneously and also in directly neighbouring cells (Fig. 19 C after 1:15). In addition, I quantified the apical migration of stem cell nuclei in K15 mut. I

analysed the 139 divisions and found in only 54 % (apical: 75, basal: 64) nuclear division occurring apically. In the wt, I observed apical migration during mitosis in 81 % (apical: 44, basal: 10) of divisions. This showed that the migration of nuclei is significantly affected in K15 mut (p=0.00009). These phenotypes of malformed neuromasts, higher proliferation, and altered INM in stem cells in the K15 mut indicates that the mutation of K15 affects the behaviour of neuromast stem cells.

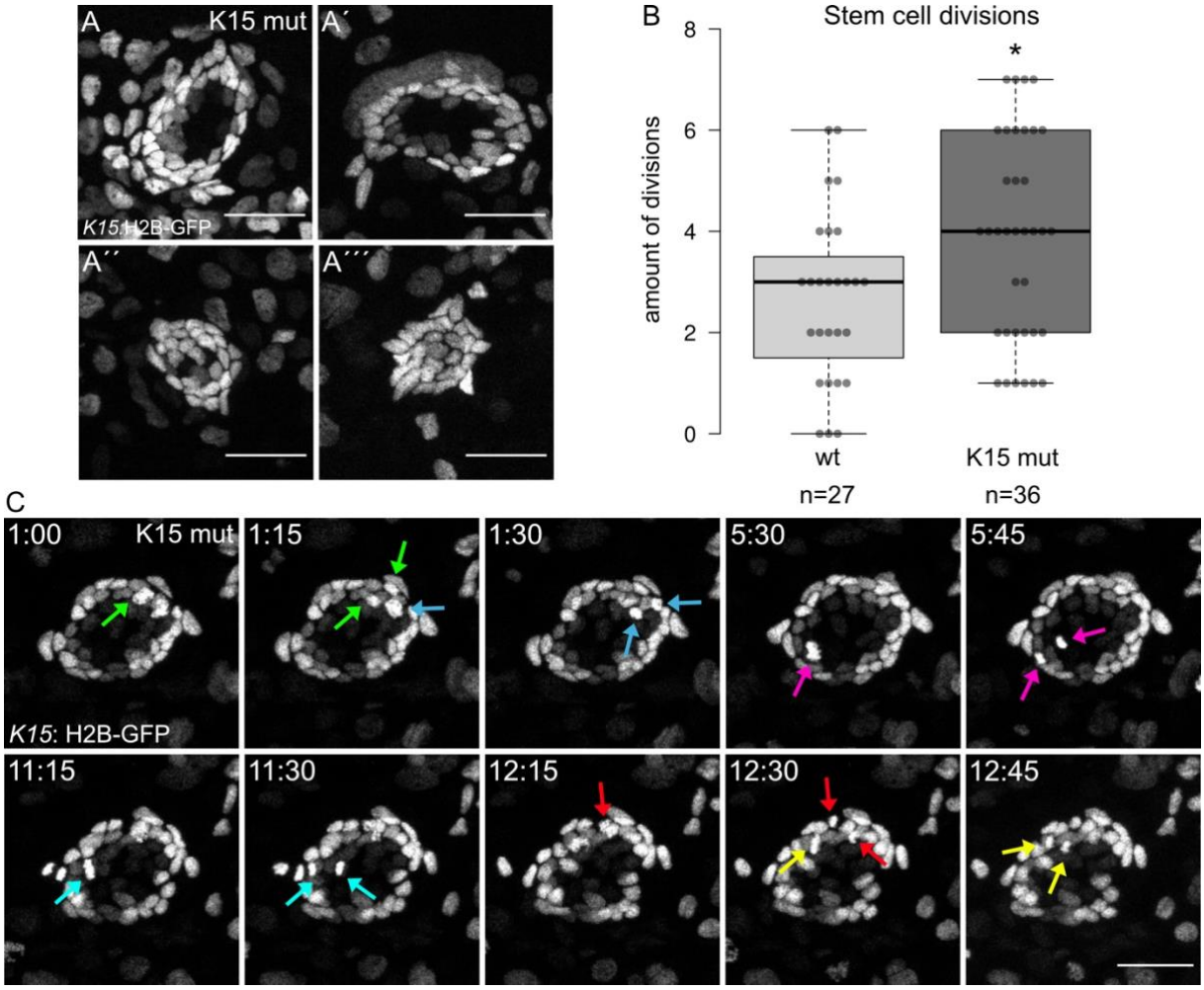

Figure 19: K15 mutation affects neuromast shapes and change stem cell proliferation

(A-A´´´) Different example of neuromast from the K15 mut displaying the abnormal shapes of neuromasts by H2B-GFP+ expression from Tg(*K15*:H2B-GFP). Scale bar shows 25 µm. (B) Boxplot showing the neuromast stem cell divisions detected by live imaging comparing the amount of division of wildtype to K15 mut (t-test = 0.015). (C) Image of a neuromast from the K15 mut showing H2B-GFP+ neuromast stem cell nuclei from Tg(K15:H2B-GFP) from a timelapse movie, where neuromasts were imaged every 15 min over 18 h. The arrows with their respective colour indicate individual divisions. Some divisions happened simultaneously.

3.9 Transplantations affected the proliferation of neuromast stem cells

To induce different levels of K15 expressions within one organism, blastula transplantation is an excellent method to generate unique mosaic embryos, in which the identity of individual cells can be determined by specific markers. Thereby, I transplanted blastula cells from one embryo (donor) into another embryo at blastula stage (host). To recognise the origin of the different organisms, distinguishable donor and host transgenic lines were used. I first characterised the behaviour of transplanted neuromast stem cells by transplanting wt Tg(*K15*:H2B-RFP) into wt Tg(*K15*:H2B-GFP) to later have the ability to compare the behaviour of K15 oe and K15 mut in the context of wt neuromast stem cells. I assessed the proliferation activity by measuring the amount of donor and host clones from 7 dpf to 14 dpf (Fig. 20 A). First of all, I was successful in generating chimeric neuromasts, consisting out of donor and host stem cells (Fig. 20 B-B´´). I followed the donor and host clones after a 7-day growth phase, and it revealed that NSCs derived from transplanted cells can have a different proliferation rate than host NSCs (Fig. 20 C-C´´). I quantified the change in number of stem cells from donor and host clones of in total 10 neuromasts from 3 individual hatchlings and I categorised the proliferation behaviour into 3 groups: no change in proliferation, increased and decreased proliferation (Fig. 21). I defined these proliferation changes by comparing the changes in donor and host clones. In the category of no change of proliferation, the stem cells of donor and host increased to the same extent after 7 days of growth. In the increased proliferation group, the donor clones increased in comparison to the host and vice versa in the reduced proliferation group.

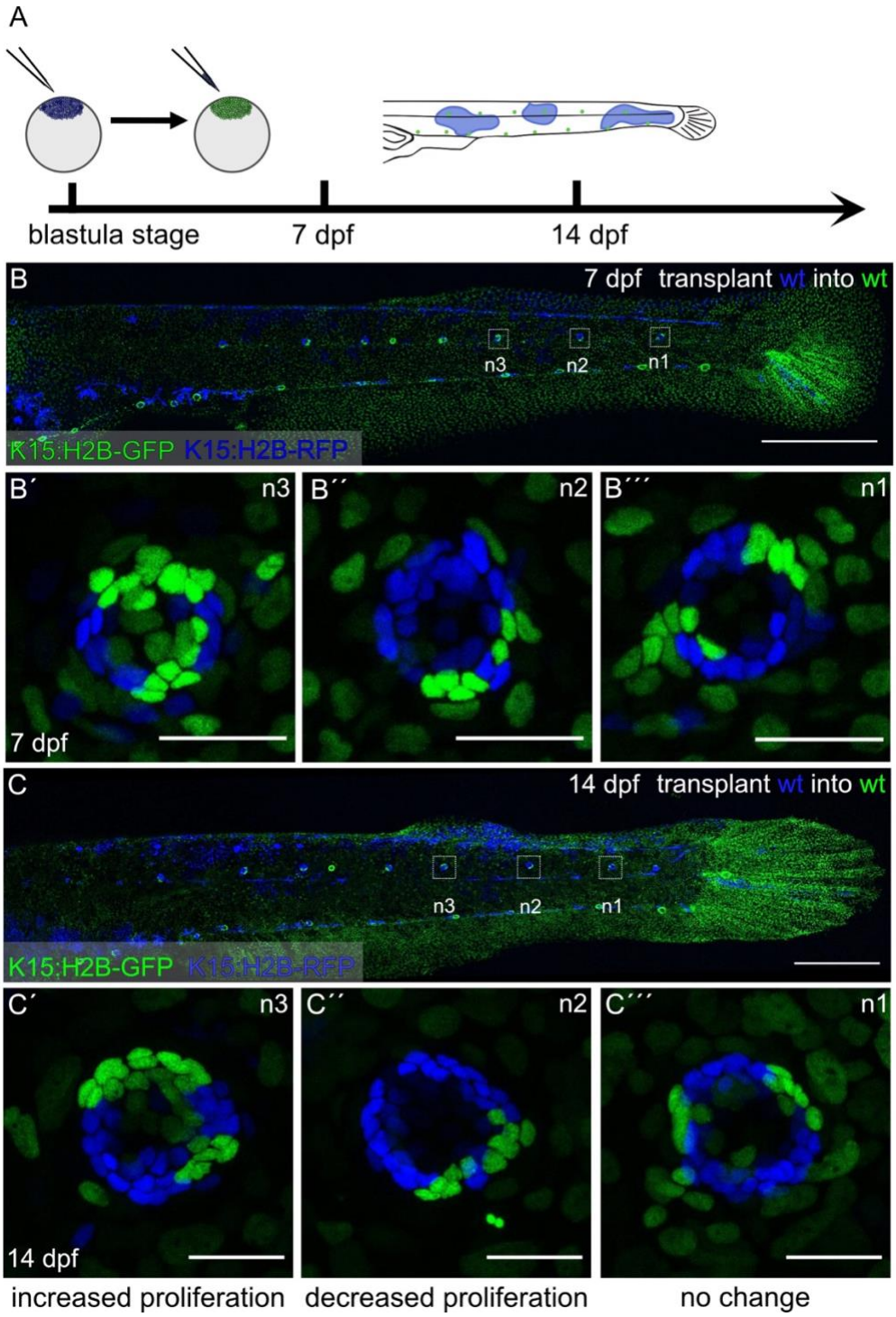

Figure 20: Control transplantation of wildtype into wildtype

(A) Schematic drawing of blastula transplantation showing how blastula cells from one donor were transferred to a host blastula. These embryos were then raised and imaged at 7 dpf and again after 14 dpf, to see the proliferation change of clones. In (B) one hatchling, 7 dpf, is represented which was transplanted with wildtypes cells from Tg(K15:H2B-RFP) into wildtype Tg(K15:H2B-GFP). Scale bar shows 500 µm. The dotted squares are indicating chimeric neuromasts which are zoomed in in (B´-B´´´). These individual neuromasts are composed out of donor and host stem cells, displayed in blue (donor) and green (host). Scale bar indicates 25 µm. (C) the same embryo was imaged 14 dpf, with the same zoom in into the three neuromasts in (C´-C´´´). Both the donor and the host stem cells were quantified over time and the proliferation could be classified into increased proliferation of donor (C´), decreased proliferation of donor (C´´) and no change in proliferation (C´´´). Scale bar indicates 25 µm.

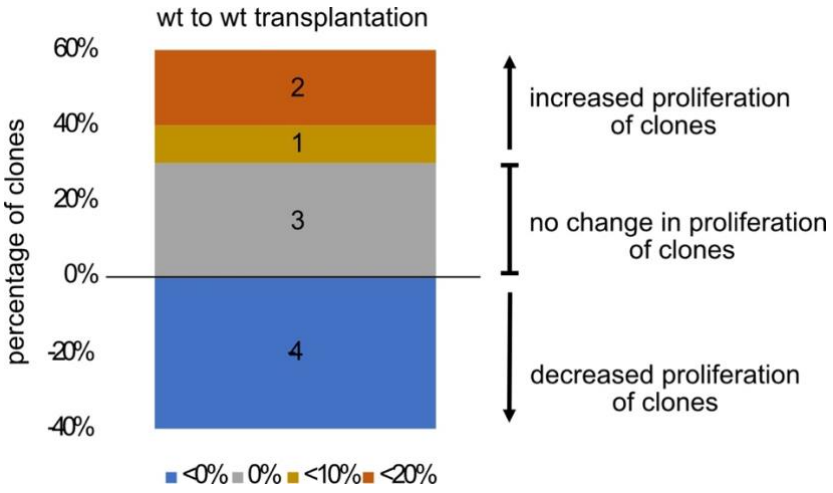

Figure 21: Quantification of proliferation changes after transplantation of wildtype to wildtype
10 chimeric neuromasts from three embryos were analysed over 7 days and proliferation changes was measured by quantifying the individual stem cells coming from donor or host. 4/10 neuromast showed a decrease of proliferation, whereas 3/10 did not show any changes in proliferation between donor and host stem cell. The increase of proliferation was further subdivided into their extend of proliferation increase. 1/10 showed up to 10 % more proliferation, whereas 2/10 showed more than 10 % increase of proliferation.

In 30 % of the chimeric neuromasts I detected no change in proliferation between donor and host stem cells (3/10). In 40 % of the chimeric neuromasts, I measured a decrease of the donor clones (4/10), whereas in the remaining 30 % (3/10) I observed an increase in donor clone (Fig. 21). Moreover, I analysed the extent of increase of the proliferation and further grouped them according to their percentage of increasement. In one of cases, the proliferation change was below 10 %, whereas in the other two cases, the proliferation was higher than 10 %. Taken together, this showed that the stem cells can behave differently after transplantation. Whether this is due to the behaviour of the individual stem cells and how they are regulated, or the transplantation cannot be concluded exactly. I further used this behaviour of transplanted wt stem cells as a baseline to compare the changes in proliferation after transplanting K15 oe and K15 mut into wt to see which effect altered *k15* expression had on the proliferation of stem cells.

3.10 Transplanted K15 oe stem cells outcompeted wt stem cells

For the transplantation of K15 oe, I used blastula cells from the double transgenic Tg(K15:K15CDS-T2A-GFP), Tg(K15:H2B-RFP) as donors and transplanted them into wt Tg(K15:H2B-GFP) hosts to follow the progression of clones. I analysed 16 chimeric neuromasts from 6 successfully transplanted hatchlings (Fig. 22A). I categorised the proliferation changes as previously described. In 75 % of the cases (12/16), I detected an increase of donor clones from K15oe, whereas in 25 % the size of donor clones decreased (4/16). Interestingly, in this K15 oe transplantation, I never detected "no change in proliferation" between the host and donor stem cells as observed in the wt (K15 oe 0/16, wt 3/10). Furthermore, I investigated the extent of increase and decrease of K15 oe donor stem cells as previously described in the wt. In 7 cases, the increase in proliferation was up to 10 %. In 4 cases the increase was higher than 10 % and in one case the proliferation increase was more than 20 % (Fig. 22B). I never observed such high increases in proliferation in the wt cells, which indicates that the differentially high K15 expression in the K15-oe stem cells represents an advantage over the wt stem cells.

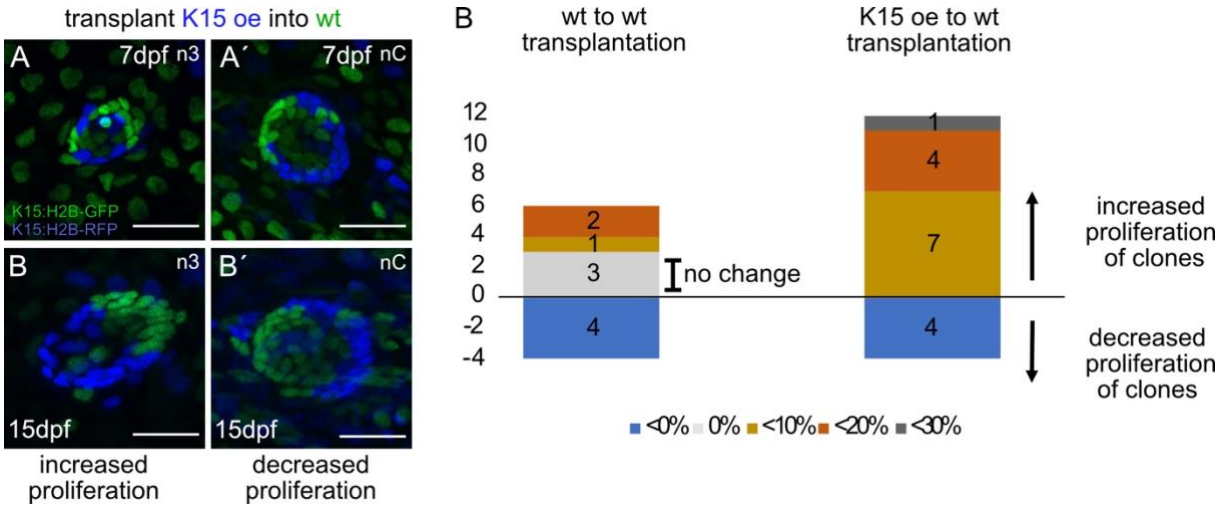

Figure 22: Transplantation of K15 overexpression into wildtype

Blastula cells from the K15 oe Tg(K15:K15CDS-T2A-eGFP), Tg(K15:H2B-RFP) were transplanted into wildtype Tg(K15:H2B-GFP). (A and A´) are representing two successful chimeric neuromasts displaying the donor cell from the K15 oe in blue and the wildtype host cell in green. Scale bar shows 25 µm. (B and B´) the same neuromasts were imaged 8 days later, showing proliferation increase (B) and decrease (B´). (C) presents the quantification of proliferation changes comparing wildtype to wildtype transplantation with K15 oe to wildtype transplantation. In total 16 neuromasts from 6 embryos could be quantified from the K15 oe transplantation. The proliferation changes are categorized as before in their extend of proliferation increase in percentage. The x-axis is showing the amount of neuromasts displaying the specific proliferation phenotype.

3.11 Transplanted K15 mut stem cells do not impact the proliferation of stem cells

To further understand how a lack of K15 influences the proliferation of stem cells, I transplanted blastula cells from the K15 mut Tg(K15:H2B-GFP) into wt Tg(K15:H2B-RFP). I analysed 18 chimeric neuromasts from 4 individual transplanted hatchlings (Fig. 23). The proliferation changes were categorised as previously mentioned. In 50 % of the cases, I measured an increase in proliferation of the K15 mut stem cells (9/18), whereas in the other 50 % I detected a decrease (9/18). Similar, to the K15 oe transplantation, I never detected "no change in proliferation" (0/18). By further investigating the proportion of increase of the donor K15 mut stem cells, 7 cases showed an increase by up to 10%, while only two cases exceeded that. This is similar to what I detected in the wt-to-wt transplantation, suggesting that the K15 mutation does not have a major impact on the stem cell proliferation in the context of a wt background.

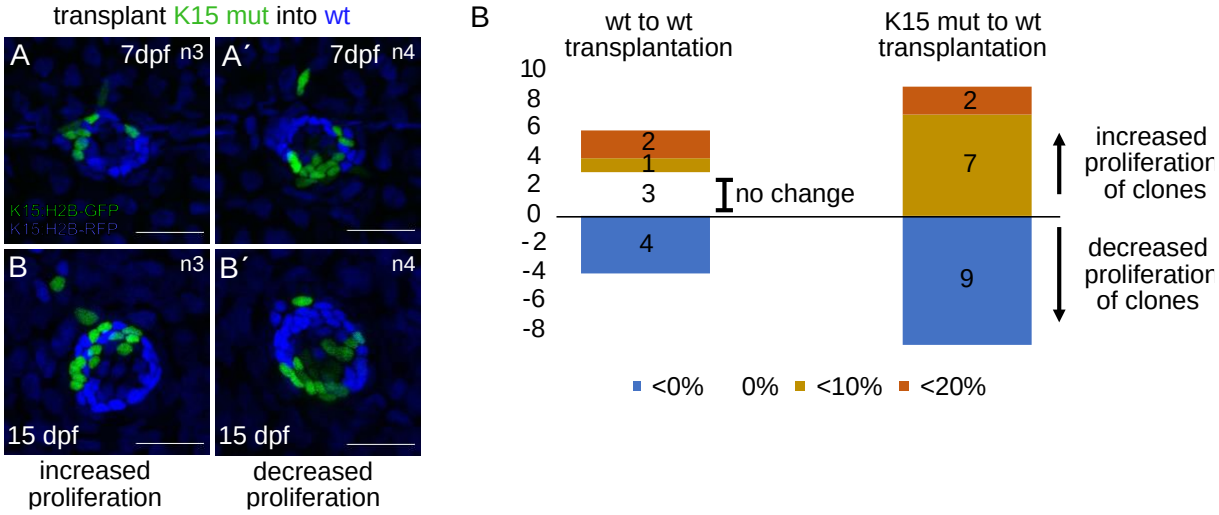

Figure 23: Transplantation of K15 mutant to wildtype

Blastula cells from the K15 mutant Tg(K15:H2B-GFP) were transplanted into wildtype Tg(K15:H2B-RFP). (A and A´) are representing two successful chimeric neuromasts displaying the donor cell from the K15 mut in green and the wildtype host cell in blue. Scale bar shows 25 µm. (B and B´) the same neuromasts were imaged 8 days later, showing proliferation increase (B) and decrease (B´). (C) presents the quantification of proliferation changes comparing wildtype to wildtype transplantation with K15 mutant to wildtype transplantation.

3.12 Single cell RNA sequencing of medaka epithelial cells revealed niche cell marker

To further understand the heterogenous nature of individual neuromast stem cells, I devised a single-cell RNA sequencing (scRNA seq) experiment. Together with Javier Vazquez-Marin, we developed a single-cell dissociation protocol to specifically isolate single cells of the skin of medaka hatchling and reduce the overrepresentation of other cell types, such as muscle cells, to be able to identify individual clusters within the epithelium. Dissociation and scRNA seq could be successfully carried out for hatchlings of wildtype Tg(*K15:*H2B-RFP), K15 oe Tg(*K15:*K15-T2A-GFP), and K15 mut Tg(*K15*:H2B-GFP).

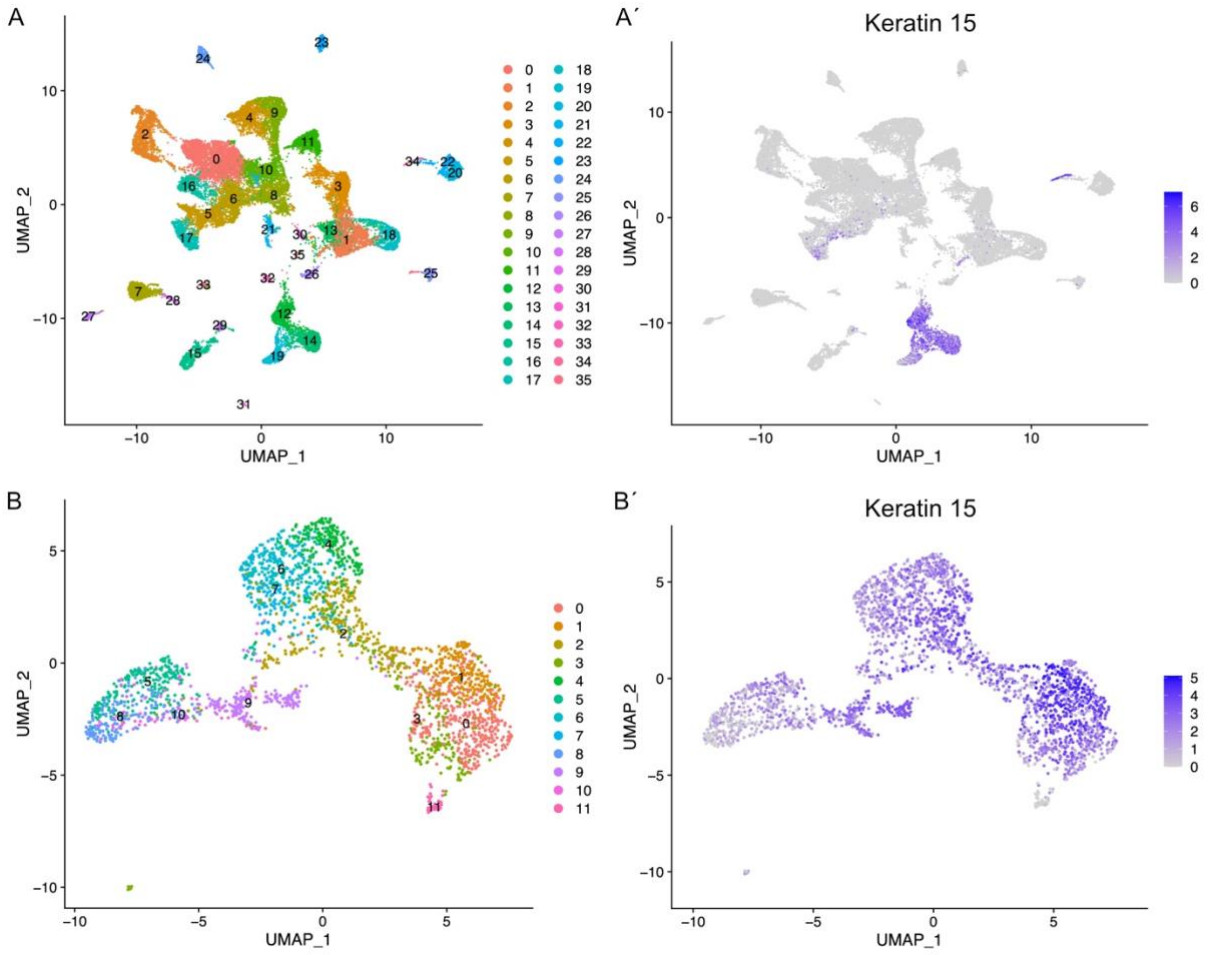

Figure 24: ScRNA seq clusters from the skin of medaka
(A) Dimensional blot of scRNA seq data displaying 35 individual clusters. (A´) shows the same blot displaying in which clusters *l15* is expressed. (B) Epithelial cluster: Re-clustered dimensional blot of the high *k15* expressing clusters (12, 14, 19) for higher resolution of individual cell types. These clusters were subclustered into 11 groups. (B´) shows expression *l15* of the epithelial cluster.

The data of the scRNA seq results of K15 wt, K15 oe, and K15 mut was integrated and displayed 35 dimensional clusters (Fig. 24 A). From those, we checked in which clusters *k15* was expressed, since K15 is used as marker for epithelial cells and neuromast stem cells. High *k15* expression was mainly found in clusters 12, 14, and 19 which already clustered separately together (Fig. 24 A′). These clusters of high *k15* expression were then clustered again to get a finer resolution of the individual cell types (Fig. 24 B, B′). With this, I screened the marker gene list, for potential candidate genes present in specific cell types. Keratins are usually co-expressed with another keratin and have a distinct interaction partner (Coulombe and Omary 2002). So far, for K15 no specialised interaction partner was found (Waseem, Alam, et al. 1999). To tackle the question whether K15 has a distinct interaction partner in medaka, I studied the expression of other keratins present in the same clusters of K15. Thereby, I identified Keratin1c19e (K1c19e), which was co-expressed in similar clusters as K15 (Fig. 25 A-A′′). Together with Jie Ji, a bachelor student from the Bachelor of Biowissenschaften, I designed a probe for *in-situ* hybridisation to further investigate in which cell types *k1c19e* is expressed. This revealed that *k1c19e* is also expressed in epithelial cells on the skin. Moreover, I detected a strong expression around the neuromast with elongated cells which are the niche cells of the neuromast (Fig. 25 B-B′′). To confirm this finding, I designed a promotor construct of *K1c19e* to generate a fluorescent transgenic line and follow the expression of *k1c19e in vivo.* Together with Jie Ji, we generated the construct *K1c19e*:H2B-RFP and injected this into wildtypes. In the injected generation, this already revealed that *k1c19e* is expressed in epithelial and niche cells. The niche cells are identified by their elongated nuclei shape (Fig. 25 C′′′, indicated by arrows). This transgenic line will build the basis to further understand the nature of the niche stem cell interaction.

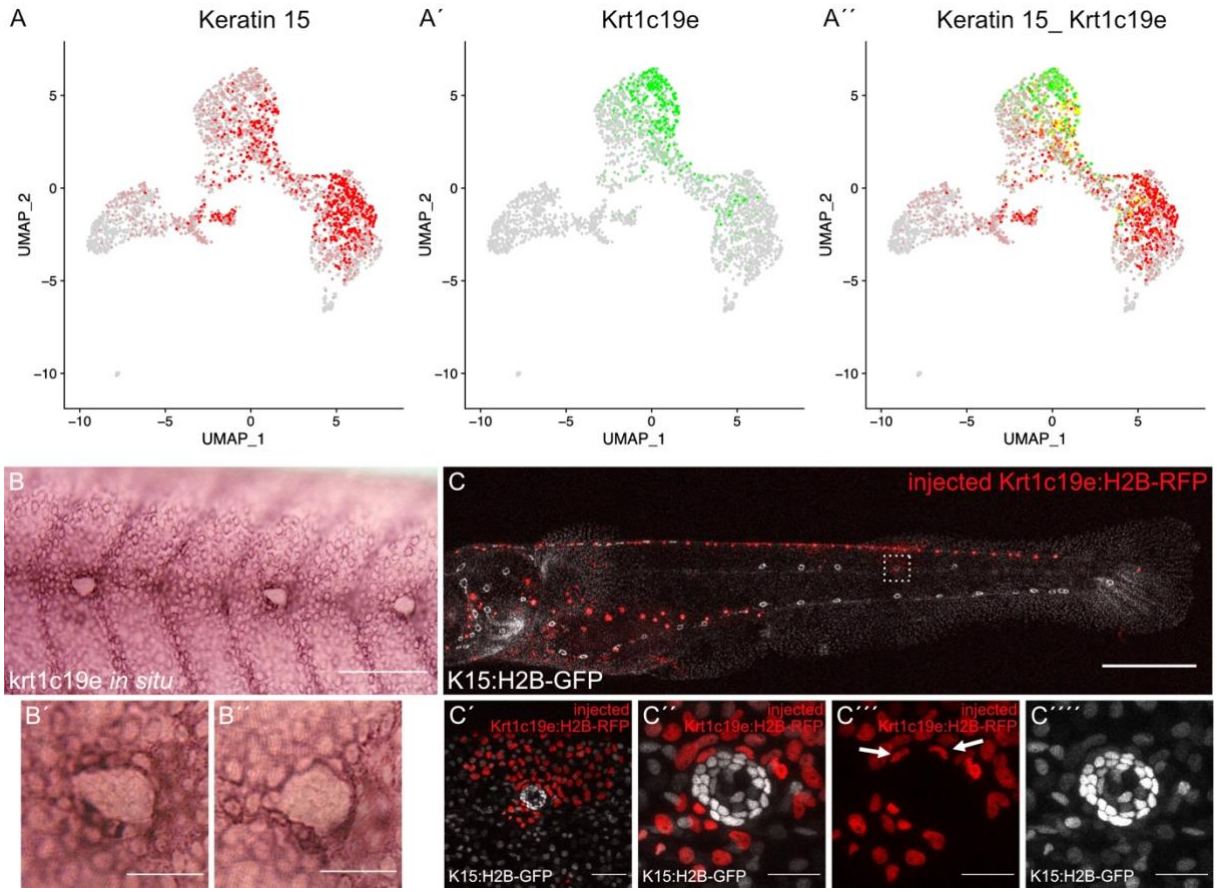

Figure 25: *Krt1c19e* expression in epithelial cells and neuromast niche cells

(A-A´´) Dimensional blot of the epithelial clusters comparing the expression of *K15* and *Krt1c19e*. (A) shows expression of *K15* within the clusters. (A´) shows expression of *Krt1c19e* and (A´´) shows the overlap of both genes in the epithelial clusters. (B-B´´) Displaying the *Krt1c19e* mRNA expression detected by *in situ* hybridisation with NBT/BCIP. (B) shows the tail of a hatchling and (B´, B´´) show zoom ins of neuromasts, displaying *Krt1c19e* mRNA expression. Scale bar indicates 25 µm. (C) Hatchling injected with Krt1c19e:H2B-RFP shows H2B-RFP + epithelial cells in red and H2B-GFP + neuromast stem cell nuclei in grey from Tg(K15:H2B-GFP). Scale bar indicates 100 µm. (C´and C´´) show zoom ins of the same neuromast, displaying H2B-RFP+ epithelial nuclei in red, surrounding the neuromast shown by H2B-GFP expression in grey. (C´´´) displays the H2B-RFP+ nuclei from the injection of Krt1c19e:H2B-RFP. The arrows indicate the elongated nuclei shape from transformed niche cells. (C´´´´) shows H2B-GFP+ neuromast stem cells from Tg(K15:H2B-GFP). Scale bar indicates 25 µm.

3.13 Identification of epithelial fin cells by scRNA seq:

Furthermore, I investigated the other subclusters present in the epithelial scRNA seq cluster which showed lower expression of *k15*. In cluster 5 and 9 (Fig. 24 B, Fig. 26 A), I identified the expression of *actinodin 1 (and1)* which is important for the fin formation in zebrafish (Heude, Shaikho, and Ekker 2014; Phan et al. 2019). To test the expression of *and1* in medaka, Jie Ji and I designed a probe for *in-situ* hybridisation against *and1* and performed whole-mount *in situ* hybridisation. *And1* was expressed in the membranous fins surrounding the hatchling, in the caudal fin and in the pectoral fins (Fig 26B, B′, B′′). This validated the expression of *and1* in fins from zebrafish.

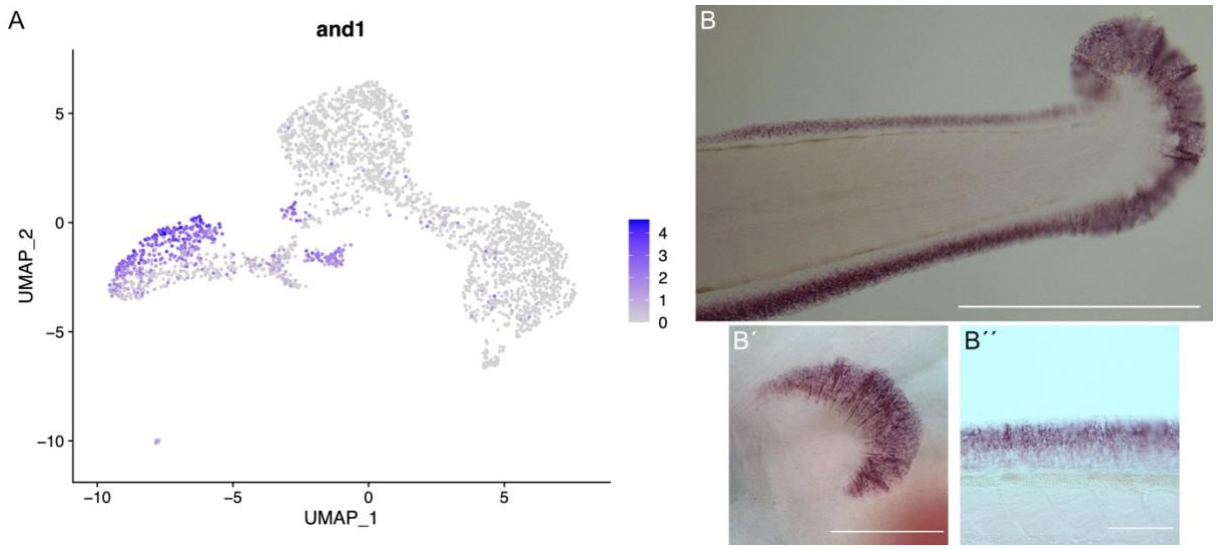

Figure 26: And 1 expression in fins

(A) Dimensional blot of the epithelial clusters showing the expression of *and1*. (B-B′′) Displays the *and1* mRNA expression detected by in situ hybridisation with NBT/BCIP, showing in (B) expression in the membranous and caudal fins. Scale bar indicates 500 µm. (B′) shows a zoom in into the pectoral fin. Scale bar indicates 100 µm. (B′′) depicts a zoom in into the membranous fins. Scale bar shows 50 µm.

4 Discussion

Adult stem cells are of fundamental importance for life. They are crucial for homeostatic growth and regeneration in all multicellular organisms. The key property of adult stem cells is to maintain the stem cell pool, and generate new differentiated cells as a response to signals from their environment (Siminovitch, McCulloch, and Till 1963). Self-renewal and differentiation must be precisely controlled to ensure the correct balance of cell types in a tissue. Fish have constantly active proliferating stem cells, giving them the extraordinary ability to grow throughout their lives (Ding et al. 2010). While increasing in overall body size, the organs of the fish maintain proper scaling and thus maintain functionality. How stem cells are orchestrated to increase the size of an organ while simultaneously maintaining proper scaling is still not fully understood. The organs of the posterior lateral line are ideal to understand how the challenging balance of homeostasis and growth is maintained by the stem cells in post-embryonic medaka. While neuromast stem cells proliferate to generate new progenitor cells that give rise to new hair cells, the function of the neuromast, the perception of their environment by the hair cells, must be maintained (Cruz et al. 2015). Moreover, the stem cell integrity must be sustained and this requires precise coordination and communication between the cells to ensure the functionality of this organ. In this thesis, I have shown how stem cells of the neuromast are coordinated in homeostatic growth and how the epidermal stem cell marker K15 affects their proliferation.

4.1 Neuromast stem cells (NSCs) actively proliferate during homeostasis

Hair cells of the neuromasts constantly need to be replenished, since they are abrased due to their exposure to the environment. Therefore, a certain number of active stem cells is essential to ensure the proper number of hair cells. In comparison to other organs, the fraction of undifferentiated cells in the neuromast is relatively high, containing mostly stem cells and progenitor cells. One question was therefore whether the stem cells display heterogeneity in behaviour in terms of proliferative activity (active or dormant). In this thesis I assessed the proliferation of neuromast stem cells (NSCs) by Bromodeoxyuridine (BrdU) incorporation to understand how NSCs are regulated in homeostasis. I was able to show that in the medaka neuromast all stem cells are proliferating at this stage of development, indicating that in the

neuromast, there is no pool of quiescent stem cells. All stem cells cycle actively within the organ. These results were obtained at the early hatchling stage which is an early post-embryonic stage, in which the stem cells might still be more proliferatively active compared to later stages. Making use of the natural occurring age variation of neuromasts from anterior to posterior, which is due to the establishment of the posterior lateral line by a migrating primordium (Seleit, et al. 2017), I could show that independent of the relative age of the neuromast the proliferation rate stays constant. Hence, the high proliferation activity of the stem cells in the neuromast of freshly hatched larvae does not seem to be due to residual embryonic stem cell activity. To prove that NSCs in juvenile or even adult fish show a similar proliferative pattern, BrdU incorporation experiments could be performed in older stages. This would conclusively show whether proliferation is reduced in older neuromasts, indicating that the organs are still developing in earlier stages. However, juvenile and adult fish also constantly produce new hair cells, requiring actively proliferating stem cells. It is not yet known how stem cells in medaka contribute to the formation of new hair cells and how the balance between generating progenitor cells and maintaining stem cells is achieved. For zebrafish it was shown that after ablation of hair cells with neomycin at 5 dpf the direct source for replacing and generating new hair cells are the progenitor cells and not the stem cells (Ma, Rubel, and Raible 2008; Cruz et al. 2015). Cruz et al tested this also in homeostatic conditions, in which hair cells are lost naturally throughout the lifespan of fish. These hair cells were still continuously renewed by symmetrically dividing progenitor cells. After repeated ablation attempts, they found that the number of progenitor cells remained constant (Cruz et al. 2015). This shows that even though the stem cells of the neuromast are not the direct source of cells providing new hairs cells, progenitor cells are continuously renewed by the stem cells to ensure a constant number of progenitor cells. Therefore, the continuous need of new support cells could be another explanation for the high proliferation of stem cells in medaka. In this work I have investigated the proliferation and regulation of NSCs, but so far it is not entirely clear how the stem cells in medaka differentiate into progenitor cells. To test this hypothesis of stem cells giving rise to progenitor cells after hair cell ablation, lineage tracing experiments could help to better understand how the stem cells contribute to the pool of progenitor cells. In addition, NSC proliferation after blocking hair cell differentiation in medaka hatchlings at 7 dpf could be assessed to determine whether stem cells continue to proliferate even though no new hair cells are formed. In zebrafish, the synthetic polyaromatic chemical SP600125 which is an inhibitor of the JNK signalling was found to block hair cell differentiation (He et al. 2016). In this way, it would be possible to understand if and how stem cells are regulated by feedback signalling

from progenitor and hair cells. Furthermore, this experimental setup could reveal whether the high proliferation in early hatchlings is a homeostatic effect of continuous loss of hair cells or an embryonic effect of the ongoing development of NSCs in medaka.

4.2 Increased anterior proliferation of NSCs in post-embryonic growth

The proliferation of NSCs was further investigated by time lapse imaging, to better understand how NSCs behave *in vivo*. Thereby, I observed that NSCs of the midline neuromasts display a positional bias of divisions towards the anterior side of the neuromast organ, indicating that NSCs are differentially regulated within one organ. Stem cells are normally embedded in so-called niches, which form the microenvironment of stem cells and are involved in their regulation (Woods and Guezguez 2021; Lee et al. 2012). It is possible that the NSCs at the anterior side of the neuromast receive other signalling cues from the niche that induce a higher proliferation. So far, it is not known why NSCs are more proliferative active anteriorly. As fish grow throughout their lives, neuromasts must also adapt to the larger body size by increasing the number of neuromasts to ensure the perception of their surroundings. As they grow, adult medaka fish generate new neuromast organs which are arranged in clusters called stitches similar to zebrafish (Nuñez et al. 2009). So far it is not known how these neuromast stiches are formed in post-embryonic growth in medaka. First hints were found in the caudal neuromast in medaka in a study from our lab. It was described how the first new neuromast is formed post-embryonically. Here it was shown that NSCs in the anterior part of the caudal neuromast give rise to the new organ by anterior migration of individual NSCs (Gross et al. 2022). Neuromasts from the midline will also form clusters of neuromast distributed across the body of the adult fish but how these organs are generated is not known. A plausible explanation could therefore be that neuromasts in the midline show a similar behaviour to NSCs in the caudal neuromast to form new organs, and that NSCs therefore proliferate more actively anteriorly. To test this hypothesis, photoconvertible fluorescent proteins such as EOS could be used to track the behaviour of NSCs over time (Benton 2018). This allows anterior NSCs to be photoconverted and tracked to understand if and how they form new organs post-embryonically. In this way, the lineage of the stem cells could be followed to understand what happens to the highly proliferative anterior NSCs.

4.3 Proliferation control in NSCs

Using live imaging, I followed the process of mitosis in NSCs in vivo and tracked dividing nuclei. Comparison with the data obtained in the BrdU incorporation event, which marked cells in S-phase, revealed a discrepancy. More cells were found in S-Phase, indicating actively cycling cells, than dividing cells during live-imaging. This suggests that NSCs rest after S-phase in G2. Possibly this arrest after the S phase ensures a pool of stem cells that is ready to divide at any time. This enables the neuromast to react quickly to induced changes in the organ and to form new cells as efficiently as possible. So far, the control and length of the NSC cell cycle in medaka has not been determined. The duration of the entire cell cycle would provide information on how stem cells are regulated and whether they can enter quiescent states. With sequential incorporation pulses of BrdU and then 5-ethynyl-2'-deoxyuridine (EdU) it is possible to estimate the full cell cycle length (Harris, Zalucki, and Piper 2018). The main time keepers during the cell cycle are the gap phases which decide whether a cell progresses with the next cell cycle phase (Cheung and Rando 2013; Bertoli, Skotheim, and de Bruin 2013). Therefore, it would be particularly interesting to measure the length of the gap phases. To follow the time of individual cell cycle phases, the fluorescent ubiquitination-based cell cycle indicator FUCCI system can be used. The FUCCI system contains two fluorescent probes which express fluorescent fusion proteins specific for the cell cycle phases; cdt1 for G1 and geminin for S/G2/M phase. In this approach the time for G1 alone and S/G2/M can be determined, by a colour change from orange in G1 and green in all other cell cycle phases (Sugiyama et al. 2009; Dolfi et al. 2019). Nevertheless, it is difficult to resolve the individual cell cycle phases and only in combination it is possible to determine the length of the cell cycle phases. Endogenous labelling of PCNA, however, showed that all cell cycle phases can be resolved by following the expression of *PCNA* (Leung et al. 2011). In medaka skin cells, it was shown how the expression of *PCNA* follow certain characteristic for specific cell cycle phases (Seleit, Aulehla, and Paix 2021). Therefore, the *PCNA* expression can be utilised to follow the cell cycle phases in NSCs. In zebrafish neuroepithelia, *PCNA* expression could be correlated with nuclear behaviour of interkinetic nuclear migration and they were able to measure the individual cell cycle phases (Leung et al. 2011). The result of fewer mitotically active NSCs than NSCs that are BrdU+ suggests that the NSCs follow an internal cell cycle control. It is not yet known how the cell cycle of NSCs is regulated and which cell cycle checkpoints are active in medaka NSCs. Classical check points during the cell cycle are cyclin-dependent kinases, such as p21, p53 and retinoblastoma protein (RB) (Sunada et al. 2021; Barnum and O'Connell 2014; de Gooijer et al. 2017). Especially, p53 is known as tumour suppressor and act as a DNA damage control by

arresting the cell cycle once DNA damage was detected and induce apoptosis to remove defective cells (Donehower et al. 1992). Thus, to understand how cell cycle arrests are controlled in medaka NSCS, antibody staining against p53 could be performed. In zebrafish they showed that p53 is not expressed in early development. However, after stress induction with the cyclin-dependent kinase inhibitor R-roscovitine, high expression of *p53* was observed in the retina, gut and liver of zebrafish (Lee et al. 2008). This showed that p53 regulates the cell cycle responses in zebrafish. Therefore, it is possible that in medaka similar mechanisms are used for cell cycle control. Understanding which cell cycle checkpoints are utilised in NSCs will provide a better understanding of how NSCS are regulated in general.

4.4 NSCs oscillate according to the cell cycle, reminiscent of interkinetic nuclear migration

NSCs are elongated cells which are arranged in a volcano like shape. I observed that the nuclei of NSCs are located at the basal side of the cell and upon cell division, nuclei migrate apically. This nuclear behaviour is known as interkinetic nuclear migration (INM) which can be observed in many stratified epithelial tissues of many organisms such as in the brain or retina (Leung et al. 2011; Lahne and Hyde 2016; Tsuda et al. 2010). INM is a complex process and it can vary enormously depending on the organism and the tissue. It was already discovered nearly one century ago in neuroepithelia of developing chick embryos (Sauer 1935; Sauer and Walker 1959). The reason for INM is generally not understood and still under debate.

So far, INM has only been detected in medaka neuroepithelia, but has not yet been described in medaka NSCs (Tsuda et al. 2010). As the neuromast is very compact and stem cell nuclei are located basally, the nuclei may not have enough space to divide at the basal side. Mitosis is an elaborate process that requires proper DNA condensation into chromosomes, the organisation of the spindle and the separation of the chromosome by the spindle. All this needs space which might not be available at the basal side of the cell of the NSCs. Therefore, INM could be a cellular mechanism to solve the problem of spatial constraints. If the cell nuclei are distributed differently within their cells, more cells can be accommodated in a given space (Miyata 2008). Another explanation for INM could be the induction of a change in stem cell fate. Epithelial cells often express certain polarity markers and have cell organelles only at specific locations within the cells, as was shown for mammalian neuroepithelial cells (Buckley and St Johnston 2022). Through the different distribution of polarity markers, INM can influence which markers are passed on to the daughter cells and thus influence which cell fate the daughter cells adopt.

In mouse brains, the evolutionary conserved membrane-bound protein Numb is specifically located at the apical crescent of the cell and its division orientation determines whether cells divide symmetrically or asymmetrically. In the case of asymmetric division, Numb is passed on only to one daughter cell and thereby a change in cell fate is induced (Chenn et al. 1998; Zhong et al. 1996). In addition, I showed that centrosomes in medaka neuromasts are located apically. Centrosomes belong to the microtubule organisation centres in cells and play a crucial role in the segregation of chromosomes during mitosis. They are thought to trigger the onset of mitosis as soon as the cell nucleus has reached the centrosomes (Miyata 2008; Schenk et al. 2009). Therefore, nuclei need to migrate apically to the centrosomes to initiate division and to properly divide during mitosis. This suggests that INM in NSCs might be associated to the centrosomes. Whether this is the reason for NSCs to undergo mitosis at the apical side is not clear.

Contrary to this idea, I observed in some cases that division occurred at the basal side of the cell, suggesting an independency of the centrosomes. In more recent studies on the zebrafish retina, it was found that INM behaviour is independent of the localisation of the centrosomes. Using DN-N-cadherin and colcemide treatment, they were able to disrupt the association of centrosomes and nuclei at the apical site. Although the nucleus and centrosome met basally, apical INM still took place. By interfering with the expression of the Cyclin-dependent kinase 1 (CDK1) and its upstream regulator Wee1 during the cell cycle, they were able to identify CDK1 as the main driver of the apical migration during G2. The CDK1 inhibitor R03306 blocked the migration of INM during G2, whereas the Wee1 inhibitor PD0166285, triggered the activation of CDK1, resulting in premature INM already in S-phase (Strzyz et al. 2015).

To test whether centrosome localisation at the apical site in medaka NSCs is the reason of INM or not, similar experiments could be performed as described for the zebrafish retina. Interfering with the centrosome position could indicate whether INM in NSCs depends on centrosome position. In addition, the dependency of CDK1 could be analysed by testing the CDK1 inhibitor R03306 and Wee1 inhibitor PD0166285, to see whether NSCs behave similarly as in the retina of zebrafish (Vassilev 2006; Leijen, Beijnen, and Schellens 2010; Strzyz et al. 2015). This would shed light on how INM is regulated in NSCs of medaka and what role it plays in stem cell behaviour.

4.5 Upregulation of *Keratin 15* in NSCs during apical migration in G2/M phase

In general, INM can be found in a variety of tissues and is not restricted to vertebrates (Meyer, Ikmi, and Gibson 2011). This shows that INM is a universal process that is important for all species. It is therefore important to better understand how INM is orchestrated. The distances which nuclei need to overcome during INM is also very diverse, ranging from 3-4 nuclei width in zebrafish retina until up to 10 nuclei width in mammalian neocortex (Miyata 2008; Taverna and Huttner 2010). Therefore, the mechanisms to drive the migration during INM can also be very different. During time-lapse imaging of NSCs, I not only observed the process of INM, but also a correlative upregulation of *Keratin 15 (K15)* in these cells during G2/M phase. This dynamic expression of *k15* in medaka NSCs indicates that its differential expression during the cell cycle might play a role during INM. In medaka NSCs, it is not known which components of the cytoskeleton are involved in INM. The process of INM has been intensively studied in recent years to understand the basal- apical motion during G2 and the opposite migration in G1. Migration during the G2 phase is described as an active process, as the nuclei move rapidly to the apical side compared to G1 (Leung et al. 2011). In addition, several motor proteins, such as microtubules and dynein as well as actin and myosin, have been shown to be involved in apical movement during INM in different organisms. (Tsai et al. 2010; Tsai et al. 2005; Kosodo et al. 2011; Leung et al. 2011; Norden et al. 2009). In contrast, it is still unclear, whether the downward migration in G1 is actively driven by cytoskeleton components or whether the nucleus is passively displaced by neighbouring nuclei entering mitosis (Schenk et al. 2009; Kosodo et al. 2011). K15 is a cytoskeleton component, similar to actin and microtubules and belongs to the family of intermediate filaments (Waseem, Dogan, et al. 1999; Liu et al. 2003). So far, Keratins have not been found to be involved in the process of INM, but since Keratins are also part of the cytoskeleton and are involved in a variety of processes in epithelial cells, it might be that K15 plays a role in INM (Coulombe and Omary 2002). The upregulation of *k15* expression during G2 possibly indicates a potential role during INM. Therefore, understanding the function of K15 is essential to provide a better understanding of the behaviour of NSCs. The role of K15 in NSCs is discussed in more detail in the following sections.

4.6 K15-GFP fusion impacts embryonic development in medaka

Understanding the dynamic expression of *k15* and its localisation within a cell during the cell cycle was one focus of this work. Unfortunately, the generation of an endogenous protein tag line for K15 in medaka was not feasible. In medaka, *K15* is not only expressed in the NSCs but also in the epithelial cells of the skin. In my attempts to generate an endogenous protein tag for K15, I labelled only very few epithelial cells. Those K15-GFP+ epithelial cells showed properly localised expression of K15 as a fine network within the cell, but most embryos with K15-GFP+ cells died. This strongly suggests that the fusion of K15 with GFP is lethal, indicating a critical function of K15.

In the course of my work for this thesis, I have also generated a CRISPR/Cas9 generated K15 mutant. In this K15 mutant I could not observe any lethality of the fish, which suggests that this K15 mutant variant does not affect the survival of the fish. This indicates that the fusion of K15 with GFP has a stronger influence on the development of medaka embryos than the truncated K15 from my K15 mutants. The K15 fusion was generated by tagging K15 at the N- or C-terminus of the gene, whereas the K15 mut is a result of a premature stop in the centre of the gene. The N- and the C-terminus of Keratins are known to be highly post translationally modified, and their post translational modification is important for their function (Omary et al. 1998; Li et al. 2023). Therefore, it is possible that the K15 fusion interferes with the proper posttranslational regulation of K15 and leads to a dominant-negative version of K15. Moreover, Keratins are intermediate filaments which form heterodimers with other Keratins. For K15 no common interaction partner is known, however from the human disorder *epidermolysis bullosa simplex* it was shown, that K15 is expressed in the same cells as K5 and K14 and K15 can compensate for the loss of K14 (Peters et al. 2001; Waseem, Alam, et al. 1999). This emphasises that Keratins can compensate for the loss of other Keratins. Therefore, one plausible explanation for the survival of K15 mutants in medaka could be genetic compensation. In zebrafish, the phenotypic differences between knockdown and knockout experiments were highlighted and it was shown how the loss of a gene can be compensated by its paralogue (Rothschild et al. 2020). Therefore, it is possible that the differences in lethality of the GFP-tagged K15 and K15 mutants can be due to genetic compensation in the K15 mutants. To test this hypothesis, also K15 morphants could be generated by treating the embryos with antisense morpholino oligos against K15 to compare the phenotypes between a knockout and a knockdown.

In addition, K15 consists of 440 amino acids (aa) and properly formed Keratin filaments only have a diameter of 10 nm. GFP has a size of 238 aa which is close to the size of K15 (Prasher

et al. 1992). Since each K15 monomer will be tagged with a GFP that is similar in size to K15, it can be assumed that protein folding and filament assembly are challenging. Since many monomers will assemble together to form intermediate filaments, the fusion of GFP and K15 inhibits the proper folding of the protein. From cell culture experiments it is known that Keratins can be tagged with fluorescent proteins and the structure and localisation of the K15 can be visualised (Bose et al. 2012). However, during the development many changes occur in which cells massively divide and rearrange to form a fully functional organism. Therefore, the correct folding of the K15 protein seems to be of great importance in the developing medaka embryo. The lethality of embryos with GFP- tagged K15 points towards that a non-functioning K15 fusion is more detrimental than no K15, as if K15 is lost, other Keratins could potentially take over the function of K15.

4.7 K15 acts as proliferation pacer

The expression of *k15* is dynamically controlled and the time-lapse imaging of the destabilised GFP expression under the *K15* promotor has shown that *k15* was upregulated during G2-M phase suggesting a potential role in the regulation of the cell cycle. To find out whether *K15* upregulation during G2 is just a correlation or whether there is causality between cell cycle progression and *K15* upregulation, I tested how altered *K15* expression affects NSC proliferation. This revealed that K15 is modifying the proliferation behaviour of NSCs by reducing the proliferation in the K15 overexpression and increasing the proliferation in K15 mutants. To date, it is not known what functional role K15 plays in the regulation of NSCs. However, these results suggest that K15 not only acts as a stem cell marker for NSCs but also regulates the behaviour of stem cells, similar to a tumour suppressor. Tumour suppressors regulate the cell cycle and thereby affect proliferation of cells. Further, tumour suppressors can induce apoptosis of cells in which defective DNA was detected (Sherr 2004). As previously mentioned, many tumour suppressor genes have already been identified such as p53, p21 and retinoblastoma which are important cell cycle checkpoint regulators (Engeland 2022; Vlatkovic et al. 2022). Keratins are generally known as structural proteins for the cytoskeleton to support the stability of epithelial cells (Aebi et al. 1983). However, it has been shown that Keratins are also important for the regulation of certain signalling pathways. Keratins, such as K10, K8 and K18, are involved in the Akt signalling pathway (Santos et al. 2002; Lim et al. 2021). The Akt signalling influences the cell cycle and dysregulation of Akt is associated with various forms of cancer (Fadhal 2023). In cervical cancer tissue, K17 was identified to regulate the cell cycle by influencing the tumour suppressor p27. K17 can be released from the intermediate filaments

and can translocate actively into the nucleus via a nuclear localisation signal (NLS) where it induces the translocation and degradation of p27 (Escobar-Hoyos et al. 2015; Baraks et al. 2022). All K17, K10, K18 and K15 belong to the type 1 acidic intermediate filament (Jacob et al. 2018). It is therefore possible that K15 may have a similar effect on the cell cycle progression as the other keratins in this class. However, according to a preliminary result of antibody staining against K15, no expression of K15 was detected in the nucleus of the cells in the epithelium (unpublished). Therefore, it is unlikely that K15 plays a function within the cell nucleus. However, the expression of trans localised K15 may be so low or only party of the K15 protein relocate into the nucleus that it cannot be detected by antibody staining. Furthermore, K15 might act on several checkpoints during the cell cycle and by this influencing the progression of the cell cycle. For K15, it is not yet known whether and at which cell cycle checkpoints it could influence the cell cycle progression. The BrdU incorporation assay revealed that the proliferation effect induced by K15 can already be observed in S-phase, as fewer stem cells were proliferatively active in the K15 overexpression and vice versa in the K15 mutant. This suggests that K15 already induces changes in the cell cycle during G1 to S-phase. To test this hypothesis, certain checkpoint marker as p53 and p27 could be analysed in NSCs in the context of K15 overexpression and K15 mutant to determine whether the expression of p53 and p27 is altered. This would reveal whether and how K15 influences the cell cycle transitions.

4.8 K15 influences cell fate

In neuromasts of medaka, K15 is used as a marker for the stem cells and high *k15* expression is associated with dividing NSCs. The supporting cells, which are the progenitor cells of the neuromast organ, no longer express K15. Also, the recruited epithelial cells, which form the niche cells of the neuromast organ, were once K15+ and have downregulated K15 expression after changing their cell fate into niche cells (Onistschenko, et al. 2023; Seleit, Krämer, et al. 2017). Keratins are frequently used as stem cell markers and their expression is tissue type specific. Interestingly, the expression of Keratins also changes depending on the differentiation state of the cell. More differentiated epithelial cells, for example, express K8 and K18, while epidermal stem cells express K5 with K14 (Coulombe and Omary 2002; Schwarz et al. 2015). This suggests that a change in keratin expression correlates with a change in cell fate. Therefore, the question arose whether and how altered keratin expression can influence the change in cell fate or whether keratin expression follows the cell fate change. In my K15 overexpression (K15 oe) and K15 mutants (K15 mut), I observed altered behaviour of INM. In both conditions less

NSC nuclei migrated apically during G2/M phase and division occurred basally. As already mentioned, K15 is a cytoskeletal component and might be involved in the migration of INM. Moreover, INM can also act as a modulator of cell fate (Chenn et al. 1998; Del Bene et al. 2008). In early development of the retina in zebrafish, it was discovered that altered behaviour in INM is changing the fate of retinal progenitor cells. They studied a Dynactin 1 mutant which affects the migration of INM, in which more nuclei stay basally instead of migrating apically during the cell cycle. This was associated with an earlier exit of the cell cycle and a cell fate change into retinal ganglion cells (Del Bene et al. 2008). By influencing INM, K15 might therefore affect NSC fate. In order to further elucidate the possible effect of K15 on INM and cell fate, I generated chimeric neuromasts in which the NSCs consisted of K15 oe and wildtype or K15 mut and wildtype. In general, I observed growth of NSCs, and furthermore, I was also able to determine the ratio in which NSCs with wildtype *k15* expression and altered *k15* expression increased. In the chimeric neuromasts with K15 oe and wildtype NSCs, K15 oe NSCs were able to outcompete the wildtype NSCs. This suggests that K15 oe NSCs have an advantage over wildtype NSCs., The results from the stable transgenic line of K15 oe indicate that K15 oe NSCs proliferate less than in the wildtype. Therefore, the proliferation cannot be the cause for the higher number of K15 oe NSCs. One explanation could be that, the overexpressed K15 NSCs, even if they proliferate less, continue to produce stem cells, but generate little to no differentiated progeny compared to the wildtype NSCs. The wildtype NSCs gradually produce differentiated cells, so that eventually there are fewer wildtype NSCs in the neuromast than K15 oe NSCs. This would explain the overrepresentation of K15 oe NSCs after 2 weeks. In the wildtype, I normally observe that *k15* is dynamically expressed in NSCs. However, this dynamic expression could be altered in the K15 oe and thus influence the fate of the stem cells. The continuous expression of *k15* could act as signal to maintain stem cell properties. If K15 acts as a signal for the NSCs to remain stem cells, I would expect to observe the exact the opposite effect from K15 mut transplantation, namely the loss of K15 mut NSCs over time. However, the K15 mut NSCs were still present after 2 weeks of growth, and no significant effect of losing K15 mut NSCs was detected. Rather, I observed a similar effect of proliferation as in the wildtype control transplants. One reason for this could be that since K15 mut NSCs generally proliferate more than the wildtype, the loss of K15 mut NSCs by their potential cell fate change can be compensated. To test this hypothesis, BrdU incorporation experiments could be performed in transplanted embryos to compare the proliferation rate of the altered K15 expressing NSCs within one organ. In addition, lineage tracing of the K15 oe NSCs could reveal how NSCs of the K15 oe are contributing to the differentiated progeny and

vice versa in the K15 mut. This would elucidate how altered K15 expression in NSCs affects cell fate and whether K15 functions as a general regulator of cell fate in NSCs.

4.9 ScRNA seq data to identify marker genes in neuromasts

ScRNA seq data opens up new dimensions for understanding the regulation of cells. Each cell has a unique gene expression and ScRNA seq provides information about its transcriptional status. Cells with similar transcriptional patterns group together and form clusters. The scRNA seq data set of the medaka skin, which I generated in this thesis, was used to better understand the expression of Keratins. Keratins usually form heterodimers with other keratins. Type 1 keratins always aggregate with type 2 Keratins (Jacob et al. 2018). Interestingly, K15 has no distinct interaction partner (Waseem, Alam, et al. 1999). Nevertheless, I was interested in dissecting which other Keratins are expressed in the same clusters as K15 to better understand the tissue and differentiation dependent expression of Keratins (Coulombe and Omary 2002). I selected Krt1c19e as a candidate, since it was expressed in the same clusters as K15. I have identified Krt1c19e as a marker for the niche cells of neuromasts. From previous studies in our lab, the neuromast niche were investigated by following the K15+ epithelial cells transforming into border cells. The transformation was reported on the change of their nuclei shape from rounded to elongated. However, after transformation into niche cells, K15 expression diminished and therefore later studies on the niche cells could not be obtained. In addition, the recruitment of epithelial cells was studied in zebrafish and similar behaviour of epithelial cells transforming into niche cells were seen (Onistschenko et al. 2023; Seleit, Krämer, et al. 2017). The *krt1c19e* expression results of this thesis showed strong expression in the skin and in the niche cells surrounding the NSCs. From zebrafish embryos, *krt1c19e* is known to be expressed in the basal epidermal layer and can also be found in cells surrounding the neuromasts. In the adult zebrafish, this *krt1c19e* expression is reduced and more restricted to the fins. Interestingly, strong *krt1c19e* expression was still obtained in p63 positive epidermal cells surrounding the neuromast which are likely the niche cells of the neuromast (Lee, Asharani, and Carney 2014). This indicates that Krt1c19e can not only be used as neuromast niche marker during the development but rather stays a stable marker for the niche cells in adult fish. Therefore, this stable expression of *krt1c19e* as niche cell marker will enable us to better understand how the stem cell niche interaction takes place and how it is maintained during post-embryonic growth. These results highlight how the scRNA seq data can be used to identify new marker genes for the neuromast. Further investigations of this data set could provide unique markers for the progenitor cells. In zebrafish progenitor studies, different progenitor cell pools were found with

distinct characteristics. Thereby they could classify the progenitor cells into four subgroups: central supports cells, dorsal/ventral amplifying cells, anterior/ posterior quiescent cells and mantle cells. Each of these cell pools transcribe different subsets of genes and behave differently in homeostasis and regeneration of hair cells. The central support cells are characterised by *isl1* and *lfng* expression and are the direct source for generating new hair cells. The dorsal/ventral amplifying cells express *wnt2* and *sost* and are highly proliferative but do not directly contribute to the hair cells. In contrast, the anterior/ posterior support cells are more quiescent and express *si:ch73-261i21.5*. The mantle cells in zebrafish express *tspan1*, form this ring like shape of stem cells and are associated with high dormancy (Lush et al. 2019; Thomas and Raible 2019). This is in contrast to what I observed in this thesis in medaka, in which NSCs are highly proliferative active. In addition, I compared the marker genes for the individual support cell types in my scRNA dataset with those of zebrafish. I could not find any congruency with the expression of these marker genes for the support cells in medaka. This indicates that the homeostasis and hair cell production of neuromasts is likely differently regulated in zebrafish and medaka. Therefore, this scRNA sequencing data set may help to further analyse the downstream cell types within the neuromast in medaka to clarify how the individual cell types are regulated.

5 Conclusion

In this thesis, I illustrated the relevance of the stem cell marker Keratin 15 (K15) in NSCs, as it is acting as a regulator of stem cell proliferation. Moreover, K15 not only acts as a cell cycle pacer but is capable to also influence the fate of the stem cells. This emphasises the previously undiscovered potential of keratins and their control in stem cells and contributes to a better understanding of possible roles of keratins in the development of cancer.

Taken together, this work provides new insights on how stem cells are regulated in homeostatic conditions and highlights the importance of keratins as regulators of stem cells.

6 Materials and Methods

6.1 Materials

6.1.1 Medaka fish lines

Table 2: Fish stocks used and generated in this thesis

Name	Stock number	Source
CR(K15_mut)	10311, 10504, 10906,	This thesis
Sc(K15:H2B-eGFP)	9433, 10224, 10487, 10779	(Seleit, et al. 2017)
SC(K15:H2B-RFP)	9430, 9963, 10225, 1048, 10792	(Seleit, Krämer, et al. 2017)
SC(K15:K15CDS-T2A-GFP)	9711, 9880, 10356, 10503, 10908	This thesis
SC(K15:d2GFP_K15:H2B-RFP)	10673	This thesis
SC(K15:mYFP)	9905	(Seleit, Krämer, et al. 2017
Wildtype Cab	8813, 9698, 10052, 10346	(Wittbrodt, Shima, and Schartl 2002)

6.1.2 cDNA templates from 20k library

Table 3: cDNA templates taken from the 20k library and used in this thesis

Gene name	Clone ID
K15	Cons_P24_M_04
And1	Cons_P43_K_04
Krt1c19e	Cons_P09_B_11

6.1.3 Oligo pools

Table 4: Oligo pool order for HCR used in this thesis

Pool name	Sequence
B3_Ola_k15_18	GTCCCTGCCTCTATATCTttGTCAAACAAGATCTGGTATTCTCGA
B3_Ola_k15_18	AATCTCCATCTCCAGTCTGGTCTTGttCCACTCAACTTTAACCCG
B3_Ola_k15_18	GTCCCTGCCTCTATATCTttACTAACTGCTCCTCCAGAACTGATA

B3_Ola_k15_18 TGGTGTTCCATGTCGTTGCGCATCAttCCACTCAACTTTAACCCG
B3_Ola_k15_18 GTCCCTGCCTCTATATCTttAAAAGCGTGCCTCTGTTTCGTGTAA
B3_Ola_k15_18 TTTGCTGGAAGGCAGAGATCTGAGAttCCACTCAACTTTAACCCG
B3_Ola_k15_18 GTCCCTGCCTCTATATCTttTTGAGACTGCAGCTCTATTTGCAGG
B3_Ola_k15_18 GCCCTCCAGAGCAGCTTTCAAACTGttCCACTCAACTTTAACCCG
B3_Ola_k15_18 GTCCCTGCCTCTATATCTttTCGGACTTTGACGAGATTAAAGTTT
B3_Ola_k15_18 TGAAGTGTCCGATTGAGATCTGAGAttCCACTCAACTTTAACCCG
B3_Ola_k15_18 GTCCCTGCCTCTATATCTttCCTCTGCCTTTTTATCGTACCACTC
B3_Ola_k15_18 GTTTCACAGACATCTCTGACTTCAGttCCACTCAACTTTAACCCG
B3_Ola_k15_18 GTCCCTGCCTCTATATCTttGGCCTCGTACTGCTCACGGATCTCA
B3_Ola_k15_18 AAGTTCTTTCTTGTTTTTATTAGCCttCCACTCAACTTTAACCCG
B3_Ola_k15_18 GTCCCTGCCTCTATATCTttTTTGCGTCCACCTCAACGTTGACCT
B3_Ola_k15_18 ATGATGGCACTCAAGTCCTCCTGTGttCCACTCAACTTTAACCCG
B3_Ola_k15_18 GTCCCTGCCTCTATATCTttTTTCCTCCTCGTGGTTCTTCTTGAG
B3_Ola_k15_18 CAGTGACCTGAGTCCTCATTGACGCttCCACTCAACTTTAACCCG
B3_Ola_k15_18 GTCCCTGCCTCTATATCTttCTGGAGCTCCAAGTCTGACCTGGCA
B3_Ola_k15_18 GACCAGCTCCTCCCTGAGGCCTTCAttCCACTCAACTTTAACCCG
B3_Ola_k15_18 GTCCCTGCCTCTATATCTttTCAGCAATGTCTGCCTCCACTGACT
B3_Ola_k15_18 GTCAGCTGGTCAAGCACTCTCCTCAttCCACTCAACTTTAACCCG
B3_Ola_k15_18 GTCCCTGCCTCTATATCTttTTCTGAAGTCATCAGCGGCCAGCCT
B3_Ola_k15_18 GCATGCAGAGCTCGGTCTCAAACTTttCCACTCAACTTTAACCCG
B3_Ola_k15_18 GTCCCTGCCTCTATATCTttTTTGGTACGGTACCCGTCCTGGATC
B3_Ola_k15_18 GTTATCCAAAGAAATTTGAATGCTTttCCACTCAACTTTAACCCG
B3_Ola_k15_18 GTCCCTGCCTCTATATCTttAACTTTGAATAGTCACGGCCGGCGG
B3_Ola_k15_18 CCCTGCAGTTCTACGATGGTGGCATttCCACTCAACTTTAACCCG

B3_Ola_k15_18	GTCCCTGCCTCTATATCTttTCTTGAGCTCGAGCTCACTGTTC GC
B3_Ola_k15_18	CAGCTTTGCTGTCCAGGAAATTTCGttCCACTCAACTTTAACC CG
B3_Ola_k15_18	GTCCCTGCCTCTATATCTttGCTGGCAAGCCGGTCATTGAGGT TC
B3_Ola_k15_18	CTCCAGGGTGCGCACCTTCTCCAGGttCCACTCAACTTTAACC CG
B3_Ola_k15_18	GTCCCTGCCTCTATATCTttTGGAAGTCTCCACTGCCTGCACC GC
B3_Ola_k15_18	ATGGTGGCCTTGTCATTGGCTCCAAttCCACTCAACTTTAACC CG
B3_Ola_k15_18	GTCCCTGCCTCTATATCTttCTGAGCCAAAAGCAAAACCACC AGA
B3_Ola_k15_18	CACCGCCAGCAAAGCCTGCACTACCttCCACTCAACTTTAAC CCG

6.1.4 Plasmids

Table 5: Plasmids which were used and generated in this thesis

Name	Stock number	Source
K15:H2B-GFP	4694	Lab stock/ Ali Seleit
I- SceI/ K15:H2B-RFP	4837	Lab stock/ Liz Ambrosio
K15:mCherry-γ-tubulin	5858	mCherry-Gamma-Tubulin-17 was a gift from Michael Davidson (Addgene plasmid #55050; http://n2t.net/addgene:55050 ; RRID:Addgene_55050)
Krt1c19e:H2B-RFP	6238	This thesis
K15:d2GFP	4817	Lab stock/ Isabel Krämer
Keratin15:mYFP	4450	Lab stock/ Ali Seleit
pGGDest(K15_5´HF_eGFPwCR13_K15-3´HF)	5839	This thesis
pGEMTeasy\K15-T2A-GFP	5841	This thesis
DR274(K15_3´UTR_T1)	5907	This thesis
DR274(K15_3´UTR_T3)	5908	This thesis
DR274(K15_exon 7_T1)	5909	This thesis
DR274(K15_exon 7_T2)	5910	This thesis
pGEMTeasy\ K15 CDS	5893	This thesis
pJET1.2(K15CDS-flexilinker-d2GFP)	6128	This thesis

K15::K15CDS-Flexilinker-d2GFP	6143	This thesis
pGEMTeasy\ Krt1c19e promotor	6237	This thesis
Krt1c19e::H2BRFP	6238	This thesis

6.1.5 Primers

Table 6: Primers used in this thesis

JW number	Primer	sequence
JW2892	GFP rev	TCGATGTTGTGGCGGATCTTGAAG
JW3384	M13 fwd	TGTAAAACGACGGCCAG
JW7807	K15 Crispr_check fwd	GGGACCAGAGTCTCTGTTTCC
JW7857	K15 Crispr_check rev	TTGGTGTTCCATGTCGTTGC
JW9581	K15 Fusion_T2A_rev	TCTCCAGCCTGCTTCAGCAGGCTGAAGT TTGTAGCAGCAGCAGAGGAAACCTGTGA GGAG
JW9583	EGFP_T2A_Fusion fwd	AGCAGGCTGGAGACGTGGAGGAGAACC CTGGACCTATGGTGAGCAAGGGC
JW9584	EGFP_T2A-Fusion rev	CTCCCCCTGAACCTGAAA
JW9872	K15 fwd on shorter annotation	GAGGAGCACAACATCTCAG
JW9873	K15 fwd at ATG	ATGAGTAACTATTCTAGCATGCA
JW9874	K15 rev without T2A (same as JW9581)	CTCCTCACAGGTTTCCTCT
JW9875	K15 rev on shorter annotation	TTCAGGTGATGACTTCAGAC
JW10028	K15 5´HF rev (BsaI oh; EV3 oh)	GCCGGTCTCAAGGTAACCTGTGAGGAGG ATGTCA
JW10029	K15 5´HF fwd (BsaI oh; pDest oh)	GCCGGTCTCAGTATCCGAAACAGAGGCA CGCTTTTC
JW10030	K15 3´HF fwd (BsaI oh; EV3 oh)	GCCGGTCTCAACTACCCCACAAAGCTAA ATCGGGGT
JW10031	K15 3`HF rev (BsaI oh; pDest oh)	GCCGGTCTCACTTAGGTTCCTGGAAAAC CTGGAT
JW10034	K15 seq endogenous tag fwd	CTCTGGAGGGCCAATTACAC
JW10035	K15 seq endogenous tag rev	TTTGGAGTCAAAGGTGGAGC
JW10036	K15 sgRNA T1 oligo fwd	TAGGGACTGACAACAGAGCACC
JW10037	K15 sgRNA T1 oligo rev	AAACGGTGCTCTGTTGTCAGTC
JW10038	K15 sgRNAT3 oligo fwd	TAGGGAGAAGCAACAACGGTTC
JW10039	K15 sgRNAT3 oligo rev	AAACGAACCGTTGTTGCTTCTC
JW10040	K15 ORF T2A EGFP - JW9581 with T2A from Karen	CCTCCACGTCACCGCATGTTAGAAGACT TCCTCTGCCCTCAGAGGAAACCTGTGAG GAG

JW10153	K15 sgRNAT1 olifo fwd new	TAGGCTCACAGGTTTCCTCTTA
JW10154	K15 sgRNA T1 oligo rev new	AAACTAAGAGGAAACCTGTGAG
JW10155	K15 sgRNA T2 oligo fwd new	TAGGCTTCATCTTTTCCTTAAG
JW10156	K15 sgRNA T2 oligo rev new	AAACCTTAAGGAAAAGATGAAG
JW10157	K15 3´HF new fwd	GCCGGTCTCAACTACCGGAAAAGATGAAGGGCGACA
JW10158	K15 3´HF new rev	GCCGGTCTCACTTACCCCGATTTAGCTTTGTGGA
JW10915	K15H2B backbone fwd	GCCGGTCTCAACCTCTTAAAGCGGCCGCGACTCT
JW10916	K15H2B backbone rev	GCCGGTCTCAAGCCCTTAGCGCTGGTGTACTTGG
JW10931	K15CDS fwd	GCCGGTCTCAACCTCCATGAGTAACTATTCTAGCATGCA
JW10932	K15CDS rev	GCCGGTCTCAAGCCAGAGGAAACCTGTGAGGAG
JW10933	K15 d2GFP backbone fwd	GCCGGTCTCAGGCTCCGTGAGCAAGGGCGAG
JW10934	K15 d2GFP backbone rev	GCCGGTCTCAAGGTTTGTGCAGTGTGGTCG
JW11135	K15CDS_fwd_sal1	GGGGTCGACGGTATGAGTAACTATTCTAGCATGCA
JW11136	K15CDS_rev_FlexilinkerOH	CGATCCGCCACCGCCAGAGCCACCTCCGCCTGAACCGCCTCCACCGCTCAGAGAGGAAACCTGTGAGGAG
JW11137	d2GFP_fwd_FlexilinkerOH	TCTGGCGGTGGCGGATCGGGAGGCGGTGGAAGTGCAGCCGCGGGTACCACTACCGGATCCATGGTGAGCAAGGGCGAG
JW11138	d2GFP_rev_Xba1	AGTTCTAGATGGGTGCTACACATTGATCCTAGCAGAAGC

6.1.6 sgRNAs

Table 7: sgRNA s which were generated and used in this thesis

gRNA	Sequence
K15 gRNA 1 (cloned by Ali Seleit)	TGACCGGCTTGCCAGCTACCTGG
K15 gRNA 2 (cloned by Ali Seleit)	CACTGGTCAGGTCAACGTTGAGG
K15 crRNA T1_N-terminal	GCCTGAGCCAGCATAGACGCTGG
K15 crRNA T2_N-terminal	TCCAGCGTCTATGCTGGCTCAGG

K15 sgRNA 4_C-terminal	CCTCTTAAGGAAAAGATGAAGGG

6.1.7 Chemicals and reagents

Table 8: Chemicals and reagents used in this thesis

Description	Source of Supply
2-isopropanol	Sigma-Aldrich
4-Di-2-ASP	Sigma-Aldrich
Acetone	Sigma-Aldrich
Agar	Roth
Agarose	Fisher BioReagents
Alkaline Phosphatase	Sigma-Aldrich
Ampicillin	Roth
Anti-Digoxigenin AP Fab fragment	Roche
BCIP (5-bromo-4-chlor-3-indolyl phosphate)	Sigma-Aldrich
Blocking Reagent	Sigma-Aldrich
Borax anhydrous	Fluka
Bovine Serum Albumin (BSA)	NEB
BrdU (5-Bromo-2-deoxyuridine)	Sigma-Aldrich
Calcium chloride ($CaCl_2$)	AppliChem
Calcium chloride dihydrate ($CaCl_2*2H_2O$)	AppliChem
Collagenase	Sigma-Aldrich
DAPI (4´, 6-Diamidino-2-Phenyindole)	Sigma-Aldrich
Deoxyadenosine triphosphate (dATP)	Thermo Fisher Scientific
Deoxynucleotide triphosphate (dNTPs)	Sigma-Aldrich
Digoxigenin-11-UTP	Roche
Disodium hydrogen phosphate dihydrate ($Na_2HPO_4*2H_2O$)	Sigma-Aldrich
Dispase	Stem cell Technologies
Dimethyl sulfoxide (DMSO)	Roth
Dulbecco´s modified eagle medium (DMEM)	Gibco
DMEM/ F-12	Gibco
Ethanol (EtOH)	Merck
Ethidium bromide (EtBr)	Sigma-Aldrich

Ethylenediaminetetraacetic acid (EDTA)	Sigma-Aldrich
Fetal bovine serum (FBS)	Gibco
Formamide	Sigma-Aldrich
GeneRuler DNA Ladder Mix	Thermo Fisher Scientific
Glycerol	Sigma-Aldrich
Glycine	Sigma-Aldrich
Goat Serum	Sigma-Aldrich
Heparin	Gibco
Hydrogen chloride (HCL)	Merck
Hydrogen peroxide (H_2O_2)	Sigma-Aldrich
I-Sce1 (Meganuclease)	NEB
Kanamycin	Roth
LB-Broth Lennox	Sigma-Aldrich
Low melt agarose	Roth
One Shot® Mach1TM-T1R Chemically Competent *E. coli*	Thermo Fisher Scientific
Magnesium chloride ($MgCl_2$)	AppliChem
Magnesium sulphate heptahydrate	Merck
Maleic acid	Roth
Methanol (MeOH)	Roth
Natural Goat Serum (NGS)	Sigma-Aldrich
NBT (4-nitro blue tetrazolium chloride)	Sigma-Aldrich
Paraformaldehyde (PFA)	Sigma-Aldrich
Penicillin- Streptomycin	Sigma-Aldrich
Polyethylene glycol – 4000 (PEG_4000)	Thermo Fisher Scientific
Potassium acetate (Kac)	AplliChem
Potassium chloride (KCl)	AppliChem
Potassium dihydrogen phosphate (KH_2PO_4)	Merck
Potassium hydroxide (KOH)	Merck
Red sea salt	Red sea
RNase A	Sigma-Aldrich
RNase free water	Sigma-Aldrich
RNA loading Dye 2x	Thermo Fisher Scientific
Sheep serum	Sigma-Aldrich
Sodium chloride (NaCl)	Sigma-Aldrich

Sodium citrate	Sigma-Aldrich
Sodium dodecyl sulphate sodium salt (SDS)	Serva
Sodium hydrogen carbonate ($NaHCO_3$)	Merck
Sodium hydroxide (NaOH)	Sigma-Aldrich
T4 DNA LIGASE	Thermo Fisher Scientific
Tricaine (MS-222)	Sigma-Aldrich
Tris base	Sigma-Aldrich
Tris-hydrochloride (Tris-HCL)	Sigma-Aldrich
Trizol Reagent	Life Technologies (Invitrogen)
Trypsin	Sigma-Aldrich
Tween20	Sigma-Aldrich
Torula RNA	Sigma-Aldrich
X-Gal	Thermo Fisher Scientific
Yeast extract	Roth

6.1.8 Media and solutions

Table 9: Medias and solutions used in this thesis

Description	Ingredients	Composition
Blocking solution for immunostainings	Natural goat serum	10 %
	PTW	1 x
Blocking buffer for *in situ* hybridization	Malate buffer	1 x
	Blocking reagent	2 %
	Tween 20	0.1 %
Borax phosphate buffer	Saturated Borax solution	4 ml
	PTW 1 x	6 ml
Embryo rearing medium (ERM, 1x)	Sodium chloride	17 mM
	Potassium chloride	0.4 mM
	Calcium chloride dihydrate	0.27 mM
	Magnesium sulphate heptahydrate	0.66 mM
EtBr bath	Ethidium bromide	0.02 %
Fin Clip Buffer	Tris/HCl	0.4 M
	NaCl	0.15 M
	SDS 20%	0.1 %

	EDTA pH 8	5 mM
Hatch Medium Medaka (10x)	10x ERM	1l
	Methylene blue	1ml
Hybridization mix	Heparin	50 µg/ ml
	Formamide	50 %
	20 x SSC	5 x
	Torula RNA	5 mg/ ml
	Tween20	0,1 %
LB medium	Bacto-Tryptone	12 g/l
	Yeast extract	5 g/l
	Sodium chloride	5 g/l
LB plates	Bacto-Tryptone	10 g/l
	Yeast extract	5 g/l
	Sodium chloride	10 g/l
	Agar	15 g/l
Maleate buffer (2x)	Maleic acid	200 mM
	NaCl	300 mM
	Tween20	0.1 %
P1	Glucose	50 mM
	Tris-HCL	50 mM
	EDTA	10 mM
	pH 8, stored at 4°C	
P2	Sodium hydroxide	0.2 N
	SDS	1 %
P3	Potassium acetate	5 M
10 x PBS pH7.3	NaCl	1.2 M
	$Na_2HPO_4 * 2H_2O$	0.35 M
	KH_2PO_4	25 mM
1 x PTW	10x PBS	1x
	Tween20	0.1 %
4 % PFA/ 1x PTW	16 % Paraformaldehyde	4 %
	10x PTW	1 x
Prestaining buffer	Tris/HCl pH 7.5	100 mM
	NaCl	100 mM

	Tween20	0.1 %
SSC (20 x)	NaCl	3 M
	Sodium citrate	0.3 M
SCCT (5 x)	SSC 20 x	5 x
	Tween20	0.1 %
SSCT (4 x)	SSC 20 x	4 x
	Tween20	0.1 %
SSCT (2 x)	SSC 20 x	2 x
	Tween20	0.1 %
SSCT (0.2 x)	SSC 20 x	0.2 x
	Tween20	0.1 %
Staining Buffer	Tris HCL pH 9.5	100 mM
	NaCl	100 mM
	$MgCl_2$	50 mM
	Tween20	0.1%
Staining Solution NBT/BCIP	NBT	337.5 µg/ml
	BCIP	175 µg/ml
	In staining Buffer	
TAE (50x)	Tris base	242 g/l
	Glacial acetic acid	5.71 %
	EDTA	50 mM
	pH 8.5	
TB (1x)	Tris-HCL	10 mM
	EDTA	1 mM
	pH 8	
Tricaine 20x	Ethyl 3-aminobenzoate methane-sulfonate salt	4 g/l
	Sodium hydrogen phosphate	10 g/l
	H_2O	Up to 1 l
	pH 7- 7.5	
Yamamoto (10x)	NaCl	171 mM
	KCl	4 mM
	$CaCl_{2*}$ $2H_2O$	2.7 mM
	$MgCl_{2*}$ $6H_2O$	4.9 mM

	$NaHCO_3$	24 mM

6.1.9 Enzymes and buffers

Table 10: Enzymes and buffers used in this thesis

	Description	Source of Supply
Enzymes	DNaseI	Thermo Fisher Scientific
	Hatching enzyme	Homemade
	I-Sce1 Meganuclease	NEB
	Proteinase K	Roche
	Q5 High-Fidelity DNA polymerase	NEB
	Sp6 Polymerase	Roche
	T7 Polymerase	Roche
	T4 DNA ligase	Thermo Fisher Scientific
Buffers	10x I-Sce1 Buffer	NEB
	10x T4 DNA ligase buffer	Thermo Fisher Scientific
	5x Q5 Reaction buffer	NEB
	Amplification buffer (HCR)	Molecular Instruments
	Hybridization buffer (HCR)	Molecular Instruments
	PBS	Gibco
	Restriction enzyme buffer	NEB
	Wash buffer (HCR)	Molecular Instruments

6.1.10 Antibodies and conjugates

Table 11: Antibodies and conjugates used in this thesis

Antibody/ conjugate	Host	Concentration	Source of Supply
α- BrdU	Rat	1/200	Abcam, ab6326
α- GFP	Mouse	1/500	Invitrogen, A11120
α-RFP	rabbit	1/500	Invitrogen, R10367
α-γ-tubulin	mouse	1/500	Sigma-Aldrich, T5326-25UL
α-Dig-AP Fab fragment	sheep	1/2000	Roche, REF 11093274910
α-rabbit-549	Goat	1/500	Jackson, 112-505-144

α-mouse-488	Goat	1/500	Invitrogen, A11029
α-rat-633	Goat	1/500	Invitrogen, A21094
Hairpin B3H1		15 pmol	Molecular Instruments
Hairpin B3H2		15 pmol	Molecular Instruments

6.1.11 Kits

Table 12: Kits used in this thesis

Kit	Source of Supply
Monarch® DNA gel Extraction Kit	NEB
Monarch® PCR & DNA cleanup Kit	NEB
mMessage mMachine Kit Sp6 Transcription	Life technologies (Invitrogen)
RNeasy Mini Kit	Qiagen
Midiprep Kit	Qiagen
pGEMTeasy	Promega
TOPO TA cloning kit	Life technologies (Invitrogen)

6.1.12 Consumables

Table 13: Consumables used in this thesis

Description	Source of Supply
Eppendorf tubes	Sarstedt
5 cm dish	Greiner
6 well plates	Greiner
10 cm dish	Sarstedt
24 well plates	Greiner
Borosilicate capillaries standard wall with filament OD 1.0 mm x 0.58 mm	Harvard Apparatus
Cell Saver Tips	Biozym
Cover slips	Roth
Entsorgungsbeutel	Roth

Falcon tubes	Sarstedt
Filter tips	Steinbrenner
Glass beads	Roth
Glass petri dish	Roth
Injection molds	Homemade
Immersion Typ G (Sp8)	Leica
Immersol W (Sp5)	Zeiss
Miniprep Röhrchen	Sarstedt
MaTek dish	NeoLab
Nitril gloves	NeoLab
Pasteur pipettes	Roth
PCR stripes	Sarstedt
PCR single tubes	Kisker
Pestles	Eppendorf
Scalpel blades	Roth
Tips	Steinbrenner
Transplantation molds	Homemade
Whatman paper	Sigma-Aldrich

6.1.13 Equipment

Table 14: Equipment which was used in this thesis

Description	Source of Supply
Bakterial Shaker INNOVA 44	New Brunswick
C1000 Touch™ Thermal Cycler	Bio-Rad
Centrifuge	Eppendorf
DeNovix DS-11 spectrophotometer	DeNovix
DM5000 B DIC microscope	Leica
Electrophoresis chamber	PeqLab Biotechnologies GmbH
Forceps	Dumont
Freezer	Liebherr
Fridge	Liebherr
Fish incubators	Haraeus instruments and RuMed
Incubators (32°C, 37°C, 60°C)	Binder
InjectMan N12	Eppendorf

Leica TCS SP8	Leica
Leica TCS SP5	Leica
Leica TCS SPE	Leica
Microwave	Samsung
Milli-Q water filtration station	Merck
Mini- centrifuge	neoLab
Needle puller P30	Sutter Instruments Co USA
Nikon SMZ18 stereomicroscope	Nikon
Olympus SZX7	Olympus
pH-meter	Sartorius
Pipettes (2 µl, 10 µl)	Eppendorf
Pipettes (20 µl, 200 µl, 1 ml)	Gilson
Power supply (gel electrophoresis)	Bio-Rad
Rotating arm	Homemade
Scale	Sartorius
Stereomicroscope Zeiss Stemi 2000	Zeiss
UV-Gel Documentation System	Intas
UV table	Vilber Lourmat
Vortex	Scientific Industries, Inc.
Water bath	GFÖ
Zeiss Axio Imager M1	Zeiss

6.1.14 Software and Applications

Table 15: Software and Applications used in this thesis

Description	Source of Supply
Affinity Designer	Affinity
CCTop	(Stemmer et al. 2015)
Endnote	Clarivate Analytics
Fiji	(Schindelin et al. 2012)
FileMaker Pro	FileMaker, Inc.
Geneious	Biomatter Limited
LAS X software	Leica
Microsoft Office	Microsoft

6.2 Methods

6.2.1 Fish Husbandry

For this thesis Medaka fish (*Oryzias latipes*) were used which were kept according to Tierschutzgesetz 111, Abs.1, Nr1 (Haltungserlaubnis AZ35-9185.64 and AZ35-9185.64/BH KIT) and the European Union animal welfare guideline. All the fish were maintained in a closed recirculation system at 28°C and 18°C, respectively on a 14 h light /10 h dark cycle.

6.2.2 Hatching of embryos

For embryo hatching which are still in the chorion (before stage 38), embryos were rolled on sandpaper to induce small holes into the chorion. Then these embryos were incubated in a drop of homemade hatching enzyme for 45 min – 60 min at 32°C on a 6- well plate dish. Afterwards, embryos were rinsed with 1x ERM. Hatched embryos were then transferred into glass plates.

6.2.3 Mounting

For live imaging, embryos were anesthetized in 1 x Tricaine for 5 min and mounted in 0.6 % low- melting point agarose in matek dishes. After embedding the fish, the matek dish was covered with 1 x Tricaine in 1 x ERM to keep the embryo anesthetized during the timeframe of imaging. Afterwards, embryos were put into 1 x ERM to recover from anaesthesia.
Fixed fish samples were mounted in the same way and covered with 1x PTW, but leaving out the anaesthesia.

6.2.4 Fixation of fish

To fix hatched fish (stage 39), fish were anesthetized with Tricaine for 10- 15 min and fixed with 4 % PFA/ 1 x PTW overnight at 4°C. For storage the 4% PFA/ 1 x PTW was replaced with 1% PFA/ 1 x PTW. For immunostainings, 4% PFA/ 1 x PTW was replaced with 100 % EtOH in several dilution steps (25 % EtOH/ 1x PTW, 50 % EtOH/ 1x PTW, 75% EtOH/ 1 x PTW, 100% EtOH). For *in-situ* hybridisation, fixative was replaced with 100 % MeOH after washing with 1 x PTW for 3 times.

6.2.5 Whole-mount immunostaining

Embryos were fixed as previously described and stored in 100 % EtOH. For the immunostaining, embryos were then rehydrated in several steps by adding PTW. First with 75 % EtOH/ 1x PTW, 50 % EtOH/ 1x PTW, 25% EtOH/ 1 x PTW and finally with 1 x PTW. At each dilution step the embryos were incubated for 5 min while shaking. Then, the embryos were

transferred into glass flasks and treated with precooled 100 % acetone for 12 min at -20°C to permeabilize the tissue for the antibody staining. After this, the embryos were washed two times for 5 min with 1 x PTW on a shaker. For blocking, embryos were put back into 2 ml Eppendorf tubes and put into blocking solution (10 % NGS in 1 x PTW) for 2 h at room temperature at a shaker. Primary antibodies were prepared in staining solution (1 % NGS in 1x PTW) with their corresponding dilution. Embryos were incubated with the antibodies overnight at 4°C on a rotating wheel. On the next day, the primary antibody was removed by washing the embryos 6 x with 1 x PTW for 5 min each. The secondary antibody was prepared in 1 % NSG in 1 x PTW as well with its corresponding dilution. Embryos were also incubated overnight at 4° C on the rotating wheel. On the following day, the secondary antibody was washed off by exchanging with 1 x PTW and exchange of the washing buffer for 6 x for 5 min. Afterwards, the samples were proceeded for imaging. In case, embryos were not directly imaged, embryos were post-fixed with and kept in 1 % PFA/ 1 x PTW.

6.2.6 BrdU incorporation and staining

For the BrdU incorporation, BrdU solution was freshly prepared by using 0.04 g BrdU powder in 50 ml of 1 x ERM. The BrdU solution was then shaken for 20 min at 37°C for proper dissolving. Then according the desired pulse, embryos were put into the BrdU solution (6h/ 24h/ 48h). For longer BrdU incorporations the BrdU solution was changed after 24h with a fresh BrdU solution. After finishing the pulse, the embryos were washed three times with 1 x ERM. Depending on the chase, the embryos were then raised or directly fixed as previously described. For the BrdU staining, first an antibody staining was performed as described in the whole-mount immunostaining. In connection, the BrdU staining was directly proceeded by first washing the embryos three times for 10 min in 1x PTW. Then the embryos were postfixed with 4% PFA/ 1 x PTW at room temperature for 30 min and then washed for three times for 10 min with 1 x PTW. As an antigen retrieval 2 N HCL and 0.5 % triton X were used for 60 min at 37°C. Then the embryos were washed again three times 10 min with 1 x PTW. For the pH recovery, Borax solution (4 ml of saturated Borax solution in 6 ml 1x PTW) was added to the embryos for 15 min at room temperature. Then embryos were washed again three times 10 min with 1 x PTW and then blocked for 2 h with 10 % NGS in 1 x PTW. After blocking, the embryos were washed two times for 5 min in 1 x PTW and then the primary antibody against BrdU (1:200 in 1 % NGS) was applied overnight at 4°C. On the following day, the embryos were washed six times for 10 min with 1 x PTW and the secondary antibody (1:500 in 1% NGS) was

applied overnight at 4°C. On the next day, embryos were washed six times 10 min in 1 x PTW and were ready for imaging.

6.2.7 Imaging

For imaging, confocal laser scanning microscopy at the Leica TCS SPE, Leica SP5 II and Leica SP8 was used. Time-lapse imaging was carried out by imaging neuromasts every 15 – 30 min up to 18 h. The *in-situ* hybridisations were imaged with Leica DIC DB5000 microscope.

6.2.8 Image processing

Images were analyzed and processed with FIJI. For cell tracking the FIJI plugin manual tracking and for stitching of larger images the plugin pairwise stitching was used (Preibisch, Saalfeld, and Tomancak 2009; Ershov et al. 2022). Moreover, the LASX software was used for 3D reconstructions. The figures were made using Affinity Designer.

6.2.9 Data processing

Analysed data were represented in graphs generated either by Excel or BoxPlotR (Spitzer et al. 2014).

6.2.10 4-Di-2-ASP staining

For quantifying the number of neuromasts in non-transgenic embryos, 4-Di-2 -ASP was used to stain neuromast hair cells. Therefore, fish were incubated in 1/1000 4-Di-2-ASP in 1 x ERM for 30 min – 1h and then screened using the GFP filter at the binocular.

6.2.11 Microinjection of one-cell stage Medaka

In order to get one-cell stage medaka embryos, adult fish were separated for males and females one day before. On the next day, males and females were reunited and after 20- 30 min freshly fertilized embryos could be collected and then separated by using forceps. The eggs were put into a self-made injection mold prepared with 1,5 % agarose in H2O. The embryos were aligned, so that the single cell is laying on top. Depending on the injection purpose (transgenesis or mutagenesis) distinct injection mixes were prepared. For transgenesis, 1 µl of I-SceI (5u/ µl), 1,25 µl I-SceI buffer (10 x), 12,5 µl Yamamoto buffer (10 x), 10 ng/ µl DNA and filled up to 25 µl of H2O. For mutagenesis, the CRISPR/Cas9 tool was used, using 150 ng/ µl Cas9 mRNA, 15 ng/ µl sgRNAs and filled up with H2O to 10 µl. Injection was then performed with a glass needle injecting into the one-cell stage of Medaka.

6.2.12 Transplantation of blastulae

Transplantation of cells were performed in blastula stage. Therefore, embryos were collected early in the morning and kept at 32°C in order to increase developmental speed. Once embryos had reached stage 8, embryos were dechorionized as previously described in hatching of embryos. Transplantation was carried out at stage 10 -11 by transferring individual cells as described (Fuhrmann, Onistschenko, and Centanin 2021)

6.2.13 Whole mount *in-situ* hybridisation

For whole mount *in-situ* hybridisation, embryos were fixed as previously described. After fixation embryos were stored in 100 % MeOH. Each washing step was performed on a shaking platform. For starting the *in-situ* hybridisation, embryos were rehydrated in a rehydration series using 75 % MeOH/ 1 x PTW, 50 % MeOH/ 1 x PTW and 25 % MeOH/ 1 x PTW each 5 min. Afterwards, embryos were rinsed 2 x 5 min with 1 x PTW. Then embryos were digested with 10 µg/ml Proteinase K to open the pores for the probe. Digestion was carried out for 10 min at room temperature without shaking. To stop the reaction, embryos were post-fixed with 4 % PFA/ 1x PTW for 20 min and then washed 5 x for 5 min in 1 x PTW. For starting the hybridisation, hybridisation mix were warmed up to room temperature and embryos were then prehybridised for 2 h at 65°C. In the meantime, probes (*K15:* 6 µl, *and1:* 10 µl, *krt1c19e:* 10 µl) were denatured in 200 µl hybridisation mix by heating up the mix to 80°C for 10 min. Right after that the probe was added to the embryos after removing prehybridization solution. The probe hybridisation was carried out over night at 65°C. On the following day, 50 % formamide/ 2 x SSCT buffer, 2 x SSCT, 0.2 x SSCT buffers were preheated to 65°C prior to usage. All washing steps were carried out in a 65°C water bath. Embryos were first washed 2 x 30 min with 50 % formamide/ 2 x SSCT, then once with 2 x SSCT for 15 min and finally 2 x 30 min with 0.2 x SSCT. Afterwards, embryos were blocked for 2 h with blocking buffer for *in-situ* hybridisation while slowly moving on a shaker at room temperature. Embryos were then covered with the premixed anti-digoxigenin-AP Fab fragments (1:2000) in blocking buffer and incubated over night at 4°C on a slowly moving rotator. On the next day, embryos were transferred into 6-well plates for washing 6 x 10 min with 1 x PTW. Then embryos were transferred to 24-well plates and equilibrated with freshly made prestaining buffer 2 x 5 min. Then NBT (337.5 µg/ ml) and BCIP (175 µg/ ml) was added to the freshly made staining buffer and added to the embryos. Staining was carried out in the dark until signal was clearly visible

(*K15:* 30 min, *and1:* 15 min, *krt1c19e:* 45 min). Embryos were then washed 3 x 5 min with 1 x PTW and prepared for imaging.

6.2.14 Probe design for HCR RNA-FISH

The HCR probe for *K15* (ENSORLG00000012618.2) was designed against the unique coding sequence, based on the Japanese medaka HdrR ASM223467v1 transcriptome using the open-source protocol from https://github.com/rwnull/insitu_probe_generator. Pooled probes (50 pmol) were ordered at IDT Oligo pools.

6.2.15 HCR™ RNA-FISH

Fixed embryos, stored in 100 % MeOH, were rehydrated as previously described in whole mount *in-situ* hybridisation. After washing it twice 5 min with 1 x PTW, embryos were digested with 10 µg/ml Proteinase K for 3 min. To stop the digestion, embryos were washed 2 x with 2 mg/ml glycine in 1 x PTW. Then embryos were post-fixed for 20 min with 4 % PFA/ 1x PTW on ice and then washed again 2 x with 1 x PTW at RT. For probe hybridisation, embryos were incubated in 50 % hybridisation buffer (Molecular Instruments)/ 1 x PTW for 5 min at room temperature and then pre-hybridised in 37°C prewarmed 100 % hybridisation buffer for 1h at 37°C. Then 4 pmol of probe were prepared in 250 µl of hybridisation buffer and heated up to 37°C. Previous hybridisation buffer was removed from the embryos and replaced by the probe mix and incubated over night at 37°C. On the next day, the probe was washed away with preheated probe wash buffer (Molecular Instruments) 4 x 15 min at 37°C. Then, washing was continued with 2 x 5 min with 5 x SSCT at room temperature and then 3 x 5 min with 1 x PTW. For the detection, embryos were pre-amplified for 5 min with amplification buffer (Molecular Instruments) at room temperature. Hairpins were prepared by using 5 µl of each hairpin (H1B3, H2B3) and put individually into PCR tubes and heated up to 95°C for 90 sec. After denaturation, hairpins were cooled down for 30 min in the dark at room temperature. Cooled hairpins were pooled in 250 µl of amplification buffer and embryos were then incubated with this hairpin mix over night at room temperature in the dark. On the following day, amplification was terminated by washing the embryos at room temperature 2 x 5 min with 5 x SSCT, 2 x 30 min with 5 x SSCT/ 1:500 DAPI to stain the nuclei and then 1 x 5 min with 5 x SSCT. Embryos were then washed once with 1 x PTW for 5 min and then left over night in 1 x PTW. Embryos were the mounted for imaging at the SP8.

6.2.16 Genotyping

For genotyping of embryos or adult fish, individual embryos or a small piece of a fin was put into 100 µl 50 mM NaOH. To extract the genomic DNA, the embryos were broken up with a pestle and then cooked at 95°C for 20 min. Then 25 µl of 50 mM Tris/HCL pH8 was added. The supernatant could then be used for PCR.

6.2.17 Polymerase Chain Reaction (PCR)

To amplify a desired piece of DNA, PCR was done. For the PCR reaction, 10 µl of 5 x Q5 buffer, 1 µl of 10 mM dNTPS, 1 µl of 10 mM forward primer, 1 µl of 10 mM reverse primer, 0,3 µl of Q5 polymerase, 1 µl of DNA and 35.7 µl H_2O were mixed resulting in a final volume of 50 µl. Q5 amplifies 1 kb in 30 sec and extension time was calculated respectively to the size of the desired DNA fragment. The annealing temperature was calculated for the individual primers using NEB Tm calculator (https://tmcalculator.neb.com). The PCR was run on the PCR cycler machine as shown in the table for 30 cycles.

Table 16: PCR cycle program used on this thesis

	Cycler Program:		
1.	98°C	1 min	DNA Denaturation
2.	98°C	30 sec	DNA Denaturation
3.	Tm °C	30 sec	Primer Annealing
4.	72°C	- min	Extension
5.	repeat to step 2	29 x	Repeat
6.	72°C	5 min	Filling in
7.	10°C	10'	Cool down

6.2.18 Agarose gel electrophoresis

To analyse the PCR reaction, agarose gel electrophoresis was performed. Therefore, 1 – 1.5 % agarose in 1 x TAE gel was poured. In each of the PCR samples 6 x loading dye was added. Then the samples were loaded on the agarose gel together with a DNA ladder and run at 120 V for 45 min – 1h depending on the DNA fragment size. Depending whether it is an analytical or a quantitative analysis, only 5 µl or the whole sample was loaded onto the agarose gel, respectively. Afterwards, the gel was stained in an Ethidium bromide bath for 15 min and then imaged at a gel documentation station. For the quantitative approach, the desired DNA fragment was cut out of the gel with a scalpel and was extracted.

6.2.19 Gel extraction

For DNA gel extraction, the Monarch DNA gel extraction kit was used as described in the manual. The DNA was then eluted in 15 min of prewarmed (50°C) H_2O. The DNA concentration was measured using a DeNovix DS-11 spectrophotometer.

6.2.20 PCR clean-up

For PCR clean up, the Monarch PCR & DNA Clean up kit was used as described in the manual and DNA was eluted in 15 min of prewarmed (50° C) H2O. DNA concentration was measured using a DeNovix DS-11 spectrophotometer.

6.2.21 Restriction Digest

For restriction digests, plasmid DNA (4- 8 µg for cloning, 2 µl of Mini for test digest) was digested with 0,5 – 1 µl of specific restriction enzymes, 10 x Cutsmart buffer and filled up with H2O (final volume 30 µl for cloning and final volume 10 µl for test digest) at 37°C for 1h-overnight. Afterwards, the restriction digest was examined using agarose gel electrophoresis.

6.2.22 DNA ligation

DNA ligation was carried out by using a 3:1 ratio of insert to vector backbone. The insert was either PCR amplified or generated by restriction digest. The insert concentration was calculated via the formula (vector concentration * insert length/ vector length) * 3 = insert concentration). For the vector backbone a concentration of 25- 50 ng was used. The ligation was performed using 10 x T4 ligase buffer, 1 µl of T4 ligase, the corresponding amount of insert and vector and H_2O filled up to 10 µl. As control, the same reaction was performed without using the insert.

6.2.23 Transformation of Shot® Mach1TM-T1R Chemically Competent *E. coli*

For transformation, the Shot® Mach1TM-T1R Chemically Competent *E. coli* bacteria were thawed on ice and then 1- 5 µl of ligation was added to the bacteria. After incubation of 15 min on ice, the bacteria were heat shocked at 42°C for 45 sec. Then the bacteria were put back on ice for another 2 min and 300 µl of TB-medium was added. The bacteria were then incubated at 37°C for 1 h at a shaker and already prepared LB-plates with corresponding antibiotics were prewarmed at 37°C. After this incubation, the bacteria were plated and were put at 37°C overnight. On the next day, colonies could be picked for mini culture inoculation in 3- 4 ml of LB-Medium with corresponding antibiotics.

6.2.24 Extraction of plasmid DNA

After the mini culture inoculation, the plasmid DNA was extracted by transferring 2 ml of culture into a 2 ml Eppendorf tube. The culture was then centrifuged for 2 min at 14000 rpm. The supernatant was then discarded and the pellet was resuspended by using 250 µl P1 resuspension buffer by rigorously pipetting up and down. Then 250 µl of P2 lysis buffer was added and inverted 5-6x before 250 µl P3 neutralization buffer was added. The samples were again inverted 5-6 x before centrifuging 10 min at 4°C at full speed. The supernatant was transferred into a fresh 1.5 ml Eppendorf tube and 600 µl of Isopropanol was added and mixed rigorously. The samples were centrifuged again for 10 min at 4° C at full speed. The supernatant was discarded and the DNA pellet was washed with 400 µl 70 % EtOH. Then the samples were centrifuged again for 5 min at full speed and afterwards the EtOH was removed fully. The pellet was dissolved in 30 µl of H2O by shaking it at 37°C. For microinjections, the plasmid DNA was extracted by using the Qiagen Plasmid big Mini Kit, as described in the manual.

6.2.25 Sequencing

Sequencing of DNA was performed by Eurofins MWG Operon with either commercial primers from Eurofins MWG Operon or specific primers selected for the desired DNA fragment.

6.2.26 Single cell dissociation

Dissociation for single cell RNA sequencing was performed for hatchlings of *K15* wildtypes Tg(K15:H2B-GFP) and Tg(K15:H2B-RFP), *K15* overexpression Tg(K15:K15CDS-T2A-GFP) and *K15* mutants CR(K15_mutant), Tg(K15:H2B-GFP). Therefore, the tails of the hatchlings were cut with a scalpel and transferred and washed twice with ice-cold 1 x PBS. Then PBS was removed and replaced by 30°C prewarmed dissociation cocktail (230 µl of 2.5 % trypsin, 230 µl of 1U/ µl dispase and 40 µl of 100 mg/ ml collagenase). The tissue was dissociated by harsh pipetting with 1 ml tips every 30 sec for 30 sec while in between keeping it at 30°C. After 20 min epithelium was fully dissociated and dissociation was stopped by adding 800 µl of washing buffer (DMEM- 10% FBS). Then samples were centrifuged for 5 min at 800 G at 8°C and afterwards kept on ice. The pellet was then washed twice by removing the supernatant and resuspending with 1 ml of 1 x PBS and centrifuging again. After the second wash, the sample was resuspended in 500 µl of washing buffer and filtered through a 40 µm strainer. Filter was then washed by adding 500 µl of washing buffer to get all dissociated cells. The filtered samples were centrifuged again for 5 min at 800 G at 8°C, supernatant was removed and pellet was resuspended in 250 µl of DMEM/ F12. Then 6 µl of sample and 6 µl of pre-filtered trypan blue

was mixed and checked for cell viability in a cell counter. For sequencing, the final suspension should contain 10000 cells in 43.2 µl DMEM/ F12 and samples were submitted on ice to the Deep Sequencing Core Facility.

6.2.27 Library preparation and sequencing

The library preparation for the single cell suspension was carried out by David Ibberson and Bianka Berki at the Deep Sequencing Core Facility of Heidelberg University and prepared according to the 10 x Genomics protocol. The libraries were sequenced on NextSeq 2000 at EMBL. The data was processed by Javier Vazquez-Marin and clusters analysed and validated by Javier Vazquez-Marin and myself.

References

Aebi, U., W. E. Fowler, P. Rew, and T. T. Sun. 1983. 'The fibrillar substructure of keratin filaments unraveled', *J Cell Biol*, 97: 1131-43.

Baraks, G., R. Tseng, C. H. Pan, S. Kasliwal, C. V. Leiton, K. R. Shroyer, and L. F. Escobar-Hoyos. 2022. 'Dissecting the Oncogenic Roles of Keratin 17 in the Hallmarks of Cancer', *Cancer Res*, 82: 1159-66.

Barker, N., J. H. van Es, J. Kuipers, P. Kujala, M. van den Born, M. Cozijnsen, A. Haegebarth, J. Korving, H. Begthel, P. J. Peters, and H. Clevers. 2007. 'Identification of stem cells in small intestine and colon by marker gene Lgr5', *Nature*, 449: 1003-7.

Barker, Nick, Rachel A. Ridgway, Johan H. van Es, Marc van de Wetering, Harry Begthel, Maaike van den Born, Esther Danenberg, Alan R. Clarke, Owen J. Sansom, and Hans Clevers. 2009. 'Crypt stem cells as the cells-of-origin of intestinal cancer', *Nature*, 457: 608-11.

Barnum, K. J., and M. J. O'Connell. 2014. 'Cell cycle regulation by checkpoints', *Methods Mol Biol*, 1170: 29-40.

Benton, Matthew A. 2018. 'A revised understanding of Tribolium morphogenesis further reconciles short and long germ development', *PLOS Biology*, 16: e2005093.

Bertoli, Cosetta, Jan M. Skotheim, and Robertus A. M. de Bruin. 2013. 'Control of cell cycle transcription during G1 and S phases', *Nature Reviews Molecular Cell Biology*, 14: 518-28.

Blanpain, C., and E. Fuchs. 2006. 'Epidermal stem cells of the skin', *Annu Rev Cell Dev Biol*, 22: 339-73.

Bose, Amrita, Muy-Teck Teh, Iain L. Hutchison, Hong Wan, Irene M. Leigh, and Ahmad Waseem. 2012. 'Two Mechanisms Regulate Keratin K15 Expression In Keratinocytes: Role of PKC/AP-1 and FOXM1 Mediated Signalling', *PLoS One*, 7: e38599.

Brunet, T., and N. King. 2017. 'The Origin of Animal Multicellularity and Cell Differentiation', *Dev Cell*, 43: 124-40.

Buckley, Clare E., and Daniel St Johnston. 2022. 'Apical–basal polarity and the control of epithelial form and function', *Nature Reviews Molecular Cell Biology*, 23: 559-77.

Burkhart, Deborah L., and Julien Sage. 2008. 'Cellular mechanisms of tumour suppression by the retinoblastoma gene', *Nature Reviews Cancer*, 8: 671-82.

Cheang, M. C., D. Voduc, C. Bajdik, S. Leung, S. McKinney, S. K. Chia, C. M. Perou, and T. O. Nielsen. 2008. 'Basal-like breast cancer defined by five biomarkers has superior prognostic value than triple-negative phenotype', *Clin Cancer Res*, 14: 1368-76.

Chenn, Anjen, Y. Alex Zhang, Bryna T. Chang, and Susan K. McConnell. 1998. 'Intrinsic Polarity of Mammalian Neuroepithelial Cells', *Molecular and Cellular Neuroscience*, 11: 183-93.

Cheung, T. H., and T. A. Rando. 2013. 'Molecular regulation of stem cell quiescence', *Nat Rev Mol Cell Biol*, 14: 329-40.

Cooper., Geoffrey M. 2000. 'The Cell: A Molecular Approach. 2nd edition. Sunderland (MA): Sinauer Associates; 2000. Intermediate Filaments.' in, *Sunderland (MA) Sinauer Associates*.

Coulombe, P. A., and M. B. Omary. 2002. "Hard' and 'soft' principles defining the structure, function and regulation of keratin intermediate filaments', *Curr Opin Cell Biol*, 14: 110-22.

Cruz, I. A., R. Kappedal, S. M. Mackenzie, D. W. Hailey, T. L. Hoffman, T. F. Schilling, and D. W. Raible. 2015. 'Robust regeneration of adult zebrafish lateral line hair cells reflects continued precursor pool maintenance', *Dev Biol*, 402: 229-38.

de Gooijer, M. C., A. van den Top, I. Bockaj, J. H. Beijnen, T. Würdinger, and O. van Tellingen. 2017. 'The G2 checkpoint-a node-based molecular switch', *FEBS Open Bio*, 7: 439-55.

de Morree, Antoine, and Thomas A. Rando. 2023. 'Regulation of adult stem cell quiescence and its functions in the maintenance of tissue integrity', *Nature Reviews Molecular Cell Biology*, 24: 334-54.

Del Bene, Filippo, Ann M. Wehman, Brian A. Link, and Herwig Baier. 2008. 'Regulation of Neurogenesis by Interkinetic Nuclear Migration through an Apical-Basal Notch Gradient', *Cell*, 134: 1055-65.

Dijkgraaf, S. 1963. 'The functioning and significance of the lateral-line organs', *Biol Rev Camb Philos Soc*, 38: 51-105.

Ding, L., W. W. Kuhne, D. E. Hinton, J. Song, and W. S. Dynan. 2010. 'Quantifiable biomarkers of normal aging in the Japanese medaka fish (Oryzias latipes)', *PLoS One*, 5: e13287.

Ding, Sheng, and Peter G. Schultz. 2004. 'A role for chemistry in stem cell biology', *Nature Biotechnology*, 22: 833-40.

Dmello, C., S. S. Srivastava, R. Tiwari, P. R. Chaudhari, S. Sawant, and M. M. Vaidya. 2019. 'Multifaceted role of keratins in epithelial cell differentiation and transformation', *J Biosci*, 44.

Doetsch, F., I. Caille, D. A. Lim, J. M. Garcia-Verdugo, and A. Alvarez-Buylla. 1999. 'Subventricular zone astrocytes are neural stem cells in the adult mammalian brain', *Cell*, 97: 703-16.

Dolfi, Luca, Roberto Ripa, Adam Antebi, Dario Riccardo Valenzano, and Alessandro Cellerino. 2019. 'Cell cycle dynamics during diapause entry and exit in an annual killifish revealed by FUCCI technology', *EvoDevo*, 10: 29.

Donehower, L. A., M. Harvey, B. L. Slagle, M. J. McArthur, C. A. Montgomery, Jr., J. S. Butel, and A. Bradley. 1992. 'Mice deficient for p53 are developmentally normal but susceptible to spontaneous tumours', *Nature*, 356: 215-21.

Douarin, N. M. 1975. 'An experimental analysis of liver development', *Med Biol*, 53: 427-55.

Engeland, Kurt. 2022. 'Cell cycle regulation: p53-p21-RB signaling', *Cell Death & Differentiation*, 29: 946-60.

Ershov, Dmitry, Minh-Son Phan, Joanna W. Pylvänäinen, Stéphane U. Rigaud, Laure Le Blanc, Arthur Charles-Orszag, James R. W. Conway, Romain F. Laine, Nathan H. Roy, Daria Bonazzi, Guillaume Duménil, Guillaume Jacquemet, and Jean-Yves Tinevez. 2022. 'TrackMate 7: integrating state-of-the-art segmentation algorithms into tracking pipelines', *Nature Methods*, 19: 829-32.

Escobar-Hoyos, L. F., R. Shah, L. Roa-Pena, E. A. Vanner, N. Najafian, A. Banach, E. Nielsen, R. Al-Khalil, A. Akalin, D. Talmage, and K. R. Shroyer. 2015. 'Keratin-17 Promotes p27KIP1 Nuclear Export and Degradation and Offers Potential Prognostic Utility', *Cancer Res*, 75: 3650-62.

Fadhal, E. 2023. 'A Comprehensive Analysis of the PI3K/AKT Pathway: Unveiling Key Proteins and Therapeutic Targets for Cancer Treatment', *Cancer Inform*, 22: 11769351231194273.

Ferraro, F., C. L. Celso, and D. Scadden. 2010. 'Adult stem cels and their niches', *Adv Exp Med Biol*, 695: 155-68.

Fuhrmann, Jana F., Jasmin Onistschenko, and Lazaro Centanin. 2021. 'Inter-species Transplantation of Blastocysts between Medaka and Zebrafish', *Bio-protocol*, 11: e4166.

Gonzalez, M. A., and A. Bernad. 2012. 'Characteristics of adult stem cells', *Adv Exp Med Biol*, 741: 103-20.

Grabher, Clemens, and Joachim Wittbrodt. 2007. 'Meganuclease and transposon mediated transgenesis in medaka', *Genome Biology*, 8: S10.

Graf, Thomas, and Matthias Stadtfeld. 2008. 'Heterogeneity of Embryonic and Adult Stem Cells', *Cell Stem Cell*, 3: 480-83.

Groß, Karen. 2022. 'Embryonic and post-embryonic organogenesis in the medaka lateral line'.

Gross, Karen, Tuğçe Raif, Ali Seleit, Jasmin Onistschenko, Isabel Krämer, and Lazaro Centanin. 2022. 'Organ-Founder Stem Cells Mediate Post-Embryonic Neuromast Formation In Medaka', *bioRxiv*: 2022.12.16.520711.

Harris, Lachlan, Oressia Zalucki, and Michael Piper. 2018. 'BrdU/EdU dual labeling to determine the cell-cycle dynamics of defined cellular subpopulations', *Journal of Molecular Histology*, 49: 229-34.

He, Y., C. Cai, S. Sun, X. Wang, W. Li, and H. Li. 2016. 'Effect of JNK inhibitor SP600125 on hair cell regeneration in zebrafish (Danio rerio) larvae', *Oncotarget*, 7: 51640-50.

Henion, Paul D., and James A. Weston. 1997. 'Timing and pattern of cell fate restrictions in the neural crest lineage', *Development*, 124: 4351-59.

Heude, Églantine, Sarah Shaikho, and Marc Ekker. 2014. 'The dlx5a/dlx6a Genes Play Essential Roles in the Early Development of Zebrafish Median Fin and Pectoral Structures', *PLoS One*, 9: e98505.

Hoffmann, Ingrid. 2021. 'Centrosomes in mitotic spindle assembly and orientation', *Current Opinion in Structural Biology*, 66: 193-98.

Hope, K. J., L. Jin, and J. E. Dick. 2004. 'Acute myeloid leukemia originates from a hierarchy of leukemic stem cell classes that differ in self-renewal capacity', *Nat Immunol*, 5: 738-43.

Iwamatsu, T. 2004. 'Stages of normal development in the medaka Oryzias latipes', *Mech Dev*, 121: 605-18.

Jacob, J. T., P. A. Coulombe, R. Kwan, and M. B. Omary. 2018. 'Types I and II Keratin Intermediate Filaments', *Cold Spring Harb Perspect Biol*, 10.

Kirchmaier, S., K. Naruse, J. Wittbrodt, and F. Loosli. 2015. 'The genomic and genetic toolbox of the teleost medaka (Oryzias latipes)', *Genetics*, 199: 905-18.

Knosel, T., V. Emde, K. Schluns, P. M. Schlag, M. Dietel, and I. Petersen. 2006. 'Cytokeratin profiles identify diagnostic signatures in colorectal cancer using multiplex analysis of tissue microarrays', *Cell Oncol*, 28: 167-75.

Kosodo, Y., T. Suetsugu, M. Suda, Y. Mimori-Kiyosue, K. Toida, S. A. Baba, A. Kimura, and F. Matsuzaki. 2011. 'Regulation of interkinetic nuclear migration by cell cycle-coupled active and passive mechanisms in the developing brain', *EMBO J*, 30: 1690-704.

Kumar, R., A. Sharma, A. K. Pattnaik, and P. K. Varadwaj. 2010. 'Stem cells: An overview with respect to cardiovascular and renal disease', *J Nat Sci Biol Med*, 1: 43-52.

Lahne, M., and D. R. Hyde. 2016. 'Interkinetic Nuclear Migration in the Regenerating Retina', *Adv Exp Med Biol*, 854: 587-93.

Lee, C., J. Hu, S. Ralls, T. Kitamura, Y. P. Loh, Y. Yang, Y. S. Mukouyama, and S. Ahn. 2012. 'The molecular profiles of neural stem cell niche in the adult subventricular zone', *PLoS One*, 7: e50501.

Lee, Hyun O., and Caren Norden. 2013. 'Mechanisms controlling arrangements and movements of nuclei in pseudostratified epithelia', *Trends in Cell Biology*, 23: 141-50.

Lee, K. C., W. L. P. Goh, M. Xu, N. Kua, D. Lunny, J. S. Wong, D. Coomber, B. Vojtesek, E. B. Lane, and D. P. Lane. 2008. 'Detection of the p53 response in zebrafish embryos using new monoclonal antibodies', *Oncogene*, 27: 629-40.

Lee, Raymond T. H., P. V. Asharani, and Thomas J. Carney. 2014. 'Basal Keratinocytes Contribute to All Strata of the Adult Zebrafish Epidermis', *PLoS One*, 9: e84858.

Leijen, S., J. H. Beijnen, and J. H. Schellens. 2010. 'Abrogation of the G2 checkpoint by inhibition of Wee-1 kinase results in sensitization of p53-deficient tumor cells to DNA-damaging agents', *Curr Clin Pharmacol*, 5: 186-91.

Leung, Louis, Abigail V. Klopper, Stephan W. Grill, William A. Harris, and Caren Norden. 2011. 'Apical migration of nuclei during G2 is a prerequisite for all nuclear motion in zebrafish neuroepithelia', *Development*, 138: 5003-13.

Li, Pei, Katrin Rietscher, Henriette Jopp, Thomas M. Magin, and M. Bishr Omary. 2023. 'Posttranslational modifications of keratins and their associated proteins as therapeutic targets in keratin diseases', *Current Opinion in Cell Biology*, 85: 102264.

Li, X., X. Zhao, Y. Fang, X. Jiang, T. Duong, C. Fan, C. C. Huang, and S. R. Kain. 1998. 'Generation of destabilized green fluorescent protein as a transcription reporter', *J Biol Chem*, 273: 34970-5.

Lim, Y., S. Kim, H. N. Yoon, and N. O. Ku. 2021. 'Keratin 8/18 Regulate the Akt Signaling Pathway', *Int J Mol Sci*, 22.

Link, H., L. Arseniev, O. Bähre, J. G. Kadar, H. Diedrich, and H. Poliwoda. 1996. 'Transplantation of allogeneic CD34+ blood cells', *Blood*, 87: 4903-9.

Liu, Y., S. Lyle, Z. Yang, and G. Cotsarelis. 2003. 'Keratin 15 promoter targets putative epithelial stem cells in the hair follicle bulge', *J Invest Dermatol*, 121: 963-8.

Lush, Mark E., Daniel C. Diaz, Nina Koenecke, Sungmin Baek, Helena Boldt, Madeleine K. St Peter, Tatiana Gaitan-Escudero, Andres Romero-Carvajal, Elisabeth M. Busch-Nentwich, Anoja G. Perera, Kathryn E. Hall, Allison Peak, Jeffrey S. Haug, and Tatjana Piotrowski. 2019. 'scRNA-Seq reveals distinct stem cell populations that drive hair cell regeneration after loss of Fgf and Notch signaling', *Elife*, 8: e44431.

Lust, Katharina, and Joachim Wittbrodt. 2018. 'Activating the regenerative potential of Müller glia cells in a regeneration-deficient retina', *Elife*, 7: e32319.

Lyle, Stephen, Melpo Christofidou-Solomidou, Yaping Liu, David E. Elder, Steven Albelda, and George Cotsarelis. 1998. 'The C8/144B monoclonal antibody recognizes cytokeratin 15 and defines the location of human hair follicle stem cells', *Journal of Cell Science*, 111: 3179-88.

Ma, D. K., M. A. Bonaguidi, G. L. Ming, and H. Song. 2009. 'Adult neural stem cells in the mammalian central nervous system', *Cell Res*, 19: 672-82.

Ma, E. Y., E. W. Rubel, and D. W. Raible. 2008. 'Notch signaling regulates the extent of hair cell regeneration in the zebrafish lateral line', *J Neurosci*, 28: 2261-73.

Malumbres, M. 2014. 'Cyclin-dependent kinases', *Genome Biol*, 15: 122.

McCulloch, E. A., and J. E. Till. 1962. 'The sensitivity of cells from normal mouse bone marrow to gamma radiation in vitro and in vivo', *Radiat Res*, 16: 822-32.

Mendez, M. G., S. Kojima, and R. D. Goldman. 2010. 'Vimentin induces changes in cell shape, motility, and adhesion during the epithelial to mesenchymal transition', *Faseb j*, 24: 1838-51.

Meyer, Emily J, Aissam Ikmi, and Matthew C Gibson. 2011. 'Interkinetic Nuclear Migration Is a Broadly Conserved Feature of Cell Division in Pseudostratified Epithelia', *Current Biology*, 21: 485-91.

Miyata, Takaki. 2008. 'Development of three-dimensional architecture of the neuroepithelium: Role of pseudostratification and cellular 'community'', *Development, Growth & Differentiation*, 50: S105-S12.

Morrison, Sean J., and Judith Kimble. 2006. 'Asymmetric and symmetric stem-cell divisions in development and cancer', *Nature*, 441: 1068-74.

Noctor, Stephen C., Alexander C. Flint, Tamily A. Weissman, Ryan S. Dammerman, and Arnold R. Kriegstein. 2001. 'Neurons derived from radial glial cells establish radial units in neocortex', *Nature*, 409: 714-20.

Norden, C., S. Young, B. A. Link, and W. A. Harris. 2009. 'Actomyosin is the main driver of interkinetic nuclear migration in the retina', *Cell*, 138: 1195-208.

Novikoff, Alex B. 1945. 'The Concept of Integrative Levels and Biology', *Science*, 101: 209-15.

Nuñez, Viviana A., Andres F. Sarrazin, Nicolas Cubedo, Miguel L. Allende, Christine Dambly-Chaudière, and Alain Ghysen. 2009. 'Postembryonic development of the posterior lateral line in the zebrafish', *Evolution & Development*, 11: 391-404.

Obernier, Kirsten, Arantxa Cebrian-Silla, Matthew Thomson, José Ignacio Parraguez, Rio Anderson, Cristina Guinto, José Rodas Rodriguez, José-Manuel Garcia-Verdugo, and Arturo Alvarez-Buylla. 2018. 'Adult Neurogenesis Is Sustained by Symmetric Self-Renewal and Differentiation', *Cell Stem Cell*, 22: 221-34.e8.

Omary, M. B., N. O. Ku, J. Liao, and D. Price. 1998. 'Keratin modifications and solubility properties in epithelial cells and in vitro', *Subcell Biochem*, 31: 105-40.

Park, M. S., and A. Koff. 2001. 'Overview of the cell cycle', *Curr Protoc Cell Biol*, Chapter 8: Unit 8 1.

Passegué, E., C. H. Jamieson, L. E. Ailles, and I. L. Weissman. 2003. 'Normal and leukemic hematopoiesis: are leukemias a stem cell disorder or a reacquisition of stem cell characteristics?', *Proc Natl Acad Sci U S A*, 100 Suppl 1: 11842-9.

Pauklin, S., and L. Vallier. 2013. 'The cell-cycle state of stem cells determines cell fate propensity', *Cell*, 155: 135-47.

Peters, B., J. Kirfel, H. Büssow, M. Vidal, and T. M. Magin. 2001. 'Complete cytolysis and neonatal lethality in keratin 5 knockout mice reveal its fundamental role in skin integrity and in epidermolysis bullosa simplex', *Mol Biol Cell*, 12: 1775-89.

Phan, H. E., M. Northorp, R. L. Lalonde, D. Ngo, and M. A. Akimenko. 2019. 'Differential actinodin1 regulation in embryonic development and adult fin regeneration in Danio rerio', *PLoS One*, 14: e0216370.

Pietras, Eric M., Matthew R. Warr, and Emmanuelle Passegué. 2011. 'Cell cycle regulation in hematopoietic stem cells', *Journal of Cell Biology*, 195: 709-20.

Prasher, Douglas C., Virginia K. Eckenrode, William W. Ward, Frank G. Prendergast, and Milton J. Cormier. 1992. 'Primary structure of the Aequorea victoria green-fluorescent protein', *Gene*, 111: 229-33.

Preibisch, Stephan, Stephan Saalfeld, and Pavel Tomancak. 2009. 'Globally optimal stitching of tiled 3D microscopic image acquisitions', *Bioinformatics*, 25: 1463-65.

Reya, Tannishtha, Sean J. Morrison, Michael F. Clarke, and Irving L. Weissman. 2001. 'Stem cells, cancer, and cancer stem cells', *Nature*, 414: 105-11.

Rothschild, Sarah C., Sarah R. Ingram, Fu- I. Lu, Bernard Thisse, Christine Thisse, Jamie A. Parkerson, and Robert M. Tombes. 2020. 'Genetic compensation of γ CaMKII, an evolutionarily conserved gene', *Gene*, 742: 144567.

Santos, M., J. M. Paramio, A. Bravo, A. Ramirez, and J. L. Jorcano. 2002. 'The expression of keratin k10 in the basal layer of the epidermis inhibits cell proliferation and prevents skin tumorigenesis', *J Biol Chem*, 277: 19122-30.

Sauer, F. C. 1935. 'Mitosis in the neural tube', *Journal of Comparative Neurology*, 62: 377-405.

Sauer, M. E., and B. E. Walker. 1959. 'Radioautographic study of interkinetic nuclear migration in the neural tube', *Proc Soc Exp Biol Med*, 101: 557-60.

Schenk, J., M. Wilsch-Bräuninger, F. Calegari, and W. B. Huttner. 2009. 'Myosin II is required for interkinetic nuclear migration of neural progenitors', *Proc Natl Acad Sci U S A*, 106: 16487-92.

Scheres, Ben. 2007. 'Stem-cell niches: nursery rhymes across kingdoms', *Nature Reviews Molecular Cell Biology*, 8: 345-54.

Schindelin, J., I. Arganda-Carreras, E. Frise, V. Kaynig, M. Longair, T. Pietzsch, S. Preibisch, C. Rueden, S. Saalfeld, B. Schmid, J. Y. Tinevez, D. J. White, V. Hartenstein, K. Eliceiri, P. Tomancak, and A. Cardona. 2012. 'Fiji: an open-source platform for biological-image analysis', *Nat Methods*, 9: 676-82.

Schofield, R. 1978. 'The relationship between the spleen colony-forming cell and the haemopoietic stem cell', *Blood Cells*, 4: 7-25.

Schopf, J. W., and B. M. Packer. 1987. 'Early Archean (3.3-billion to 3.5-billion-year-old) microfossils from Warrawoona Group, Australia', *Science*, 237: 70-3.

Schwarz, N., R. Windoffer, T. M. Magin, and R. E. Leube. 2015. 'Dissection of keratin network formation, turnover and reorganization in living murine embryos', *Sci Rep*, 5: 9007.

Seleit, A., K. Gross, J. Onistschenko, O. P. Hoang, J. Theelke, and L. Centanin. 2022. 'Local tissue interactions govern pLL patterning in medaka', *Dev Biol*, 481: 1-13.

Seleit, A., I. Krämer, E. Ambrosio, N. Dross, U. Engel, and L. Centanin. 2017. 'Sequential organogenesis sets two parallel sensory lines in medaka', *Development*, 144: 687-97.

Seleit, A., I. Krämer, B. Riebesehl, E. Ambrosio, J. Stolper, C. Q. Lischik, N. Dross, L. Centanin 2017 ´Neural stem cells induce the formation of their physical niche during organogenesis´, eLife 6:e29173.

Seleit, Ali, Alexander Aulehla, and Alexandre Paix. 2021. 'Endogenous protein tagging in medaka using a simplified CRISPR/Cas9 knock-in approach', *Elife*, 10: e75050.

Sherr, C. J. 2004. 'Principles of tumor suppression', *Cell*, 116: 235-46.

Siminovitch, L., E. A. McCulloch, and J. E. Till. 1963. 'The Distribution of Colony-Forming Cells among Spleen Colonies', *J Cell Comp Physiol*, 62: 327-36.

Sjöqvist, M., D. Antfolk, F. Suarez-Rodriguez, and C. Sahlgren. 2021. 'From structural resilience to cell specification - Intermediate filaments as regulators of cell fate', *Faseb j*, 35: e21182.

Sogabe, S., W. L. Hatleberg, K. M. Kocot, T. E. Say, D. Stoupin, K. E. Roper, S. L. Fernandez-Valverde, S. M. Degnan, and B. M. Degnan. 2019. 'Pluripotency and the origin of animal multicellularity', *Nature*, 570: 519-22.

Spitzer, Michaela, Jan Wildenhain, Juri Rappsilber, and Mike Tyers. 2014. 'BoxPlotR: a web tool for generation of box plots', *Nature Methods*, 11: 121-22.

Stemmer, M., T. Thumberger, M. Del Sol Keyer, J. Wittbrodt, and J. L. Mateo. 2015. 'CCTop: An Intuitive, Flexible and Reliable CRISPR/Cas9 Target Prediction Tool', *PLoS One*, 10: e0124633.

Strzyz, P. J., H. O. Lee, J. Sidhaye, I. P. Weber, L. C. Leung, and C. Norden. 2015. 'Interkinetic nuclear migration is centrosome independent and ensures apical cell division to maintain tissue integrity', *Dev Cell*, 32: 203-19.

Sugiyama, M., A. Sakaue-Sawano, T. Iimura, K. Fukami, T. Kitaguchi, K. Kawakami, H. Okamoto, S. Higashijima, and A. Miyawaki. 2009. 'Illuminating cell-cycle progression in the developing zebrafish embryo', *Proc Natl Acad Sci U S A*, 106: 20812-7.

Sunada, S., H. Saito, D. Zhang, Z. Xu, and Y. Miki. 2021. 'CDK1 inhibitor controls G2/M phase transition and reverses DNA damage sensitivity', *Biochem Biophys Res Commun*, 550: 56-61.

Suzuki, S., J. Namiki, S. Shibata, Y. Mastuzaki, and H. Okano. 2010. 'The neural stem/progenitor cell marker nestin is expressed in proliferative endothelial cells, but not in mature vasculature', *J Histochem Cytochem*, 58: 721-30.

Taverna, E., and W. B. Huttner. 2010. 'Neural progenitor nuclei IN motion', *Neuron*, 67: 906-14.

Thomas, E. D., and D. W. Raible. 2019. 'Distinct progenitor populations mediate regeneration in the zebrafish lateral line', *Elife*, 8.

Tsai, J. W., Y. Chen, A. R. Kriegstein, and R. B. Vallee. 2005. 'LIS1 RNA interference blocks neural stem cell division, morphogenesis, and motility at multiple stages', *J Cell Biol*, 170: 935-45.

Tsai, J. W., W. N. Lian, S. Kemal, A. R. Kriegstein, and R. B. Vallee. 2010. 'Kinesin 3 and cytoplasmic dynein mediate interkinetic nuclear migration in neural stem cells', *Nat Neurosci*, 13: 1463-71.

Tsuda, Sachiko, Tadao Kitagawa, Shigeo Takashima, Shuichi Asakawa, Nobuyoshi Shimizu, Hiroshi Mitani, Akihiro Shima, Makiko Tsutsumi, Hiroshi Hori, Kiyoshi Naruse, Yuji Ishikawa, and Hiroyuki Takeda. 2010. 'FAK-mediated extracellular signals are essential for interkinetic nuclear migration and planar divisions in the neuroepithelium', *Journal of Cell Science*, 123: 484-96.

Van Keymeulen, Alexandra, Ana Sofia Rocha, Marielle Ousset, Benjamin Beck, Gaëlle Bouvencourt, Jason Rock, Neha Sharma, Sophie Dekoninck, and Cédric Blanpain. 2011. 'Distinct stem cells contribute to mammary gland development and maintenance', *Nature*, 479: 189-93.

Vassilev, Lyubomir T. 2006. 'Cell Cycle Synchronization at the G2/M Phase Border by Reversible Inhibition of CDK1', *Cell Cycle*, 5: 2555-56.

Vlatkovic, T., M. R. Veldwijk, F. A. Giordano, and C. Herskind. 2022. 'Targeting Cell Cycle Checkpoint Kinases to Overcome Intrinsic Radioresistance in Brain Tumor Cells', *Cancers (Basel)*, 14.

Waseem, A., B. Dogan, N. Tidman, Y. Alam, P. Purkis, S. Jackson, A. Lalli, M. Machesney, and I. M. Leigh. 1999. 'Keratin 15 expression in stratified epithelia: downregulation in activated keratinocytes', *J Invest Dermatol*, 112: 362-9.

Waseem, Ahmad, Yasmin Alam, Anand Lalli, Bilal Dogan, Nicholas Tidman, Patricia Purkis, Sarah Jackson, Michael Machesney, and Irene M. Leigh. 1999. 'Keratin 15 Expression in Stratified Epithelia: Downregulation in Activated Keratinocytes', *Journal of Investigative Dermatology*, 112: 362-69.

Wittbrodt, J., A. Shima, and M. Schartl. 2002. 'Medaka--a model organism from the far East', *Nat Rev Genet*, 3: 53-64.

Woods, K., and B. Guezguez. 2021. 'Dynamic Changes of the Bone Marrow Niche: Mesenchymal Stromal Cells and Their Progeny During Aging and Leukemia', *Front Cell Dev Biol*, 9: 714716.

Zerlin, M., S. W. Levison, and J. E. Goldman. 1995. 'Early patterns of migration, morphogenesis, and intermediate filament expression of subventricular zone cells in the postnatal rat forebrain', *J Neurosci*, 15: 7238-49.

Zhong, W., J. N. Feder, M. M. Jiang, L. Y. Jan, and Y. N. Jan. 1996. 'Asymmetric localization of a mammalian numb homolog during mouse cortical neurogenesis', *Neuron*, 17: 43-53.

Zhou, J., Q. Chen, Y. Zou, S. Zheng, and Y. Chen. 2019. 'Stem Cells and Cellular Origins of Mammary Gland: Updates in Rationale, Controversies, and Cancer Relevance', *Stem Cells Int*, 2019: 4247168.

Declaration

I herewith declare that I have written the PhD thesis “Stem cell homeostasis in medaka neuromasts – Keratin 15 as a regulator of proliferation” on my own with no other sources and aids than quoted.

Heidelberg, 2024

Acknowledgments

First of all, I would like to thank Prof Dr Lazaro Centanin for giving me the opportunity to do my PhD in his lab. You have accompanied me all these years during my Master's program and I was able to learn so much not only during my PhD but also before during my lab rotation and Master's thesis. I am enormously grateful to have had you as my PhD supervisor and Doktorvater to help me to develop all my professional skills and moreover to become the person I am now. A PhD is not always easy and you supported me in all situations both professional and personal, and gave me the freedom to overcome all the obstacles that arose during these years. It has been a pleasure to work with and for you.

I would like to thank Prof. Dr. Steffen Lemke and Prof. Dr. Fiona Doetsch for supporting me as my TAC supervisors on the way to my PhD. The lively discussion about my topic helped me to think outside the box and bring my project to the stage it is at now. I would especially like to thank Steffen for the many honest and funny conversations. Your enormous enthusiasm has shown me again and again what science can mean and that you always have to be curious, even after setbacks in science. Thank you for also being my referee. In addition, thank you, Juniorprof. Dr. Lauren Saunders and Dr. Josephine Bageritz for agreeing to be part of my defense committee.

The great working environment of the lab is also one aspect which I am very grateful for. Over the years so many people have come and go, but all left a memorial time in my head. Therefore, a big thank you goes to all the current and former members of the Centaniños.

I would like to especially thank Claudia Loosli, our mother and soul of the lab. Spending time with you in and outside of the lab was always a pleasure. We had so many fundamental conversations about life from which I learnt a lot. So please keep this spirit!

Thanks also go to Javier Vazquez-Marin for always showing great patience, interest and willingness to help. Without him, the scRNA sequencing would not have been so successful.

Over the years, many students were part of the lab and I would have never imaged that some would have taken so much part of my life during my PhD. A big thank you therefore goes to Rebecca Kern. You supported me not only in the lab when it was not easy for me but we enjoyed also so many lively discussions about science, books and movies. I would also like to thank Silvia Zanna, who made my time in the lab a few years ago unforgettable (dionysiert)

I am grateful that we are still in touch today and support each other in our careers.

My special honour goes to Karen Groß, to which I am so grateful that she has accompanied me during the first years of my PhD. I have learned so many things and you have helped me to become the researcher I am now. On top of this, we were able to build up a great friendship which have lasted over our time of the lab. Thanks for proofreading this thesis and supporting me in all professional and personal things.

Coming back to the great working environment, I would also like to thank the entire 5th floor for making the last few years such an enjoyable time. I am grateful to Tanja Kellner and Beate Wittbrodt, who I could always turn to when I needed technical help in the lab and who were always on hand with help and advice. This fits in with Thomas Thumberger, who I could always go to when I had questions about cloning, CRISPR and crazy ideas. So, thank you very much.

I would also like to thank the entire fish team: Erik Leist, Marzena Majewski and Antonino Saraceno. Without your care for the fish, all the research I did, would not have been possible.

Special thanks go to Frederike Seibold and Eva Hasel de Carvalho, who always helped with all administrative matters and sometimes made impossible things possible. You both bring so much positive energy to the floor and I've always loved popping into your offices and having a nice chat, with or without a drink at the bar. Moreover, many thanks to Eva, who proofread this work and always gave me good advice.

From a scientific point of view, I am very grateful for the many discussions with Joergen Benjaminsen, Lucie Zilova and Venera Weinhardt. They always had the time to help me and think about challenging questions.

The spirit of 5th floor was always something special. Therefore, I would like to thank all current and former members, especially Rashi, Risa, Cassian, Jana, Tina, Natalia, Encarni and Kaisa who were always there and with whom I not only had scientific discussions in the lab, at conferences retreats, but also many lively conversations about our lives outside the lab.

My special thanks go to Bettina Welz and Christina Schlagheck, who have made these last 7 years an unforgettable time. Not only did we study together and completed our Master's degrees, but we also continued our doctorates together. It is very special for me that you have accompanied me so closely during this time and I am especially grateful that we were able to overcome our obstacles together. We also had so much fun and it was always a pleasure to spend almost all lunch breaks with you. In addition, our friendship has grown and I look forward to the following years to see who we become :)

Thank you, Christina for also proofreading parts of this thesis.

Besides the lab, I am very grateful for Leonie Adelmann, who has been part of my studies for almost 10 years and has supported me all along this time. We have grown together and I am inspired by your natural curiosity about science.
I would also like to thank Michelle Rosenthal-Rückeis and Isabelle Fröhlich, with whom I started my scientific journey during the Bachelors. You were always curious about how I was developing scientifically and it was always nice to chat with you about my project.

Ein großer Dank geht auch an meine Familie und Freunde von zu Hause. Ich danke vor allem meinen Eltern, die mich immer unterstützt und mich auf diesem Weg begleitet haben. Die Zuversicht meines Vaters, hat mir immer geholfen am Ball zu bleiben, weil er schon immer wusste, dass ich meinen Doktor machen werde. Ich möchte mich auch bei Alina Werle bedanken, die, solange ich denken kann, an meiner Seite ist und mir als Freundin in allen Belangen zur Seite steht.
Last but not least, möchte ich Kevin Chajewski danken, mein Partner und bester Freund. Er stand mir bei allen Höhen und Tiefen der letzten Jahre beiseite und hat mich unterstützt, getröstet und war immer geduldig, wenn ich ein Ohr zum Zuhören gebraucht habe. Vielen Dank, dass du immer für mich da bist.

Publications

Temporal and clonal characterization of neural stem cell niche recruitment in the medaka neuromast **(2023) Onistschenko** J, Kaminsky S, Vazquez-Marín J, Gross K, Wang T, Seleit A, Dörr M, Centanin L. Cells Dev, doi: 10.1016/j.cdev.2023.203837

Inter-species Transplantation of Blastocysts between Medaka and Zebrafish **(2021)** Fuhrmann JF, **Onistschenko J**, Centanin L. Bio-protocol, doi: 10.21769/BioProtoc.4166

Local tissue interactions govern pLL patterning in medaka. **(2021)** Seleit A, Gross K, **Onistschenko J**, Hoang OP, Theelke J, Centanin L. Dev Biol, doi: 10.1016/j.ydbio.2021.09.002

Development and regeneration dynamics of the Medaka notochord. **(2020)** Seleit A, Gross K, **Onistschenko J**, Woelk M, Autorino C, Centanin L. Dev Biol, doi: 10.1016/j.ydbio.2020.03.001

List of Figures

Figure 1: Representation of symmetric and asymmetric division of stem cells 4
Figure 2: Schematic drawing of the cell cycle. 4
Figure 3: Schematic representation of intermediate filament assembly 6
Figure 4: Illustration of interkinetic nuclear migration 8
Figure 5: Posterior lateral line of medaka 10
Figure 6: Proliferation activity of neuromast stem cells in homeostasis 16
Figure 7: Active proliferation of neuromast stem cells *in vivo* 17
Figure 8: Variable positioning of NSC nuclei 18
Figure 9: Neuromast stem cells undergo interkinetic nuclear migration 19
Figure 10: Apical localisation of centrosome in neuromast stem cells 21
Figure 11: Heterogenous expression of Keratin 15 in epithelial and neuromast stem cells 23
Figure 12: K15 localisation in epithelial cells displaying the fin network of K15 24
Figure 13: Dynamic expression of K15 during the cell cycle in neuromast stem cells 26
Figure 14: Generation of K15 overexpression 27
Figure 15: Reduced proliferation in K15 oe shown by BrdU incorporation 28
Figure 16: K15 overexpression negatively affects stem cell proliferation 29
Figure 17: Generation of K15 mutants via CRISPR/cas9 30
Figure 18: Increased proliferation in K15 mut shown by BrdU incorporation 31
Figure 19: K15 mutation affects neuromast shapes and change stem cell proliferation 32
Figure 20: Control transplantation of wildtype into wildtype 34
Figure 21: Quantification of proliferation changes after transplantation of wildtype to wildtype 35
Figure 22: Transplantation of K15 overexpression into wildtype 36
Figure 23: Transplantation of K15 mutant to wildtype 37
Figure 24: ScRNA seq clusters from the skin of medaka 38
Figure 25: Krt1c19e expression in epithelial cells and neuromast niche cells 40
Figure 26: And 1 expression in fins 41

List of Tables

Table 1: Quantification of injected embryos for the endogenous tag of K15 25
Table 2: Fish stocks used and generated in this thesis 59
Table 3: cDNA templates taken from the 20k library and used in this thesis 59
Table 4: Oligo pool order for HCR used in this thesis 59
Table 5: Plasmids which were used and generated in this thesis 61
Table 6: Primers used in this thesis 62
Table 7: sgRNA s which were generated and used in this thesis 63
Table 8: Chemicals and reagents used in this thesis 64
Table 9: Medias and solutions used in this thesis 66
Table 10: Enzymes and buffers used in this thesis 69
Table 11: Antibodies and conjugates used in this thesis 69
Table 12: Kits used in this thesis 70
Table 13: Consumables used in this thesis 70
Table 14: Equipment which was used in this thesis 71
Table 15: Software and Applications used in this thesis 72
Table 16: PCR cycle program used on this thesis 78